University of Houston
Department of Mechanical Engineering
Houston, Texas 77004

ON THE STABILITY OF POISEUILLE PIPE FLOW

by

Henry J. Crowder
and
Charles Dalton
(Principal Investigator)

Technical Report No. 1

August, 1969

CASE FILE COPY

Sponsor: Manned Spacecraft Center
National Aeronautics and Space Administration

Contract: NGR-44-005-065

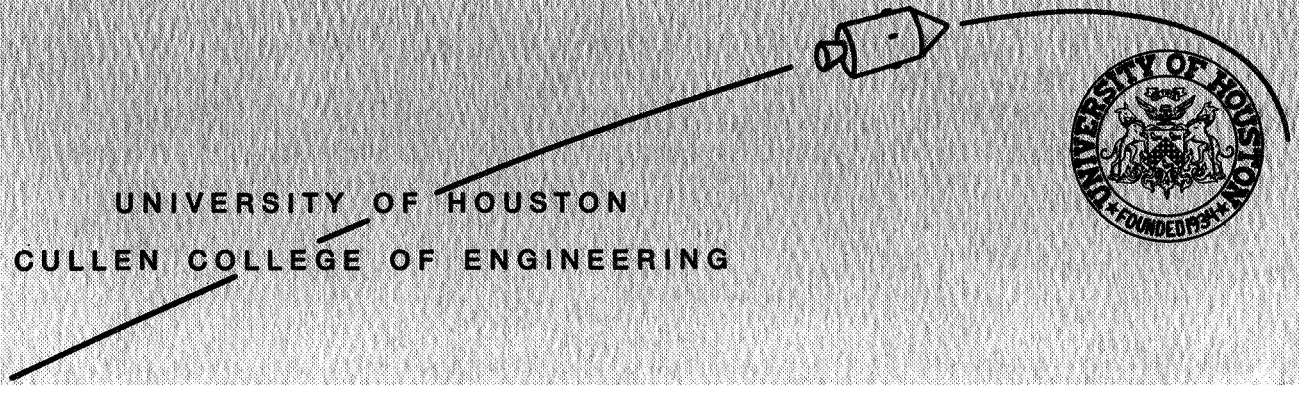

ERRATA

"ON THE STABILITY OF POISEUILLE PIPE FLOW"

by H. J. Crowder and C. Dalton
University of Houston
NASA Grant NGR-44-005-065

p. 50 Figure 3c should be labeled Figure 3b

p. 54 The ordinate on Figure 4a should be labeled G instead of F

p. 55 The ordinate on Figure 4b should be labeled G instead of F

p. 56 The ordinate on Figure 4c should be labeled G instead of F

p. 57 The ordinate on Figure 4d should be labeled G instead of F

p. 58 The ordinate on Figure 4e should be labeled G instead of F

University of Houston
Department of Mechanical Engineering
Houston, Texas 77004

ON THE STABILITY OF POISEUILLE PIPE FLOW

by

Henry J. Crowder
and
Charles Dalton
(Principal Investigator)

Technical Report No. 1

August, 1969

Sponsor: Manned Spacecraft Center
National Aeronautics and Space Administration

Contract: NGR-44-005-065

ON THE STABILITY OF POISEUILLE PIPE FLOW

by

Henry J. Crowder

and

Charles Dalton
(Principal Investigator)

Prepared under Contract NGR - 44 - 005 - 065 by the University of Houston, Houston, Texas 77004 for the Manned Spacecraft Center, NASA, Houston, Texas.

ABSTRACT

The problem of the stability of Poiseuille pipe flow was studied numerically. The finite-difference equations which were solved are approximations to the nonlinear, axisymmetric, Navier-Stokes equations in cylindrical coordinates subject to a stream-function perturbation. The disturbance to the stream function is of the form $A_m(R_1^2/2 - R_1^4/4)\sin(A_r t)$ which is axisymmetric, oscillatory and fixed in space.

The resulting solutions show the experimentally observed instability of the stream function and vorticity at Reynolds numbers of 10,000 and 100,000 for a finite-amplitude disturbance, $A_m = 1.0$. The experimentally observed stability at a Reynolds number of 1000 and $A_m = 1.0$ was also found. At a Reynolds number of 3000 and $A_m = 1.0$, a neutral stability effect was noted. For a small-amplitude case, $A_m = 0.1$, at a Reynolds number of 100,000, the solution represents a damped disturbance which is consistent with classical small-amplitude theory.

TABLE OF CONTENTS

LIST OF FIGURES

	7a. $R = 10^3$ ($A_m = 1.0$)	
	7b. $R = 3 \times 10^3$ ($A_m = 1.0$)	
	7c. $R = 10^4$ ($A_m = 1.0$)	
	7d. $R = 10^5$ ($A_m = 0.1$)	
	7e. $R = 10^5$ ($A_m = 1.0$)	69-73
8	Disturbance Vorticity, Time $\simeq$ 1.5, Radius = 0.6,	
	8a. $R = 10^3$ ($A_m = 1.0$)	
	8b. $R = 3 \times 10^3$ ($A_m = 1.0$)	
	8c. $R = 10^4$ ($A_m = 1.0$)	
	8d. $R = 10^5$ ($A_m = 0.1$)	
	8e. $R = 10^5$ ($A_m = 1.0$)	74-78
9	Disturbance Stream Function, Time $\simeq$ 2.5, Radius = 0.4,	
	9a. $R = 10^3$ ($A_m = 1.0$)	
	9b. $R = 3 \times 10^3$ ($A_m = 1.0$)	
	9c. $R = 10^4$ ($A_m = 1.0$)	
	9d. $R = 10^5$ ($A_m = 0.1$)	
	9e. $R = 10^5$ ($A_m = 1.0$)	79-83
10	Disturbance Stream Function, Time $\simeq$ 2.5, Radius = 0.6,	
	10a. $R = 10^3$ ($A_m = 1.0$)	
	10b. $R = 3 \times 10^3$ ($A_m = 1.0$)	
	10c. $R = 10^4$ ($A_m = 1.0$)	
	10d. $R = 10^5$ ($A_m = 0.1$)	
	10e. $R = 10^5$ ($A_m = 1.0$)	84-88
11	Disturbance Stream Function, Time $\simeq$ 2.5, Radius = 0.8,	
	11a. $R = 10^3$ ($A_m = 1.0$)	
	11b. $R = 3 \times 10^3$ ($A_m = 1.0$)	
	11c. $R = 10^4$ ($A_m = 1.0$)	
	11d. $R = 10^5$ ($A_m = 0.1$)	
	11e. $R = 10^5$ ($A_m = 1.0$)	89-93
12	Disturbance Vorticity, Time $\simeq$ 2.5, Radius = 0.4,	
	12a. $R = 10^3$ ($A_m = 1.0$)	
	12b. $R = 3 \times 10^3$ ($A_m = 1.0$)	
	12c. $R = 10^4$ ($A_m = 1.0$)	
	12d. $R = 10^5$ ($A_m = 0.1$)	
	12e. $R = 10^5$ ($A_m = 1.0$)	94-98

NOMENCLATURE

a,b	eigenvalues of I-A-D matrix
A,B	constants (defined, last line, page 13)
A,B,C,D	finite-difference functions
A_m	amplitude
A_r	frequency
c	wave number
d	pipe diameter
f, f(r,z,t), $f^n_{i,j}$	disturbance stream function
F	disturbance stream function (Chapter IV)
F(r)	Poiseuille pipe flow stream function
g, g(r,z,t), $g^n_{i,j}$	disturbance vorticity
G	disturbance vorticity (Chapter IV)
G(r)	Poiseuille pipe flow vorticity
H	tridiagonal matrix
i	$\sqrt{-1}$
I	identity matrix
L	length of flow field
L′, L″	operators used in Chapter III
n	mode number
o()	order function
p	pressure

$()'$	differentiation with respect to the indicated coordinate
q_o, q, Q	general quantities
r, r_i	radial coordinates
R	pipe radius
R_1	disturbance radius
R	Reynolds number
t, t_n, T	time
u	radial velocity component
v	azimuthal velocity component
V	general velocity
$\bar{V}$	vector velocity
w	axial velocity component
W	space-average velocity
$\bar{W}$	Poiseuille pipe flow velocity profile
x	general coordinate
z, z_j	axial coordinate
Z_1	axial location of disturbance
α	phase velocity
∇, ∇^2	differential operators
$\Delta r, \Delta z, \Delta t$	increments of r, z, t
$\epsilon_r, \epsilon_{g_b}, \epsilon_{g_i}$	convergence constants
θ	azimuthal coordinate
ν	kinematic viscosity
π_n, π_n'	product functions

ρ_k	I-A-D iteration parameter
Φ	general function
$(\Phi^n_{i,j})_x$	finite difference approximation to derivative with respect to x at point (r_i, z_j, t_n)
$\psi, \psi(r,z,t)$	total stream function
$\Omega, \Omega(r,z,t)$	total vorticity

Subscripts and Superscripts

i	radial index
Imax	maximum radial index
j	axial index
Jmax	maximum axial index
k, ℓ, m	iteration counters
n	time index
r, θ, z, t	partial derivative with respect to r, θ, z, t

CHAPTER I. INTRODUCTION

The problem of the stability of Poiseuille pipe flow has been of interest since it was first studied experimentally by Osborne Reynolds [14] in 1880. For the purpose of correlating his data, he defined a parametric grouping, now called the Reynolds number,

$$R_e = \frac{VR}{\nu},$$

where V is a reference velocity, R is a reference length, and ν is the kinematic viscosity of the fluid.

The object of all analytical and experimental approaches to this stability problem has been to determine the minimum Reynolds number at which fully developed laminar flow in a pipe undergoes the transition to turbulence at some position in the flow field.

Experimental approaches have usually shown the transition to turbulence, but both the minimum value of the Reynolds number for transition, and the maximum value of the Reynolds number at which laminar flow could be sustained have varied widely among the various experiments [3,8,9,14,15,20]. Perhaps the most important experimental results to this investigation are those presented by Kuethe [8] in 1956 and extended by Leite [9] in 1958.

In his experiments with air, Kuethe found that at a Reynolds number of 12,000 his disturbance generator, a frustrum of a conical airfoil of nondimensional radius 0.7, created turbulence without oscillation. At a Reynolds number of 8,000 any amplitude of oscillation was sufficient to cause turbulence. But, at a Reynolds number of 4,000, the onset of turbulence was a definite function of the amplitude of the oscillation at 25 Hz.

Leite changed the disturbance generator in the experimental apparatus to a thin sleeve oscillating near the wall. He found that for no oscillation the flow was laminar up to a Reynolds number of 20,000. He also found that the flow damped small oscillations up to a Reynolds number of 13,000, which was the limit of his experiments. In addition it was found that at frequencies above 45 Hz, all disturbances were damped over a short distance from the generator.

Previous analytical treatments of the stability problem have not been as successful as experimental approaches. The classical approach, first attempted by Sexl [8] in 1927, uses linearized small-perturbation techniques, many of which were developed for this and similar problems.

This approach begins with one of the nondimensional forms of the Navier-Stokes equations for incompressible flow,

$$\bar{V}_t + \bar{V} \cdot \nabla \bar{V} = -\nabla p + \frac{1}{R_e} \nabla^2 \bar{V}, \tag{1.1}$$

and the equation of continuity for incompressible flow,

$$\nabla \cdot \bar{V} = 0, \tag{1.2}$$

where $\bar{V}$ is the vector velocity, p is the pressure, R_e is the Reynolds number, and ∇ and ∇^2 are the applicable differential operators given by Irving and Millineux [7]. In the present method of analysis, one assumes that any quantity, q_o, is given by

$$q_o = Q + q, \tag{1.3}$$

where Q is a mean-flow quantity and q is a perturbation quantity. Further, one assumes that q is given by

$$q = \Phi(r)\ \exp(i\alpha z + in\theta - i\alpha ct), \tag{1.4}$$

where α (the phase velocity) is complex, n (the mode number) is an integer, and c (the wave number) is real. One then substitutes equation (1.4) into equation (1.3) and the resulting expression is substituted into equations (1.1) and (1.2). One retains only those terms which are first order in the exponential function, which is then divided out of the equations, to obtain [2],

$$i\alpha w + u' + \frac{u}{r} + \frac{inv}{r} = 0, \tag{1.5.1}$$

$$i\alpha(\bar{W} - c)w + \bar{W}'u + i\alpha p = \frac{1}{R_e}[w'' + \frac{1}{r}w' - (\alpha^2 + \frac{n^2}{r^2})w], \tag{1.5.2}$$

$$i\alpha(\bar{W} - c)\ u + p' = \frac{1}{R_e}[u'' + \frac{1}{r}u' - (\alpha^2 + \frac{n^2+1}{r^2})u - \frac{2in}{r^2}w], \tag{1.5.3}$$

and

$$i\alpha(\bar{W} - c)v + \frac{in}{r} p = \frac{1}{R_e}\left[v'' + \frac{1}{r}v' - (\alpha^2 + \frac{n^2+1}{r^2})v + \frac{2in}{r^2}u\right], \qquad (1.5.4)$$

where $\bar{W}$ is the main-flow velocity, u, v, and w are the perturbation velocity components in the r, θ, and z directions, respectively, and primes indicate differentiation with respect to the radial coordinate, r.

After assuming that n = 0, that is, the flow is axially symmetric, the pressure p is eliminated between equations (1.5.2) and (1.5.3), and the resulting equation is simplified using equation (1.5.1) to obtain

$$i\alpha(\bar{W} - c)(w' - i\alpha u) - \frac{\bar{W}'}{r}u + \bar{W}''u =$$

$$\frac{1}{R_e}\left[w''' + \frac{1}{r}w'' - \frac{1}{r^2}w' - \alpha^2 w' - i\alpha u'' - \frac{i\alpha}{r}u' + i\alpha^3 u\right]. \qquad (1.6)$$

We next define a stream function, ψ, by the equations

$$w = \frac{1}{r}\psi', \qquad (1.7.1)$$

and

$$u = -\frac{i\alpha}{r}\psi, \qquad (1.7.2)$$

which identically satisfies the continuity equation. Substitution of equations (1.7) into equation (1.6) and simplification results in the Orr-Sommerfield equation for axisymmetric Poiseuille pipe flow,

$$i\alpha(\bar{W} - c)(\psi'' - \frac{1}{r}\psi' - \alpha^2\psi) - i\alpha r\left(\frac{\bar{W}'}{r}\right)'\psi =$$

$$\frac{1}{R_e}\left[\psi'''' - \frac{2}{r}\psi''' + (\frac{3}{r^2} - 2\alpha^2)\psi'' - (\frac{3}{r^3} - \frac{2\alpha^2}{r})\psi' - (\frac{\alpha^2}{r^2} - \alpha^4)\psi\right]. \quad (1.8)$$

Since this is the equation for Poiseuille pipe flow,

$$\bar{W} = 1 - r^2, \quad (1.9)$$

and as a consequence of equation (1.9), the term $i\alpha r\left(\frac{\bar{W}'}{r}\right)'\psi$ in equation (1.8) vanishes identically.

Solutions to equation (1.8) have generally been obtained by assuming values for α and R_e and solving for the eigenfunctions ψ and eigenvalues c. Those solutions for which c is zero yield the so-called neutral stability curve as a function of α and R_e. All of the authors who have attempted solutions for the zeroth mode, n = 0, have reached the conclusion that the disturbance is damped [5,13,16,17]. These analytical results are not too surprising due to the experimental results of Kuethe and Leite.

For the first mode, n = 1, the corresponding form of equation (1.8) cannot be derived but both analytical and experimental approaches to this problem have been attempted. Bhat [3], in 1966, experimentally obtained instability for this mode at Reynolds numbers higher than 2,130 but he does not specify the amplitude of the disturbance he used. Lessen, Sadler and Liu [10] in 1968 reported an accompanying linear analysis. The authors found no instability for Reynolds numbers up to 30,000.

The failure of this analytical approach for Poiseuille pipe flow contrasts with the success of the corresponding approach for plane-Poiseuille flow by Thomas [22] in 1953, who numerically solved the analog of equation (1.8). Thomas' solution shows the experimentally observed instability of plane-Poiseuille flow, although the minimum Reynolds number obtained was 5,000, which was too high. It was shown by Meksyn and Stuart [12], Stuart [19], and Meksyn [11] that Thomas' results could be brought more into line with experimental results by including some of the non-linear terms of the differential equations in establishing the equations to be solved. In the final paper of the sequence, Meksyn succeeds in reducing the theoretical minimum critical Reynolds number from 5,000 to approximately 1,500 as compared with the experimentally observed value of approximately 1,000.

Another approach to the Poiseuille pipe flow stability problem has become possible with the advent of large-scale digital computers. This approach consists of solving the governing differential equations (1.1) and (1.2) in their nonlinear form for either small or large amplitude disturbances which are imposed on the flow field. Due to limited time and/or limited memory available on the present-generation computers, this approach has been restricted to treating the problem in two dimensions.

In the case of plane-Poiseuille flow, this is not a severe limitation since Squire [18] in 1933 was able to obtain a

coordinate transformation which reduces the three-dimensional eigenvalue problem to an equivalent two-dimensional problem. It should be noted that there is an effective viscosity increase caused by the transformation. The effective viscosity increase causes the transition Reynolds number for the equivalent two-dimensional problem to be greater than the transition Reynolds number for the untransformed three-dimensional problem. It should also be noted that use of the Squire transformation gives the eigenvalues but not eigenfunctions of a three-dimensional disturbance by treating an equivalent two-dimensional disturbance [2]. This theorem is generally taken to mean that the most unstable disturbance is two-dimensional. Unfortunately, due to the geometry of Poiseuille pipe flow, no such coordinate transformation is possible. Therefore, it is not known a priori that two-dimensional disturbances are more unstable than three-dimensional ones. Admitting the possibility of a more unstable three-dimensional disturbance, we feel that a solution to the two-dimensional, nonlinear problem should show the experimentally observed instability.

Due to the experimental results which have been presented, it was decided that the disturbance should be oscillatory, axially symmetric, of finite, but small, amplitude, and of low frequency. The criterion for instability will be taken to be the decay of a stream function disturbance. If the stream function disturbance does not decay with downstream axial distance for a given Reynolds

number, then the flow is deemed unstable. If the disturbance decays with downstream axial distance for a given value of the Reynolds number, then the flow is taken to be stable.

Therefore, it is this approach to the problem of the stability of Poiseuille pipe flow which has been taken in this work.

CHAPTER II. FORMULATION OF PROBLEM

Since it was decided to treat the stability of Poiseuille pipe flow in two dimensions, we assume that the flow is axially symmetric; therefore, all derivatives with respect to the azimuthal coordinate, θ, in equations (1.1) and (1.2) are assumed to be identically zero. Further, we have assumed that the azimuthal velocity component, v, is identically zero. Therefore, the forms of equations (1.1) and (1.2) which we choose to solve are

$$u_t + uu_r + wu_z = -p_r + \frac{1}{R_e}\left[u_{rr} + \frac{u_r}{r} - \frac{u}{r^2} + u_{zz}\right], \tag{2.1.a}$$

$$w_t + uw_r + ww_z = -p_z + \frac{1}{R_e}\left[w_{rr} + \frac{w_r}{r} + w_{zz}\right], \tag{2.1.b}$$

and

$$u_r + \frac{u}{r} + w_z = 0. \tag{2.1.c}$$

where u and w are the velocity components in the radial and axial directions, respectively, p is the pressure, and R_e is the Reynolds number, and subscripts denote partial differentiation with respect to the indicated coordinate.

The Reynolds number in this case is given by

$$R_e = \frac{Wd}{\nu} . \tag{2.2}$$

where W is the space-average velocity, d is the pipe diameter, and ν is the kinematic viscosity of the fluid.

The pressure is eliminated from equations (2.1) by differentiation of equation (2.1.b) with respect to r and subtracting the result from equation (2.1.a) differentiated with respect to z. After defining the vorticity, Ω, by

$$\Omega = u_z - w_r, \tag{2.3}$$

the result of the above operation may be expressed as

$$\Omega_t + (u\Omega)_r + (w\Omega)_z = \frac{1}{R_e}\left[\left(\frac{1}{r}(r\Omega)_r\right)_r + \Omega_{zz}\right]. \tag{2.4}$$

We next define a stream function, ψ, by

$$u = -\frac{\psi_z}{r}, \tag{2.5.a}$$

and

$$w = \frac{\psi_r}{r}, \tag{2.5.b}$$

such that equation (2.1.c) is identically satisfied.

Therefore, in terms of the stream function and vorticity, equations (2.4) and (2.3) may be written as

$$\Omega_t - \left(\frac{\psi_z}{r}\Omega\right)_r + \left(\frac{\psi_r}{r}\,\Omega\right)_z = \frac{1}{R_e}\left[\left(\frac{1}{r}(r\Omega)_r\right)_r + \Omega_{zz}\right], \tag{2.6.a}$$

and

$$\Omega = -\frac{1}{r}\left[\psi_{zz} + r\left(\frac{\psi_r}{r}\right)_r\right]. \tag{2.6.b}$$

Now, we make a change of variables such that upper case quantities refer to the main flow while lower case quantities

refer to the secondary flow. Therefore, let

$$\psi(r,z,t) = F(r) + f(r,z,t), \tag{2.7.a}$$

and

$$\Omega(r,z,t) = G(r) + g(r,z,t). \tag{2.7.b}$$

Since F and G are main flow quantities for Poiseuille pipe flow, they are given by

$$F(r) = \frac{1}{2}r^2 - \frac{1}{4}r^4, \tag{2.8.a}$$

and

$$G(r) = 2r. \tag{2.8.b}$$

Therefore, equations (2.6) can be written as

$$g_t - f_z\left(\frac{g}{r}\right)_r + \frac{f_r g_z}{r} + (1-r^2)g_z = \frac{1}{R_e}\left[\left(\frac{1}{r}(rg)_r\right)_r + g_{zz}\right], \tag{2.9.a}$$

and

$$f_{zz} + r\left(\frac{f_r}{r}\right)_r = -rg. \tag{2.9.b}$$

It should be noted that to this point in the development no assumption has been made which linearized equations (2.9); therefore, the equations are suitable for describing the behavior of the flow for both large and small amplitude disturbances.

Boundary Conditions

Preceding the development of the boundary conditions for the problem, we will establish the flow field on which equations (2.9) will be solved. This rectangular dimensionless field is shown in Figure 1, where the length L is much greater than 1 and much greater than Z_1. The value of L should be such that an increase

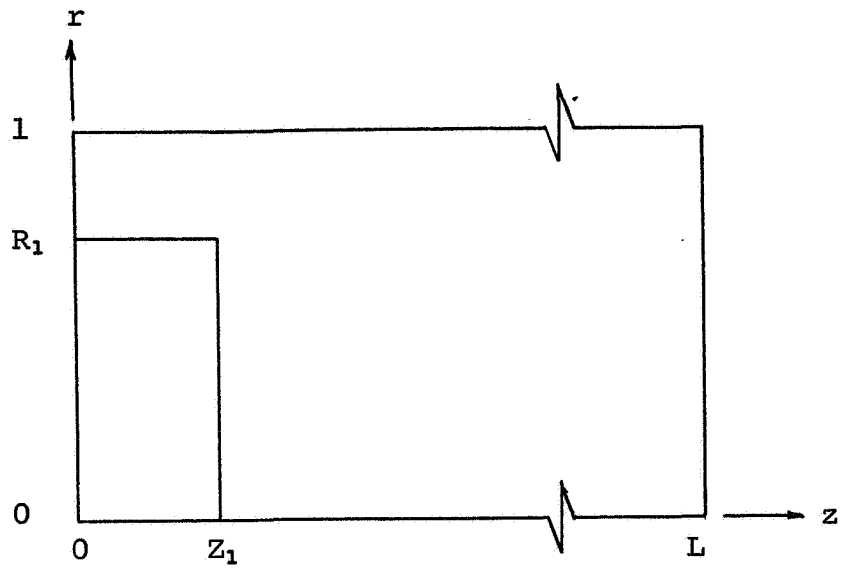

Figure 1. Flow Field

in L causes no change in the solution obtained. The line Z = 0 is arbitrarily placed in the flow with the exception that we initially assume that fully developed flow exists within and on the boundaries of the field of interest. The line r = 1 is the wall of the pipe, while the line r = 0 is the centerline of the pipe.

The boundary conditions applied at r = 1 are the normal conditions of no-slip and no flow through a solid boundary

$$u = -\frac{f_z}{r} = 0, \tag{2.10.a}$$

$$w = \frac{f_r}{r} = 0. \tag{2.10.b}$$

Axial symmetry at the center line, r = 0, implies that

$$f_r = u_r = g_r = w_r = 0. \tag{2.10.c}$$

Since the governing differential equations (2.9) are singular on the line r = 0 and we demand that every quantity be bounded on that line, we have

$$u = u_r = w_r = g = f_z = f_r = g_r = g_z = 0. \qquad (2.10.d)$$

On the line z = 0 we have assumed that fully developed pipe flow must exist. Therefore, we have

$$g = 0 \text{ on } z = 0. \qquad (2.10.e.1)$$

In order to make the solution as free as possible instead of using the condition that f = 0, we use the condition

$$f_z = 0, \qquad (2.10.e.2)$$

which allows the streamlines to move radially.

The downstream boundary conditions are somewhat harder to specify. Ideally, they are specified such that L is located so that no further change occurs in the solution by increasing L. We have followed the suggestion of Thomas and Szewczyk [22] of using

$$f_{zz} = 0, \qquad (2.10.f)$$

and either

$$g_{zz} = 0, \qquad (2.10.g.1)$$

or

$$g_z = 0, \qquad (2.10.g.2)$$

since use of $f_{zz} = Af$ and $g_{zz} = Bg$ imply periodicity of the flow

field for A and B not equal to zero. Boundary conditions (2.10.f) and either of (2.10.g) do not imply the undesired periodicity of the flow field. It should be noted that these conditions are an approximation to the condition that derivatives along a streamline are zero either for L>>1, or for streamlines parallel to the Z axis.

Two considerations govern the form of the disturbance function which may be chosen. First, the disturbance should be modeled on a physically realizable system. Second, the disturbance function should not violate the continuity equation. A disturbance of the form

$$f(R_1,\ Z_1,\ t\geq 0) = \left(\frac{R_1^2}{2} - \frac{R_1^4}{4}\right) A_m \sin A_r t, \qquad (2.11)$$

gives a disturbance to the stream function which is quite similar to the form of a disturbance generated by an infinitesimally thin hollow cylinder which is oscillated axially at the point (R_1, Z_1), where A_m is the amplitude and A_r is the period of the disturbance. Application of equation (2.9.b) yields the vorticity at the point (R_1, Z_1) as

$$g(R_1, Z_1,\ t\geq 0) = \frac{1}{R_1}\left(f_{rr} - \frac{f_r}{R_1} + f_{zz}\right). \qquad (2.12)$$

Since we assume that the disturbance is generating any deviation from the fully developed flow solution, we have for initial conditions

$$f(r,z,0) = 0, \tag{2.13.a}$$

and

$$g(r,z,0) = 0, \tag{2.13.b}$$

for

$$0 \le r \le 1, \quad 0 \le z \le L.$$

Now we turn to the derivation of the boundary condition for g on the line r = 1. Equations (2.10) are repeated along with equation (2.9.b) to facilitate the derivation,

$$u = -\frac{f_z}{r} = 0, \tag{2.10.a}$$

$$w = \frac{f_r}{r} = 0, \tag{2.10.b}$$

and

$$f_{zz} + f_{rr} - \frac{1}{r} f_r = -rg. \tag{2.9.b}$$

Since r = 1 is a solid boundary and $f_z = 0$ at every point on r = 1, we also have $f_{zz} = 0$. Therefore, we substitute this condition and equation (2.10.b) into equation (2.9.b) to obtain

$$g = -\frac{f_{rr}}{r}, \tag{2.14}$$

on the line r = 1.

We now turn to the problem of the consistency of the boundary and initial conditions. From equations (2.10.e) we have

$$f_z(0,0,t) = 0, \tag{2.15.a}$$

$$f_z(1,0,t) = 0, \tag{2.15.b}$$

$$g(0,0,t) = 0, \tag{2.15.c}$$

and

$$g(1,0,t) = 0. \tag{2.15.d}$$

Since from equation (2.10.a) we have

$$f_z(1,0,t) = 0, \tag{2.15.e}$$

therefore, from equations (2.15.b) and (2.15.e) we have

$$f_z(1,0,t) = 0, \tag{2.15.f}$$

but far upstream of $z = 0$, fully developed flow must exist; therefore, we have

$$f(1,0,t) = 0. \tag{2.16}$$

From equation (2.10.d) we have

$$g(0,z,t) = 0, \tag{2.17}$$

and from equations (2.10.d) and (2.15.a) we have

$$f_z(0,z,t) = 0. \tag{2.18}$$

Since any increase in the value of the stream function at $r = 0$ simply implies an increase in the centerline velocity, we must also have

$$f(0,z,t) = 0; \tag{2.19}$$

therefore, this is the condition which we apply.

CHAPTER III. ESTABLISHMENT OF FINITE-DIFFERENCE EQUATIONS

Grid System

The governing differential equations are nonlinear and coupled, both in the equations and through the boundary conditions. Since there is no known closed-form solution to systems of equations of this type, the method of solution which we used was the method of finite differences. In order to apply this technique, it is necessary, first, to introduce a net of grid points on the flow field of Figure 1 as shown in Figure 2.

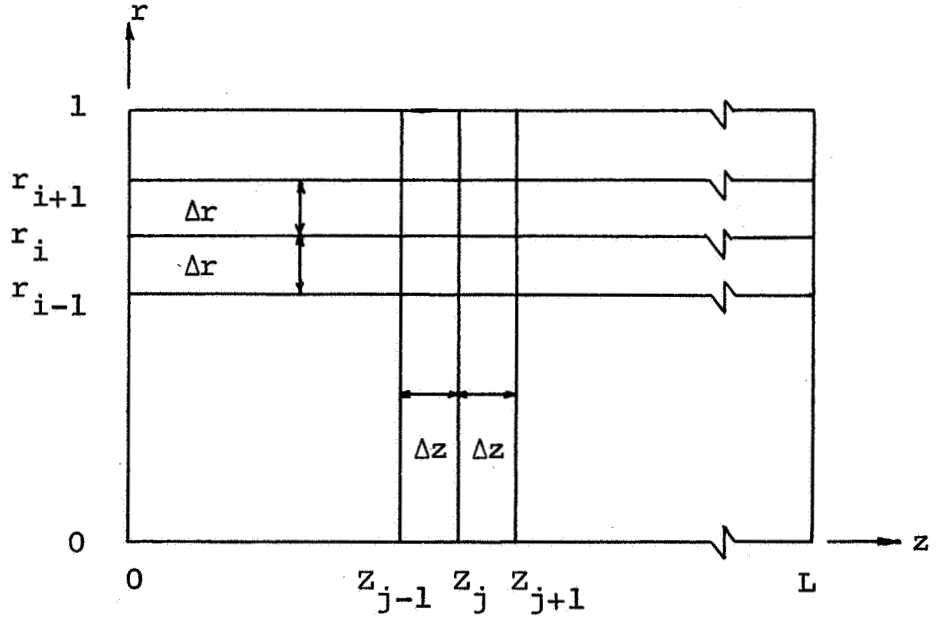

Figure 2. Grid System

Two auxiliary conditions have been imposed on the net of grid points; these are that one of the grid points is the point of the disturbance (R_1, Z_1) and that some grid line falls on each boundary of the flow field. Initially, we did not demand that

the spacing between the grid lines be equal but experimentation indicated that equal spacing yielded a more accurate solution.

The experimentation with the grid spacing showed that mesh spacings of 0.10 and 0.10 in the radial and axial directions, respectively, were a reasonable compromise between accuracy of the computation and machine storage.

Since the variable mesh spacing approach has been rejected, the analysis which follows is for an equally spaced grid in the radial and axial directions respectively. Therefore, the coordinates of a grid point are given by

$$r_i = (i-1)\,\Delta r \text{ where } 1 \le i \le Imax, \tag{3.1.a}$$

and

$$z_j = (j-1)\,\Delta z \text{ where } 1 \le j \le Jmax. \tag{3.1.b}$$

It would be more general to allow the time step to be variable, so we have

$$t_n = \sum_{\ell=0}^{n} \Delta t_\ell \text{ where } \Delta t_0 = 0, \tag{3.1.c}$$

and

$$\Delta t_{2\ell-1} = \Delta t_{2\ell},$$

for any ℓ.

Using definitions (3.1) of the grid system, we have

$$\Phi(r,z,t) = \Phi^n_{i,j} = \Phi(r_i, z_j, t_n), \tag{3.1.d}$$

for the value of any function at a grid point.

Finite-Difference Expressions

Having established the mesh system on which the finite-difference equations will be solved, we now turn our attention to the derivation of the equations. We define for use in this derivation,

$$\Phi_z = \left(\Phi^n_{i,j}\right)_z = \frac{1}{2\Delta z}\left[-\Phi^n_{i,j-1} + \Phi^n_{i,j+1}\right] + o(\Delta z^2), \qquad (3.2.a)$$

$$\Phi_{zz} = \left(\Phi^n_{i,j}\right)_{zz} = \frac{1}{\Delta z^2}\left[\Phi^n_{i,j-1} + -2\Phi^n_{i,j} + \Phi^n_{i,j+1}\right] + o(\Delta z^2), \qquad (3.2.b)$$

$$\Phi_r = \left(\Phi^n_{i,j}\right)_r = \frac{1}{2\Delta r}\left[-\Phi^n_{i-1,j} + \Phi^n_{i+1,j}\right] + o(\Delta r^2), \qquad (3.2.c)$$

$$\Phi_{rr} = \left(\Phi^n_{i,j}\right)_{rr} = \frac{1}{\Delta r^2}\left[\Phi^n_{i-1,j} + -2\Phi^n_{i,j} + \Phi^n_{i+1,j}\right] + o(\Delta r^2), \qquad (3.2.d)$$

$$\Phi_t = \left(\Phi^n_{i,j}\right)_t = \frac{1}{\Delta t_n}\left[\Phi^{n+1}_{i,j} - \Phi^n_{i,j}\right] + o(\Delta t), \qquad (3.2.e)$$

where Φ^n is the function of interest at the n^{th} iterative level.

The differential equation governing the stream function, equation (2.9.b) can be written in the following forms,

$$\rho_k f - f_{zz} = \rho_k f + f_{rr} - \frac{1}{r} f_r + rg, \qquad (3.3.a)$$

and

$$\rho_k f - f_{rr} + \frac{1}{r} f_r = \rho_k f + f_{zz} + rg, \qquad (3.3.b)$$

by adding the quantity $\rho_k f$ to both sides and factoring the equations appropriately. We now difference equations (3.3) to obtain

$$\rho_k f^{n+1,k+1}_{i,j} - \left(f^{n+1}_{i,j}\right)^{k+1}_{zz} =$$

$$\rho_k f^{n+1,k}_{i,j} + \left(f^{n+1}_{i,j}\right)^{k}_{rr} - \frac{1}{r_i}\left(f^{n+1}_{i,j}\right)^{k}_{r} + r_i\, g^{n+1}_{i,j}, \qquad (3.4.a)$$

and

$$\rho_k f^{n+1,k+2}_{i,j} - \left(f^{n+1}_{i,j}\right)^{k+2}_{rr} + \frac{1}{r_i}\left(f^{n+1}_{i,j}\right)^{k+2}_{r} =$$

$$\rho_k f^{n+1,k+1}_{i,j} + \left(f^{n+1}_{i,j}\right)^{k+1}_{zz} + r_i\, g^{n+1}_{i,j}, \qquad (3.4.b)$$

where the superscripts n and k indicate, respectively, the time step and the iteration level from which the value of the function f is taken.

Equations (3.4) can be written in the form

$$\rho_k f^{n+1,k+1}_{i,j} - A_i f^{n+1,k+1}_{i-1,j} + B_i f^{n+1,k+1}_{i,j} - C_i f^{n+1,k+1}_{i+1,j} = D_{i,j} \qquad (3.5.a)$$

and

$$\rho_k f^{n+1,k+2}_{i,j} - A_j f^{n+1,k+2}_{i,j-1} + B_j f^{n+1,k+2}_{i,j} - C_j f^{n+1,k+2}_{i,j+1} = D_{i,j} \qquad (3.5.b)$$

where the coefficients A, B, and C are functions only of the grid system and the difference operators. The terms D are functions only of the grid system, the vorticity, g, and the known stream function, f, at the last iteration. Either of equations (3.5) can be written in the general form

$$(\rho_k I + H)\bar{f} = D, \qquad (3.6)$$

where H is a tridiagonal matrix. Furthermore, due to the form of the coefficients A, B, and C, the matrix H is positive definite.

The quantities ρ_k in equations (3.3), (3.4), (3.5) and (3.6) are parameters which are added to the equations to increase the speed with which convergence to the solution is obtained. The "best" values of the ρ_k for use in equations (3.5) are given by Varga [23] and Young [24] for a square equally spaced grid for Laplace's equation to be

$$\rho_k = b\left(\frac{a}{b}\right)^{\frac{k+1}{m+1}} \quad k = 1,2,---,m \tag{3.7}$$

where a and b are respectively the maximum and minimum eigenvalues of the operator matrix H. Unfortunately, no analytical values of ρ_k can be obtained for the grid and difference equation which we have but Briley's [4] and our experiments indicate that the values of a and b above and a value of m = 5 yield the greatest convergence rate if the values of $f^n_{i,j}$ are used as initial approximations to the values of $f^{n+1}_{i,j}$.

We now begin to derive the vorticity-transport finite-difference equation. By an appropriate factoring, equation (2.9.a) can be written in the following forms:

$$g_t - f_z\left(\frac{g}{r}\right)_r - \frac{1}{R_e}\left(\frac{1}{r}(rg)_r\right)_r = -\left(\frac{f_r}{r} + 1-r^2\right)g_z + \frac{1}{R_e}\,g_{zz}, \tag{3.8.a}$$

and

$$g_t + \left(\frac{f_r}{r} + 1-r^2\right)g_z - \frac{1}{R_e}\,g_{zz} = f_z\left(\frac{g}{r}\right)_r + \frac{1}{R_e}\left(\frac{1}{r}(rg)_r\right)_r. \tag{3.8.b}$$

We now introduce the finite-difference operators (3.2) into equations (3.8) to obtain

$$\left[\frac{1}{\Delta t_n} + \frac{1}{r_i^2}\left(f_{i,j}^{n+1}\right)_z + \frac{1}{r_i^2 R_e}\right] g_{i,j}^{n+1}$$

$$- \left[\frac{1}{r_i}\left(f_{i,j}^{n+1}\right)_z + \frac{1}{r_i R_e}\right]\left(g_{i,j}^{n+1}\right)_r - \frac{1}{R_e}\left(g_{i,j}^{n+1}\right)_{rr} = \frac{1}{\Delta t_n} g_{i,j}^{n} \qquad (3.9.a)$$

$$- \left[\frac{1}{r_i}\left(f_{i,j}^{n}\right)_r + 1 - r_i^2\right]\left(g_{i,j}^{n}\right)_z + \frac{1}{R_e}\left(g_{i,j}^{n}\right)_{zz},$$

and

$$\frac{1}{\Delta t_{n+1}} g_{i,j}^{n+2} + \left[\frac{1}{r_i}\left(f_{i,j}^{n+2}\right)_r + 1 - r_i^2\right]\left(g_{i,j}^{n+2}\right)_z - \frac{1}{R_e}\left(g_{i,j}^{n+2}\right)_{zz} =$$

$$\left[\frac{1}{\Delta t_{n+1}} - \frac{1}{r_i^2}\left(f_{i,j}^{n+1}\right)_z - \frac{1}{r_i^2 R_e}\right] g_{i,j}^{n+1} \qquad (3.9.b)$$

$$+ \left[\frac{1}{r_i}\left(f_{i,j}^{n+1}\right)_z + \frac{1}{r_i R_e}\right]\left(g_{i,j}^{n+1}\right)_r + \frac{1}{R_e}\left(g_{i,j}^{n+1}\right)_{rr},$$

where, as an auxiliary condition, we demand that

$$\Delta t_{2n+2} = \Delta t_{2n+1}, \qquad (3.9.c)$$

for all n. This auxiliary condition is necessary for convergence.

Equations (3.9) can be written in the form

$$\frac{1}{\Delta t_n} g_{i,j}^{n+1} - A_{i,j}^{n+1} g_{i-1,j}^{n+1} + B_{i,j}^{n+1} g_{i,j}^{n+1} - C_{i,j}^{n+1} g_{i+1,j}^{n+1} = D_{i,j}^{n}, \qquad (3.10.a)$$

and

$$\frac{1}{\Delta t_n} g_{i,j}^{n+2} - A_{i,j}^{n+2} g_{i,j-1}^{n+2} + B_{i,j}^{n+2} g_{i,j}^{n+2} - C_{i,j}^{n+2} g_{i,j+1}^{n+2} = D_{i,j}^{n+1}, \qquad (3.10.b)$$

where the coefficients A, B, and C are functions of the unknown stream function, $f^{n+1}_{i,j}$, as well as the grid system. The terms D are functions of the known stream function, $f^{n}_{i,j}$, and vorticity, $g^{n}_{i,j}$. The time step, Δt_n, must be much less than one, and it must be the same between the n + 1 and the n + 2 time steps. We have treated the time step as a parameter which may be selected subject to the restriction equation (3.9.c) in order to improve the convergence of the iterative procedure which must be used to solve the difference equations (3.5) and (3.10).

Boundary Condition Representation

Since we have derived the difference approximations to the differential equations, we will now derive the difference approximations to the boundary conditions. The finite-difference operator which approximates the first derivative in terms of the coordinates of the grid points is [1]

$$\Phi'(x) = \sum_{k=0}^{n} L_k'(x)\,\Phi_k, \tag{3.11.a}$$

where x is the point at which Φ' is evaluated, Φ_k is the value of the function at the k^{th} grid point, and

$$L_k'(x) = \sum_{\substack{j=0 \\ j\neq k}}^{n} \frac{\pi_n(x)}{(x-x_k)(x-x_j)\pi_n'(x_k)}, \tag{3.11.b}$$

where $\pi_n(x)$ is the normal product notation and $\pi_n'(x_k)$ has the zero factor deleted from the product.

The second derivative operator is

$$\Phi''(x) = \sum_{k=0}^{n} L_k''(x)\,\Phi_k, \tag{3.11.c}$$

where

$$L_k''(x) = \sum_{\substack{j=0 \\ j\neq k}}^{n} \sum_{\substack{m=0 \\ m\neq j \\ m\neq k}}^{n} \frac{\pi_n(x)}{(x-x_k)(x-x_j)(x-x_m)\pi_n'(x)}, \tag{3.11.d}$$

where all the symbols are the same as those for $\Phi'(x)$. In the operators (3.11.a) and (3.11.c) all subscripts are relative to adjacent grid points in the x direction, therefore they are valid for partial derivatives at any n adjacent grid points, which are not necessarily equally spaced.

Since we have defined the operators which we will need, we now derive the finite-difference forms of the boundary conditions. On the line r = 0 (i = 1) we have from equations (2.17) and (2.19)

$$f^n_{1,j} = 0, \tag{3.12.a}$$

and

$$g^n_{1,j} = 0, \tag{3.12.b}$$

respectively for all j and n. On the line r = 1 (i = Imax) we have from equations (2.10.b), (2.14) and (2.16) the conditions that

$$f^n_{Imax,j} = 0, \tag{3.13.a}$$

$$\frac{1}{r_{Imax}} f'(r_{Imax}) = 0, \tag{3.13.b}$$

and

$$g^n_{Imax,j} = -\frac{1}{r_{Imax}} f''(r_{Imax}), \qquad (3.13.c)$$

where the operators are defined in equations (3.11.a) and (3.11.c). Equation (3.13.a) is used for the stream function at i = Imax. Then equation (3.13.c) is used to find the value of the vorticity. The value of the indices for the grid points in the r direction is Imax - 4 ≤ i ≤ Imax + 1. This range of grid points was used since it was found to yield more accurate results when equation (3.13.b) was used to eliminate the stream function value at Imax + 1.

From equations (2.10.e) we have for the line z = 0 (j=1)

$$f'(z=0) = 0, \qquad (3.14.a)$$

and

$$g^n_{i,1} = 0. \qquad (3.14.b)$$

At the point (R_1, Z_1) we have from equations (2.11) and (2.12)

$$f^n_{R_1,Z_1} = \left(\frac{r^2_{R_1}}{2} - \frac{r^4_{R_1}}{4}\right)\left(A_m \sin A_r t_n\right), \qquad (3.15.a)$$

and

$$g^n_{R_1,Z_1} = -\frac{1}{r_{R_1}}\left[\left(f^n_{i,j}\right)_{rr} - \frac{1}{r_{R_1}}\left(f^n_{i,j}\right)_r + \left(f^n_{i,j}\right)_{zz}\right]. \qquad (3.15.b)$$

On the downstream boundary z = L (j = Jmax) we have from (2.10.f) and (2.10.g) using equations (3.11.a) and (3.11.c) that

$$f''(z) = 0, \tag{3.16.a}$$

and either

$$g''(z) = 0, \tag{3.16.b.1}$$

or

$$g'(z) = 0. \tag{3.16.b.2}$$

In equations (3.16) the j has the range Jmax - 4 ≤ j ≤ Jmax. This range of j values is used to avoid using function values at points located outside the flow field.

The initial conditions are given from equations (2.12) and (2.13) as

$$f^{o}_{i,j} = 0, \tag{3.17.a}$$

and

$$g^{o}_{i,j} = 0. \tag{3.17.b}$$

This completes the definition of the finite-difference approximations to the boundary and initial conditions.

Solution of Finite-Difference Equations

The difference equations (3.5) and (3.10) are written to be solved using an adaptation of the Implicit-Alternating-Direction-Method (I-A-D) subject to the conditions (3.12) through (3.16). The I-A-D Method which we use in solving this problem is an adaptation of the methods developed by Young [23] and Varga [24].

Since our difference equations are not approximations to the Laplacian differential equation, and our grid is not equally

spaced on a square region, we do not know a priori that the I-A-D Method is either convergent or stable as applied to this problem. Since the I-A-D Method has proven numerically to be both stable and convergent on either similar equations or similar grids [4,6,21], we proceed cavalierly on the assumption that we will be equally fortunate.

Of all the publications in this area, the most closely allied work is that by Dixon [6] who treated both the stability of Poiseuille flow and plane Poiseuille flow. His results in the case of plane Poiseuille flow show the experimentally observed instability; but in the case of Poiseuille flow he has shown only that a disturbance imposed on the field uniformly on a radius is amplified at a Reynolds' number of 100,000. At a Reynolds' number of 10,000 the results of his calculation show that the disturbance may either be amplifying or decaying. At a Reynolds' number of 1000 his solution shows the experimentally observed decay of the disturbance. His calculation procedure was to use the Implicit-Alternating-Direction-Method for solution of the vorticity transport equation and Successive-Over-Relaxation for solution of the stream function equation. He obtained stream function values only at every odd time step. He also used the downstream boundary conditions which introduce periodicity into the flow field. Still, on the whole, his results seem to be valid. Our calculation procedure, disturbance, and downstream boundary conditions

differ considerably from those used by Dixon.

Before explicitly explaining the calculation procedure, we set forward the convergence tests that are applied. For the stream function we used

$$\left| f_{i,j}^{n,\ell,k+2m} - f_{i,j}^{n,\ell,k} \right| \leq \epsilon_f \max_{i,j} \left| f_{i,j}^{n,\ell,k+2m-1} \right|, \qquad (3.18)$$

where m is the number of ρ values used in the iterative procedure and k is the stream-function iterative counter. We chose ϵ_f such that $\epsilon_f \geq 1.0 \times 10^{-5}$.

The tests used for convergence of the vorticity are

$$\left| g_{i,j}^{n,\ell+1} - g_{i,j}^{n,\ell} \right| \leq \epsilon_{g_i} \max_{i,j} \left| g_{i,j}^{n,\ell} \right| \quad i \neq \text{Imax}, \qquad (3.19.a)$$

and

$$\left| g_{\text{Imax},j}^{n,\ell+1} - g_{\text{Imax},j}^{n,\ell} \right| \leq \epsilon_{g_b} \max_{j} \left| g_{\text{Imax},j}^{n,\ell} \right|, \qquad (3.19.b)$$

where ℓ is the vorticity iteration counter. Equation (3.19.a) was used where i < Imax and equation (3.19.b) was used when i = Imax. We demanded that $\epsilon_{g_b} = 2\epsilon_{g_i}$, and that $\epsilon_{g_i} \geq \epsilon_f$ at all iterations.

The vorticity and stream function calculations are stopped when

$$T > 20, \qquad (3.20)$$

where T is the real time, or when a solution pattern was established.

To explain the actual I-A-D Method which was employed we will trace the calculation procedure from the n time step to the n + 2 time step. The iteration counters used are ℓ for the vorticity and k for the stream function.

Step 1: Calculate $D_{i,j}^{n}$ using the right hand side of equation (3.9.a) and the values of $f_{i,j}^{n}$ and $g_{i,j}^{n}$.

Step 2: Calculate $g_{i,j}^{n+1,\ell}$ using equation (3.10.a) and the values of $f_{i,j}^{n+1,\ell-1}$ and $D_{i,j}^{n}$.

Step 3: Calculate $f_{i,j}^{n+1,\ell,k+1}$ using equation (3.5.a) and the values $g_{i,j}^{n+1,\ell}$ and $f_{i,j}^{n+1,\ell,k}$.

Step 4: Calculate $f_{i,j}^{n+1,\ell,k+2}$ using equation (3.5.b) and the values $g_{i,j}^{n+1,\ell}$ and $f_{i,j}^{n+1,\ell,k+1}$.

Step 5: If k is divisible by 2m, then apply the test in equation (3.18). If the test is passed, proceed to step 6. Otherwise, update k by 2 and repeat steps 3, 4 and 5.

Step 6: If ℓ is greater than 1, apply the tests in equations (3.19). If the tests are passed, proceed to step 7. Otherwise, update ℓ by 1 and repeat steps 2 through 6.

Step 7: Output the results of the calculations. If the test in equation (3.20) is passed or a solution pattern has been established, halt the calculation. Otherwise, update n by 1 and proceed to step 8 or step 1, depending respectively on whether step 2 or step 9 was in use for the time step being processed.

Step 8: Calculate $D_{i,j}^{n+1}$ using the right hand side of equation (3.9.b) and the values of $f_{i,j}^{n+1}$ and $g_{i,j}^{n+1}$.

Step 9: Calculate $g_{i,j}^{n+2,\ell}$ using equation (3.10.b) and the values of $f^{n+2,\ell-1}$ and $D_{i,j}^{n+1}$.

Step 10: Replace step 2 with step 9 and proceed to step 3.

In steps 2 and 9 it will be noted that for $\ell = 1$ on any time level no true values of $f_{i,j}^{n+1,\ell-1}$ exist, therefore the values of $f_{i,j}^{n}$ were used. These values of $f_{i,j}^{n}$ were also used for $f_{i,j}^{n+1,\ell,k}$ when k = 1. The only other special cases occur for n = 1 in which case the initial conditions are used for $g_{i,j}^{o}$ and $f_{i,j}^{o}$. In the above calculation procedure the boundary conditions (3.12) through (3.16) are applied in steps 2, 3, 4 and 9 with the values of the indices indicated in the step.

We have now defined the finite-difference equations and explained the calculating and testing procedures, so we move on to the display of the results.

CHAPTER IV. RESULTS

A computer program was written and run on the Scientific Data Systems Sigma 7 Computer at the University of Houston. This program performed the I-A-D calculations necessary to solve the difference equations (3.5) and (3.9) under the solution sequence steps 1-10 listed in Chapter III. The solution was carried out with a basic time step of 0.02.

Preliminary runs indicated that both nonuniform grids in the r and z directions and grids with $\Delta r \neq \Delta z$ yielded a numerical instability. (See Appendix B for a complete discussion of the numerical errors associated with the nonuniform grid system.) Therefore, the results presented here were calculated with $\Delta r = \Delta z = 0.10$. It was also found that, for the same error criteria, using double-precision arithmetic improved the convergence and cut the total computation time for each time step. The program was set up to solve the difference equations on a flow field of dimensions 1 by 11 to 25 radii in the radial and axial directions respectively.

The program selected the length of the flow field above 11 radii by testing all values one radius upstream of the downstream boundary. If one value was greater than 10^{-7}, the flow field was increased in length by one radius. The maximum length of the flow field found to be necessary was 14 radii. Since the computer-plotting routines are for even increments, the plotted flow field

is 12 radii in length. This is sufficient to show all significant changes in the variables.

As further preliminary checks, the boundary and initial conditions were changed to those of Poiseuille pipe flow and this solution was calculated for 10 time steps. The resulting solution was maintained at its correct value for a Reynolds number of 1000. Short runs were also made for the main flow case with an analogous disturbance to the one for the perturbation flow. These results are qualitatively similar to the results obtained for the perturbation flow so we use the perturbation flow solution since it is numerically more accurate.

The Reynolds numbers for which the solution was calculated are the following: At an amplitude A_m equal to 1.0, the Reynolds numbers were 1000, 3000, 10,000 and 100,000, while at an amplitude of 0.1, the only Reynolds number was 100,000. The values were selected because the solution at a Reynolds number of 1000 should be unconditionally stable. The solution at a Reynolds number of 100,000 should be unstable at an amplitude of 1.0 and possibly stable at an amplitude of 0.1. All runs were made with A_r equal to π which is within the experimentally unstable range indicated by Kuethe (1956) and Leite (1959). So, these runs provide a comparison upon which to decide whether the solutions at Reynolds numbers of 3000 and 10,000 were stable or unstable. Unfortunately, since the time step is variable and solutions were saved for plotting

at every fifth time step, the times at which solutions are available are not always directly comparable. Nevertheless, the solutions presented were selected as close together in time as possible. All results presented represent from 5 to 6½ hours of computing time each.

Summary plots, Figures 3 and 4, are presented (for all Reynolds numbers) which show how the maximum values of both the disturbance stream function (F) and disturbance vorticity (G) behave as the flow moves downstream with time. Only the first disturbance is shown in each plot since subsequent disturbances have similar trends in the maximum values. Other plots presented are for disturbance vorticity and disturbance stream function versus axial position (Z) for a given radius, time and Reynolds number. The plots which we present are for nondimensional radii of 0.4, 0.6, and 0.8 as these were felt to be generally representative of the solutions obtained since 0.6 is the radius of the disturbance and 0.4 and 0.8 are equally spaced on either side of the disturbance. Plots are shown at representative times for each Reynolds number; however, results are not shown for all radial values at every time for which plots are given. As a preliminary screening device, a printer contour plot was made of all results which were retained for ultimate presentation. These contour plots indicate that the radii selected do not always contain the maximum value of the vorticity or stream function solution at the time step. The plots in Figures 5-20 are

all scaled on the maximum value for each Reynolds number for the time step being plotted.

Preliminary runs indicated that our downstream boundary conditions had little or no effect on the solution but that the condition $g_z = 0$ (B.C.1) seemed slightly preferable. Therefore, all results presented are for this condition.

Figure 3, the summary stream function plots for all Reynolds numbers, shows how the maximum value of the disturbance stream function behaves as the disturbance is carried downstream. For a Reynolds number of 1000 and an amplitude (A_m) of 1.0, Figure 3a, the maximum value of the disturbance stream function takes on a maximum value of 0.22 and then is observed to decrease as the disturbance moves downstream. This result is consistent with what is expected since flows at a Reynolds number of 1000 are inherently stable and all disturbances must decay with time. At a Reynolds number of 3000 and an amplitude of 1.0, Figure 3b, the maximum value of the disturbance stream function increases to 0.23, decreases to 0.17 and then levels off at 0.175. The calculation at this Reynolds number did not decay with distance as the disturbance moved downstream, but neither did it amplify. Therefore, we consider this case to be neutrally stable.

For an amplitude of 1.0 and a Reynolds number of 10,000, Figure 3c, the maximum value of the stream function disturbance increased to a value of 0.23, decreased to 0.17 and then began to

climb slowly, reaching a value of 0.18 at an axial length of 5.8. The calculations for the next time step, at a time of 4.18, did not converge for this run at a Reynolds number of 10,000. Various methods (including decreasing the time step) were attempted in order to obtain convergence but these attempts met with no success. The nonconvergence of the solution was attributed to instability of the flow. Therefore, at a Reynolds number of 10,000 and an amplitude of 1.0, the flow is considered unstable because of the increase with axial distance of the maximum value of the disturbance stream function and subsequent failure of the solution to converge.

Two amplitudes were considered at a Reynolds number of 100,000. Figure 3d depicts the behavior of the maximum value of the disturbance stream function for an amplitude of 0.1 which could be taken to be a small-amplitude disturbance. The disturbance stream function maxima increased to about 0.024 just downstream of the point of application of the disturbance and then continually decreased as far as the calculation was carried. Since the disturbance stream function is decaying for this example, we consider this flow to be stable. This result is consistent with other small-amplitude investigations in that Poiseuille pipe flow seems to be stable to small-amplitude disturbances at all Reynolds numbers, i.e., Davey and Drazin (1969). The calculation for the amplitude of 1.0 at this Reynolds number, Figure 1e, produced a result almost

identical with the calculation at a Reynolds number of 10,000 with the same disturbance amplitude. Thus, we consider the small-amplitude disturbance flow to be stable and the large-amplitude disturbance (A_m = 1.0) flow to be unstable.

The disturbance vorticity plots shown in Figure 4, for the same calculations as depicted in Figure 3, have the same qualitative behavior as the disturbance stream-function plots. Therefore, the same conclusions can be drawn solely from the disturbance vorticity plots.

Comparison of the plots of the stream function and vorticity at an approximate time of 0.5 and a radius of 0.6, Figures 5 and 6, show that the maximum values appear on the radius of the disturbance for all Reynolds numbers considered. The jagged behavior of both the stream function and vorticity upstream of the disturbance seems due to damping of a disturbance wave moving upstream and counter to the main flow.

At a time of approximately 1.5 and a radial value of 0.6, Figures 7 and 8, the maximum vorticity is at the point of the disturbance as it was at earlier calculation times. The maximum value of the stream function for disturbance amplitude 1.0 at all Reynolds numbers is seen to lie on the disturbance radius and at the downstream peak of the disturbance. For the disturbance amplitude 0.1, the maximum value is at the upstream peak. It

is also observed that the first peak of the disturbance has moved approximately one radius downstream.

At a time of approximately 2.5, Figures 7-12, plots are given for all three nondimensional radial values, 0.4, 0.6 and 0.8, at each Reynolds number. Figure 9 shows the disturbance stream function at a radius of 0.4 while Figure 11 shows the disturbance stream function at a radial value of 0.8. Both figures illustrate the progression of the disturbance wave downstream at equal distances on either side of the disturbance radius. Figure 10 shows the disturbance stream function for the radial value of 0.6 (the disturbance radius). This figure indicates that the disturbance is damped at the Reynolds number of 1000 and also for the Reynolds number of 100,000 at a disturbance amplitude of 0.1. Also indicated in Figure 10 is the failure of the disturbance stream function to decrease in value for Reynolds numbers of 3000, 10,000 and 100,000 as the disturbance progresses downstream.

The disturbance vorticity plots at a time of approximately 2.5 for each of the radial values 0.4, 0.6 and 0.8 are contained in Figures 12-14. Study of these vorticity plots shows that the same observations can be made about disturbance stream function.

Another point to note in Figures 9-11 is that the disturbance stream function is a maximum at a radial value of 0.8 and that the downstream peak has moved toward the centerline of the cases considered except at a Reynolds number of 100,000 and a disturbance

amplitude of 0.1 for which the maximum disturbance stream function value remained at the disturbance radius of 0.6.

Figures 15 and 16 depict the behavior of the disturbance quantities at a time of approximately 3.5 and a radial value of 0.6. The results in Figures 15 and 16 bear a similarity to those in Figures 10 and 13 (at a time of 2.5). Again, it is noted that the values at Reynolds numbers of 1000 and 100,000 (the latter at an amplitude of 0.1) are decreasing with downstream distance, while for Reynolds numbers of 10,000 and 100,000 (at $A_m = 1.0$), the disturbance quantities are increasing with downstream distance. At a Reynolds number of 3000, no change in disturbance stream function or disturbance vorticity is noted with increasing downstream distance.

Another point of interest in Figures 15 and 16 is the marked decrease in the first negative peak of the stream function for the higher amplitude ($A_m = 1.0$) cases. For the low-amplitude ($A_m = 0.1$) case, the first negative peak is greater than the first positive peak. Note should also be taken of the strong pattern resemblance of the stream-function plots at Reynolds numbers of 3000, 10,000 and 100,000 ($A_m = 1.0$). These patterns are dissimilar from those at Reynolds numbers of 1000 and 100,000 ($A_m = 0.1$). A similar pattern resemblance is seen in the vorticity plots.

At a time of 4.0 and at a radial value of 0.6, Figures 17 and 18, results are given for all examples except one. The example for which no results are given in this case is at a Reynolds number of 100,000 and an amplitude of 1.0. As mentioned earlier, the solution for this example failed to converge. Several corrective procedures were attempted, i.e., smaller time steps and finer, more time-consuming finite differencing, to obtain convergence at this calculation time, but to no avail. We attribute the failure to converge for this one case to instability of the flow.

In Figure 17, the disturbance stream function is shown to be decreasing with downstream distance at Reynolds numbers of 1000 and 100,000, the latter of which is for an amplitude of 0.1. For Reynolds numbers of 3000 and 10,000, the disturbance stream function is increasing with downstream distance. Figure 18, the disturbance vorticity, follows the trend as discussed for the disturbance stream function at this time and radial distance.

The pattern resemblance first noted in Figures 15 and 16 has intensified in Figures 17 and 18.

The far downstream regions of the stream function for Reynolds numbers of 3000 and 10,000 are now quite similar and are markedly dissimilar from the same region at 1000. In the immediate downstream vicinity of the disturbance, plots for Reynolds numbers of 1000 and 3000 are similar but different from that at 10,000. The plots for a Reynolds number of 100,000 ($A_m = 0.1$) is not

similar to any of the other plots. Similar pattern comparison can be made for the vorticity plots.

Figures 19 and 20, the last figures presented in the calculation procedure, depict the solution at a time of approximately 4.5 and a radius of 0.6. For these conditions the solution at a Reynolds number of 10,000 and an amplitude of 1.0 failed to converge despite several (previously mentioned) corrective attempts. Again, we attribute this convergence failure to instability of the flow.

Figure 19 shows the disturbance stream function value to continue to decrease with downstream distance as time progresses for a Reynolds number of 1000 and 100,000, the latter for an amplitude of 0.1. The solution for the progressing disturbance stream function at a Reynolds number of 3000 remains at approximatly the same magnitude between Figures 17 and 19. Once again, as shown in Figure 20, the disturbance vorticity reflects the observations made for the disturbance stream function.

The patterns of the stream functions at Reynolds numbers of 1000 and 3000, Figure 19, are now seen to differ over most of the region downstream of the disturbance. The plot at a Reynolds number of 100,000 ($A_m = 0.1$) is again dissimilar from the other plots. Figure 20, for the vorticity, shows the same type of results.

CHAPTER V. SUMMARY AND CONCLUSIONS

The feasibility of a numerical technique to determine the response of Poiseuille pipe flow to a given disturbance has been demonstrated. This problem has been treated experimentally many times with well-substantiated results. Heretofore, however, no one had ever been able to show the instability of Poiseuille pipe flow to a disturbance, be it a small disturbance or a large disturbance.

The results of the preceding chapter demonstrate that the numerical approach contained herein does yield a stable solution to an axisymmetric disturbance of the form $f(R_1, Z_1, t_n) = (1.0) \cdot (\frac{R_1^2}{2} - \frac{R_1^4}{4}) \sin \pi t_n$ at a Reynolds number of 1000. The stream function disturbance is seen to decay with downstream axial distance for this example.

At a Reynolds number of 3000 and a disturbance amplitude of 1.0, the disturbance stream function is not seen to decay with increasing downstream distance; however, no growth of the disturbance stream function is noted either. This Reynolds number calculation seems to be neutrally stable.

For a Reynolds number of 10,000, the same disturbance function was found not to decay but was carried downstream with slightly increasing amplitude. This result failed to meet our

stability criterion cited in Chapter I, i.e., if the amplitude of the disturbance stream function decays with downstream axial distance, then the flow is deemed stable to the disturbance at the given Reynolds number.

At a Reynolds number of 100,000 and a disturbance amplitude of 1.0, the stream function disturbance was also amplified with downstream axial distance. This is definitely an unstable condition according to the cited criterion.

The four examples for which results have been cited were all for a disturbance amplitude of 1.0 which is, of course, a finite-amplitude disturbance. The results of these calculations have been consistent with what is expected from the physical problem for the same conditions. To examine what would happen for a small-amplitude disturbance, we considered a flow with Reynolds number of 100,000 and a disturbance amplitude of 0.1. We found for this case that the disturbance was definitely damped as it progressed downstream.

All of the results cited are consistent with experiment for the corresponding Reynolds numbers and amplitudes. Particulars of the solutions follow:

On the basis of preliminary, short computer runs, it was found that, to insure numerical stability and improve accuracy of the solution, an equally spaced grid was necessary for the solution of the finite-difference equations.

For the disturbance used, a flow field of 14 radii appears to be of sufficient length to represent an "infinite" length for the times covered by these calculations. Double-precision arithmetic was found to improve the stability of the solution and speeds the convergence as well as reducing total computing time.

For all Reynolds numbers and times the finite-amplitude disturbance stream function showed more damping toward the wall and more growth toward the centerline with axial distance downstream of the disturbance. At high calculation times at an amplitude of 1.0, we observe strong pattern resemblance between the solutions at Reynolds numbers of 3000, 10,000 and 100,000 (amplitude 1.0) but dissimilar patterns at Reynolds numbers of 1000 and 100,000 (amplitude 0.1). The amplitudes of the disturbance stream functions and vorticities at Reynolds numbers of 3000, 10,000 and 100,000 (amplitude 1.0) are again similar but they are different from those at values of 1000 and 100,000 (amplitude 0.1). We found, contrary to the results of Dixon and others, that the stream functions and vorticities at Reynolds numbers of 10,000 and 100,000 show definite amplification with distance downstream of the disturbance while they show definite damping at values of 1000 and 100,000 (amplitude 0.1). The calculation at a Reynolds number of 3000 showed no decay or amplification with downstream distance.

In conclusion, we say that Poiseuille pipe flow is unstable to an axisymmetric disturbance of the form $f(R_1, Z_1, t_n) = (1.0) \cdot (\frac{R_1^2}{2} - \frac{R_1^2}{4}) \sin \pi t_n$ at Reynolds numbers of 10,000 and 100,000 is stable at a Reynolds number of 1000 and is neutrally stable at 3000. When the disturbance amplitude is changed from 1.0 to 0.1 at a Reynolds number of 100,000, we found that the flow was stable.

References

1. Abramowitz, M., and Stegun, I. A., (ed.), Handbook of Mathematical Functions, National Bureau of Standards, Applied Mathematics Series 55, Washington, 1965.

2. Betchov, R., and Criminale, W. O., Jr., Stability of Parallel Flows, Vol. 10 of Applied Mathematics and Mechanics, Edited by F. N. Frenkiel and G. Temple, Academic Press, New York, 1967.

3. Bhat, W. V., "An Experimental Investigation of the Stability of Hagen-Poiseuille Flow Subjected to the First Mode of Azimuthally Periodic Small Disturbance," Ph.D. Dissertation, University of Rochester, Rochester, N. Y., 1966.

4. Briley, W. R., "Time-Dependent Flow in a Cylindrical Container," Ph.D. Dissertation, University of Texas at Austin, Austin, Texas, 1968.

5. Corcos, G. M. and Sellars, J. R., "On the Stability of Fully Developed Flow in a Pipe," Journal of Fluid Mechanics, Vol. 5, 1959, pp. 97-112.

6. Dixon, T. N., "A Study on Stability and Incipient Turbulence in Poiseuille and Plane Poiseuille Flow by Numerical Finite Difference Simulation," Ph.D. Dissertation, Rice University, Houston, Texas, 1966.

7. Irving, J. and Mullineux, N., Mathematics in Physics and Engineering, Academic Press, New York, 1959.

8. Kuethe, A. M., "Some Features of Boundary Layers and Transition to Turbulent Flow," Journal of the Aeronautical Sciences, Vol. 23, 1956, pp. 444-451.

9. Leite, R. J., "An Experimental Investigation of the Stability of Poiseuille Flow," Journal of Fluid Mechanics, Vol. 5, 1959, pp. 81-96.

10. Lessen, M., Sadler, S. G., Liu, Ting-Yung, "Stability of Pipe Poiseuille Flow," The Physics of Fluids, Vol. 11, 1968, pp. 1404-1409.

11. Meksyn, D., "Stability of Laminar Flow Between Parallel Planes for Two- and Three-Dimensional Finite Disturbances," Zeitschrift Für Physik, Vol. 178, 1964, pp. 159-172.

12. Meksyn, D., and Stuart, J. T., "Stability of Viscous Motion Between Parallel Planes for Finite Disturbances," Proceedings of the Royal Society, Series A, Vol. 208, 1951, pp. 517-26.

13. Pekeris, C. L., "Stability of the Laminar Flow Through a Straight Pipe of Circular Cross-Section to Infinitesimal Disturbances Which Are Symmetrical about the Axis of the Pipe," Proceedings of the National Academy of Science, Washington, Vol. 34, 1948, pp. 285-295.

14. Reynolds, O., "An Experimental Investigation of the Circumstances Which Determine Whether the Motion of Water Shall Be Direct or Sinuous, and of the Law of Resistance in Parallel Channels," Philosophical Transactions of the Royal Society, Vol. 174, 1883, pp. 935-982.

15. Sarpkaya, T., "Investigation of the Stability of Pulsating Viscous Flow," Journal of Basic Engineering, Vol. 87D, 1966, pp. 589.

16. Schensted, I. V., "Contributions to the Theory of Hydrodynamic Stability," Ph.D. Dissertation, University of Michigan, Ann Arbor, Michigan, 1961.

17. Sexl, T., "Zur Stabilitaetsfrage der Poiseuilleschen Stroemung," Annalen der Physik, Vol. 83, 1927, pp. 835-848.

18. Squire, H. B., "On the Stability of the Three-Dimensional Distrübances of Viscous Flow Between Parallel Walls," Proceedings of the Royal Society, Series A, Vol. 142, 1933, pp. 612-628.

19. Stuart, J. T., "On the Non-Linear Mechanics of Hydrodynamic Stability," Journal of Fluid Mechanics, Vol. 4, 1958, pp. 1-21.

20. Taylor, G. I., "Some Recent Developments in the Study of Turbulence," Proceedings of the Fifth International Congress of Applied Mechanics, 1938, pp. 294-310.

21. Thoman, D. C., and Szewczyk, A. A., "Numerical Solutions of Time-Dependent Two-Dimensional Flow of a Viscous Incompressible Fluid over Stationary and Rotating Cylinders," Heat Transfer and Fluid Mechanics Laboratory, Department of Mechanical Engineering, University of Notre Dame, Notre Dame, Indiana, Technical Report 66-14, 1966.

22. Thomas, L. H., "The Stability of Plane Poiseuille Flow," Physical Review, Vol. 91, 1953, pp. 780-783.

23. Varga, R. S., Matrix Iterative Analysis, Prentice-Hall, Inc., Englewood Cliffs, N. J., 1963.

24. Young, D. M., Jr., "The Numerical Solution of Elliptic and Parabolic Partial Differential Equations," Survey of Numerical Analysis, Edited by John Todd, McGraw-Hill Book Company, Inc., New York, 1962, pp. 380-435.

APPENDIX A

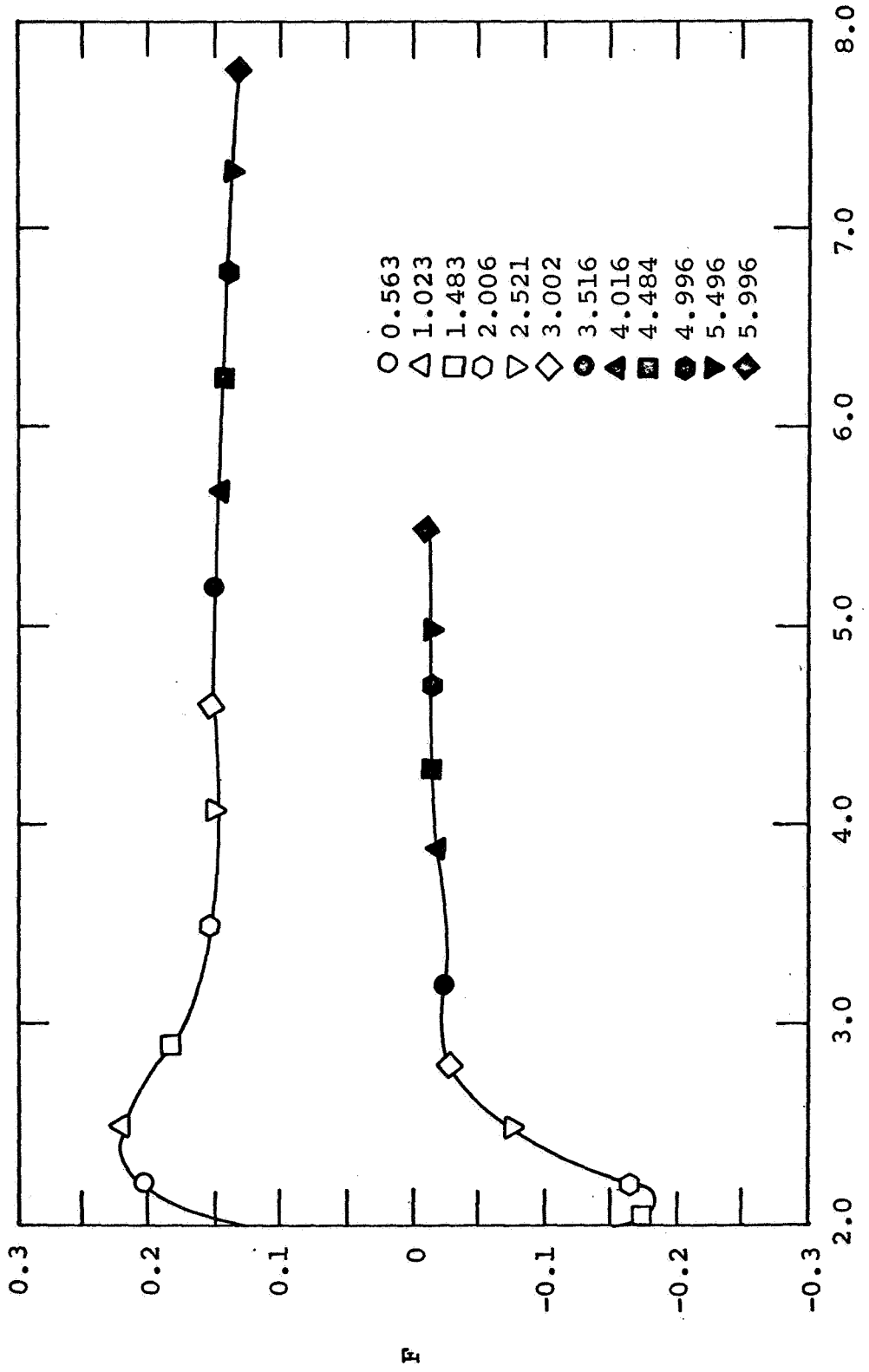

Figure 3a. Maximum Value of Disturbance Stream Function vs. Downstream Distance, $R = 10^3$, $A_m = 1.0$, $A_r = \pi$.

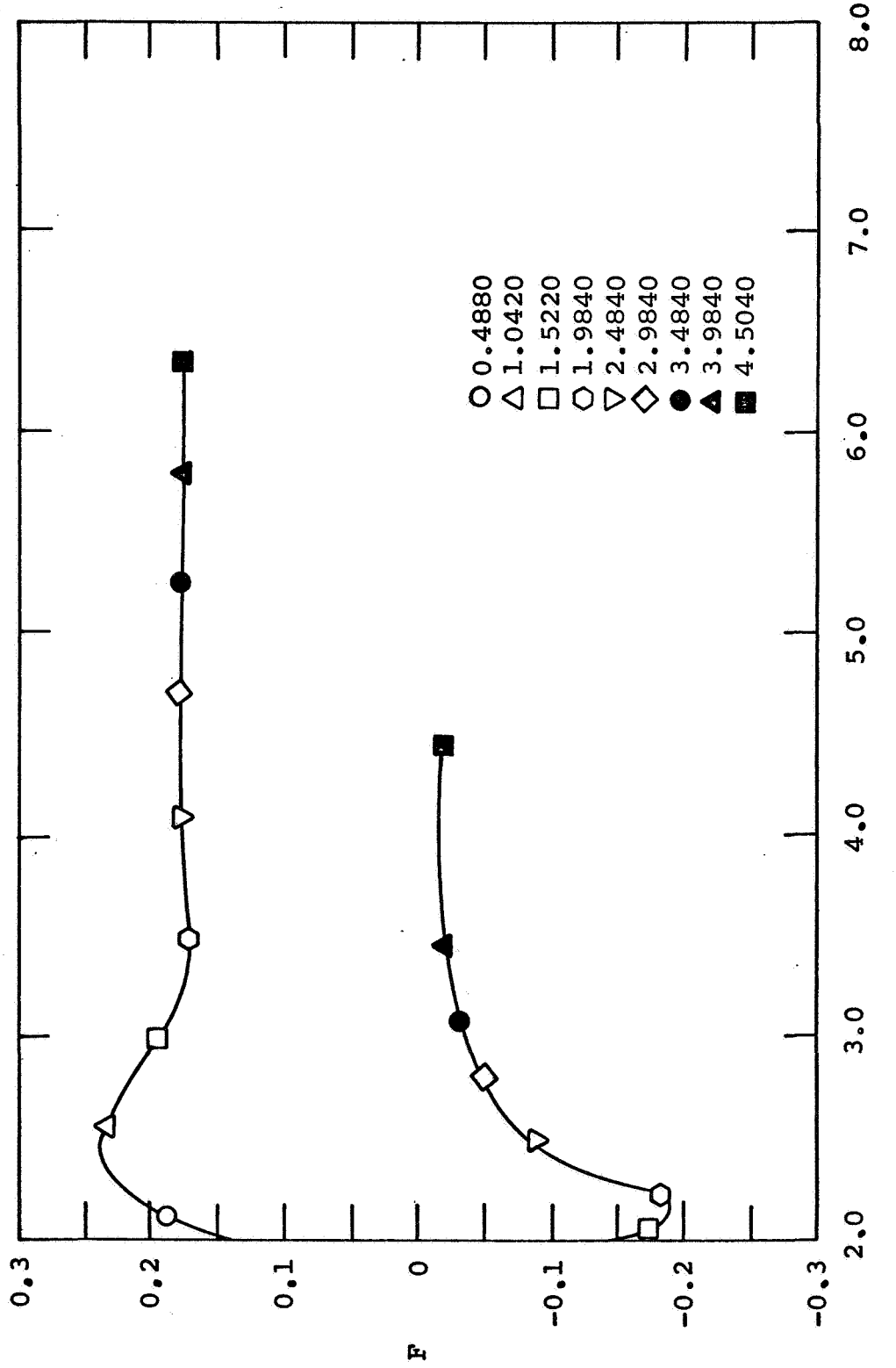

Figure 3c. Maximum Value of Disturbance Stream Function vs. Downstream Distance, $R = 3 \times 10^3$, $A_m = 1.0$, $A_r = \pi$.

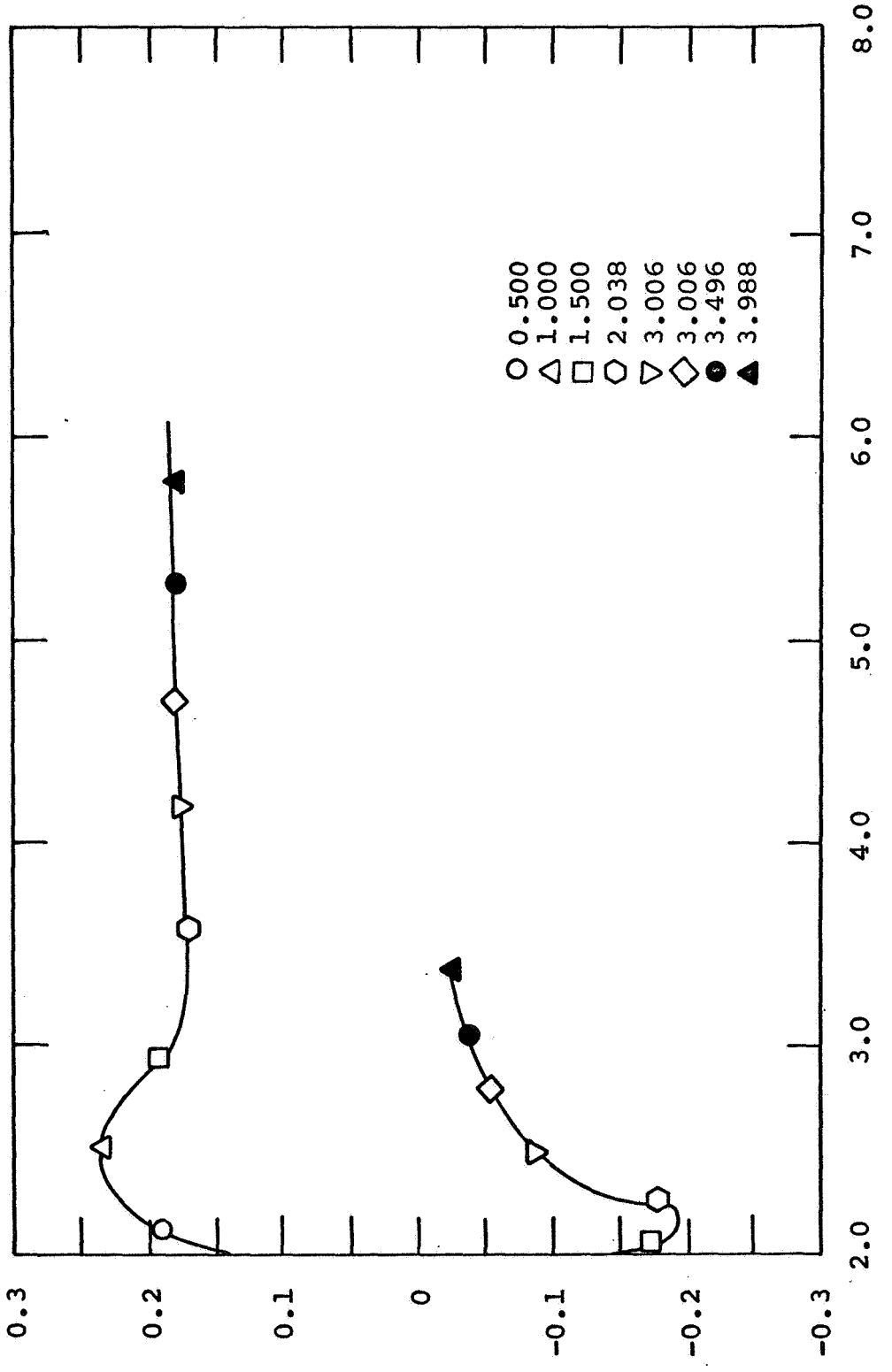

Figure 3c. Maximum Value of Disturbance Stream Function vs. Downstream Distance, $R = 10^4$, $A_m = 1.0$, $A_r = \pi$.

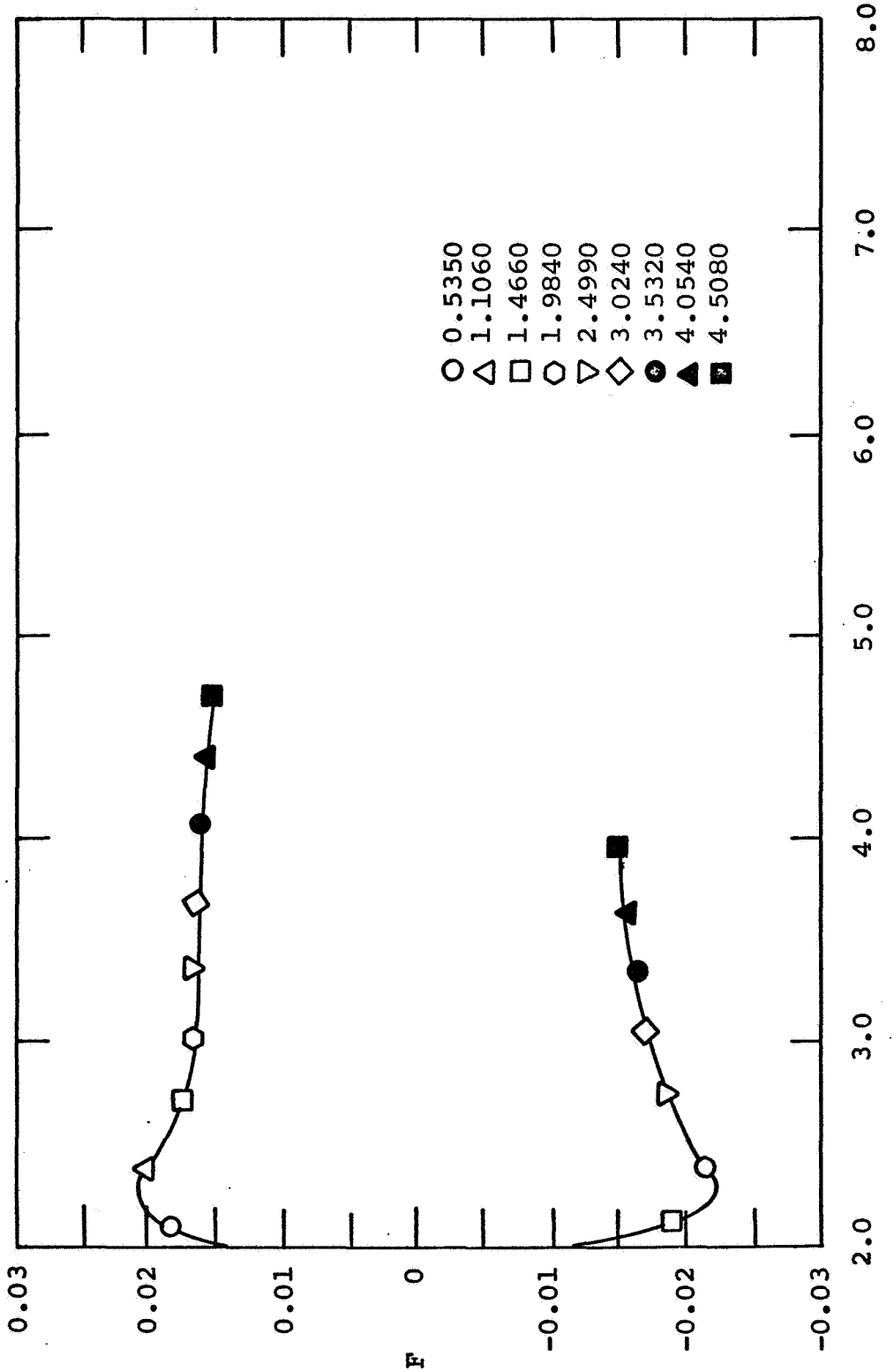

Figure 3d. Maximum Value of Disturbance Stream Function vs. Downstream Distance, $R = 10^5$, $A_m = 0.1$, $A_r = \pi$.

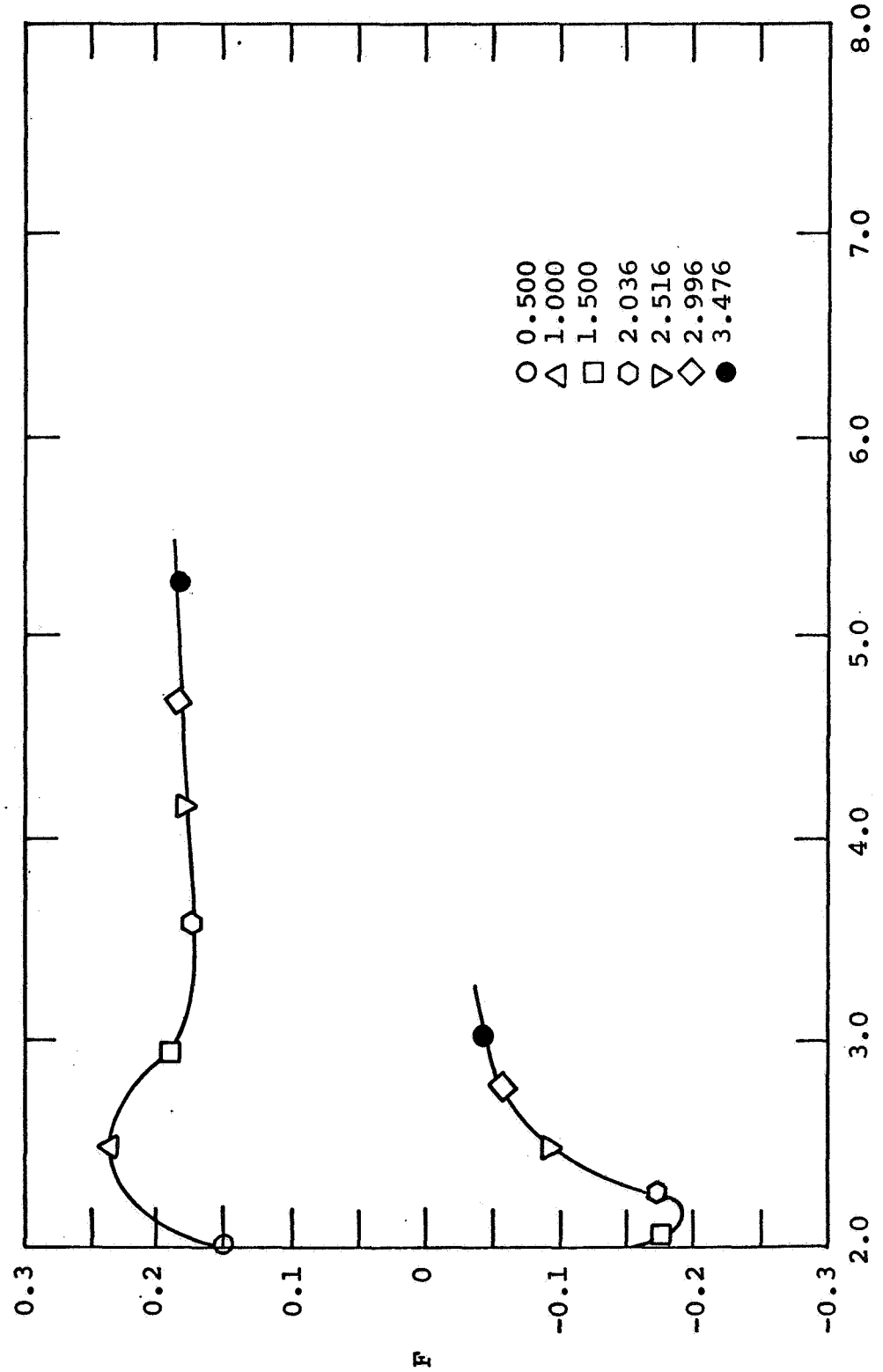

Figure 3e. Maximum Value of Disturbance Stream Function vs. Downstream Distance, $R = 10^5$, $Am = 1.0$, $Ar = \pi$.

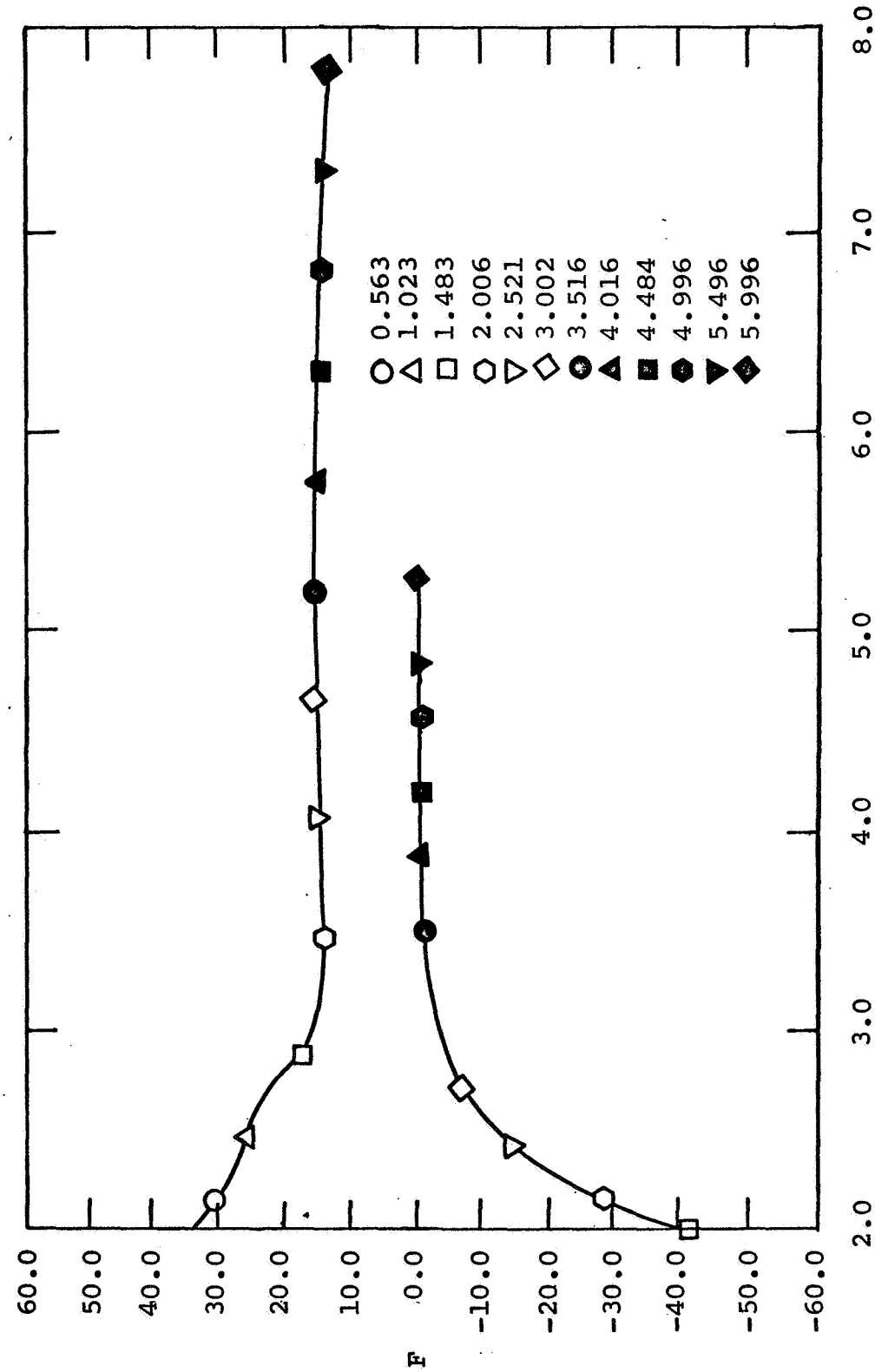

Figure 4a. Maximum Value of Disturbance Vorticity vs. Downstream Distance, $R = 10^3$, $A_m = 1.0$, $A_r = \pi$.

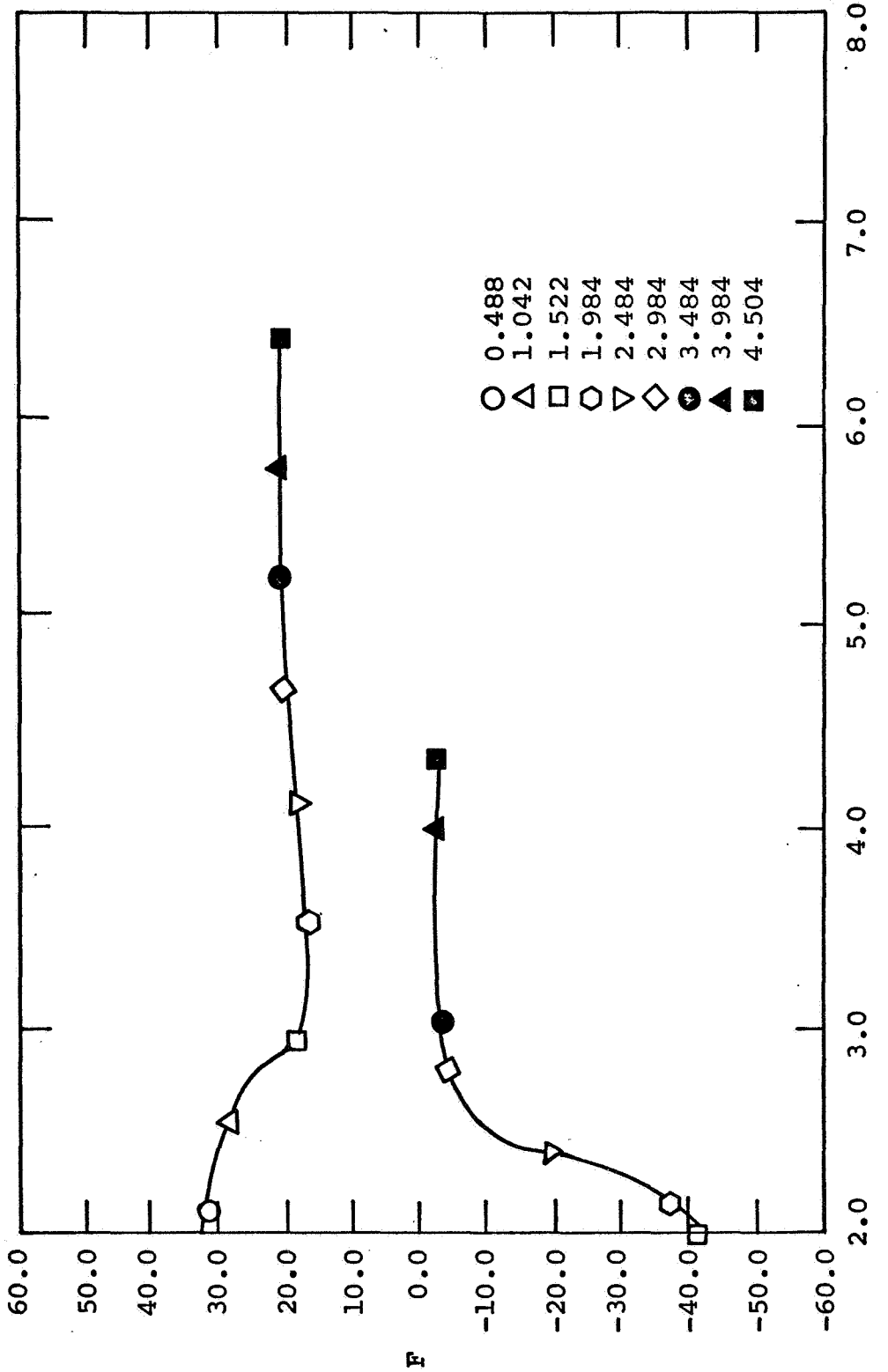

Figure 4b. Maximum Value of Disturbance Vorticity vs. Downstream Distance, $R = 3 \times 10^3$, $A_m = 1.0$, $A_\Gamma = \pi$.

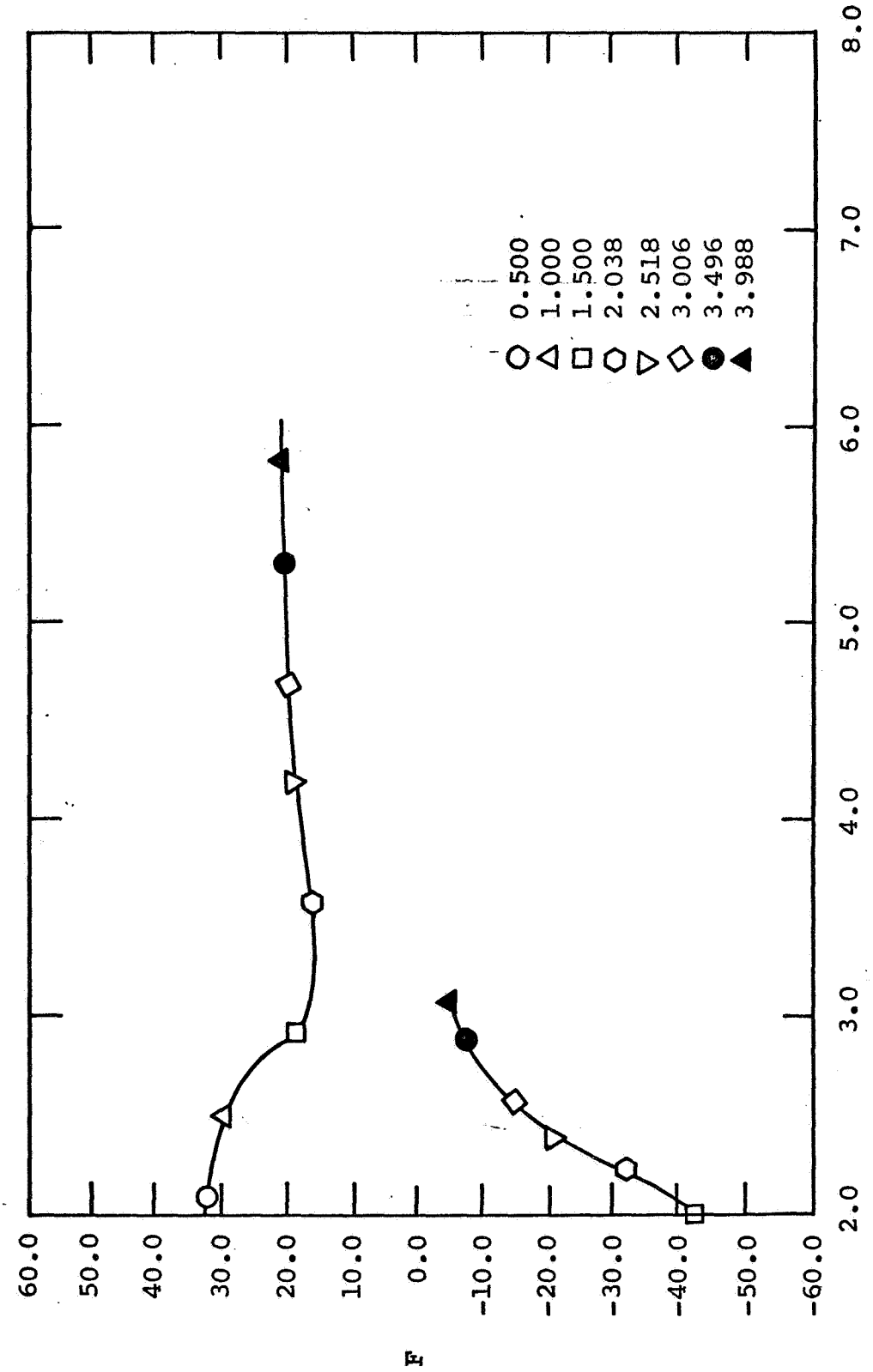

Figure 4c. Maximum Value of Disturbance Vorticity vs Downstream Distance; $R = 10^4$, $A_m = 1.0$, $A_r = \pi$.

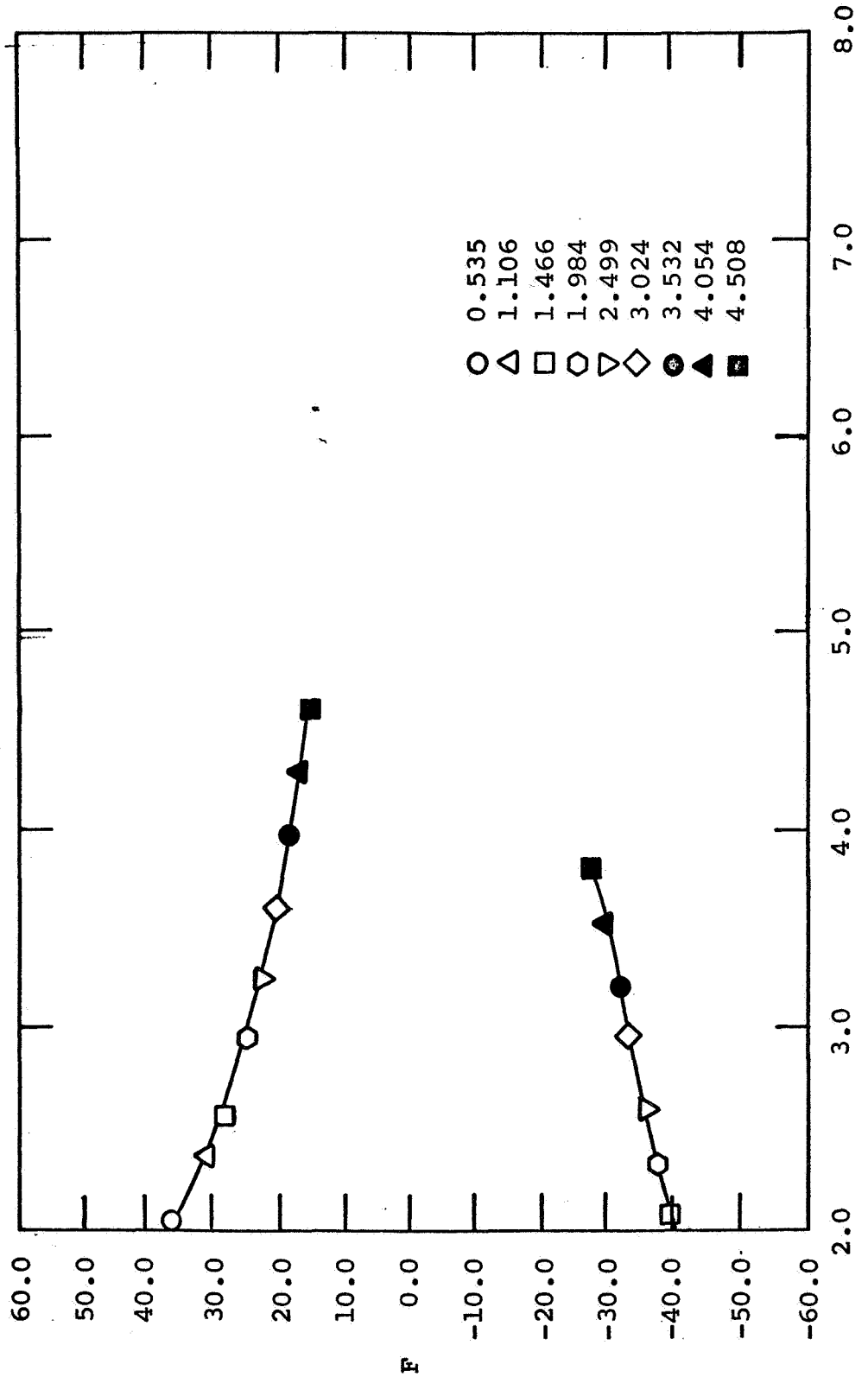

Figure 4d. Maximum Value of Disturbance Vorticity vs. Downstream Distance, $R = 10^5$, $A_m = 0.1$, $A_r = \pi$.

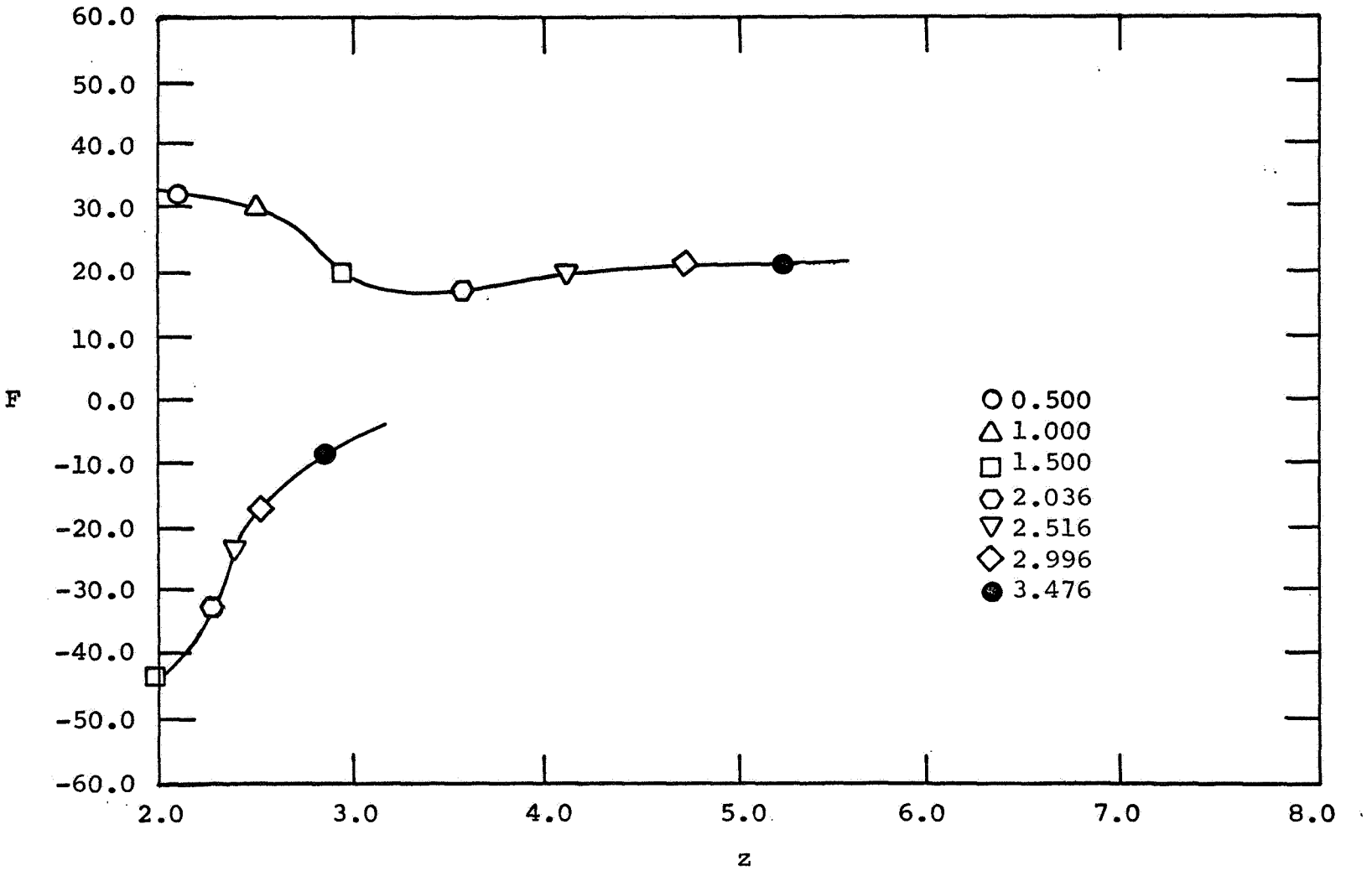

Figure 4e. Maximum Value of Disturbance Vorticity vs. Downstream Distance, $R = 10^5$, $A_m = 1.0$, $A_r = \pi$.

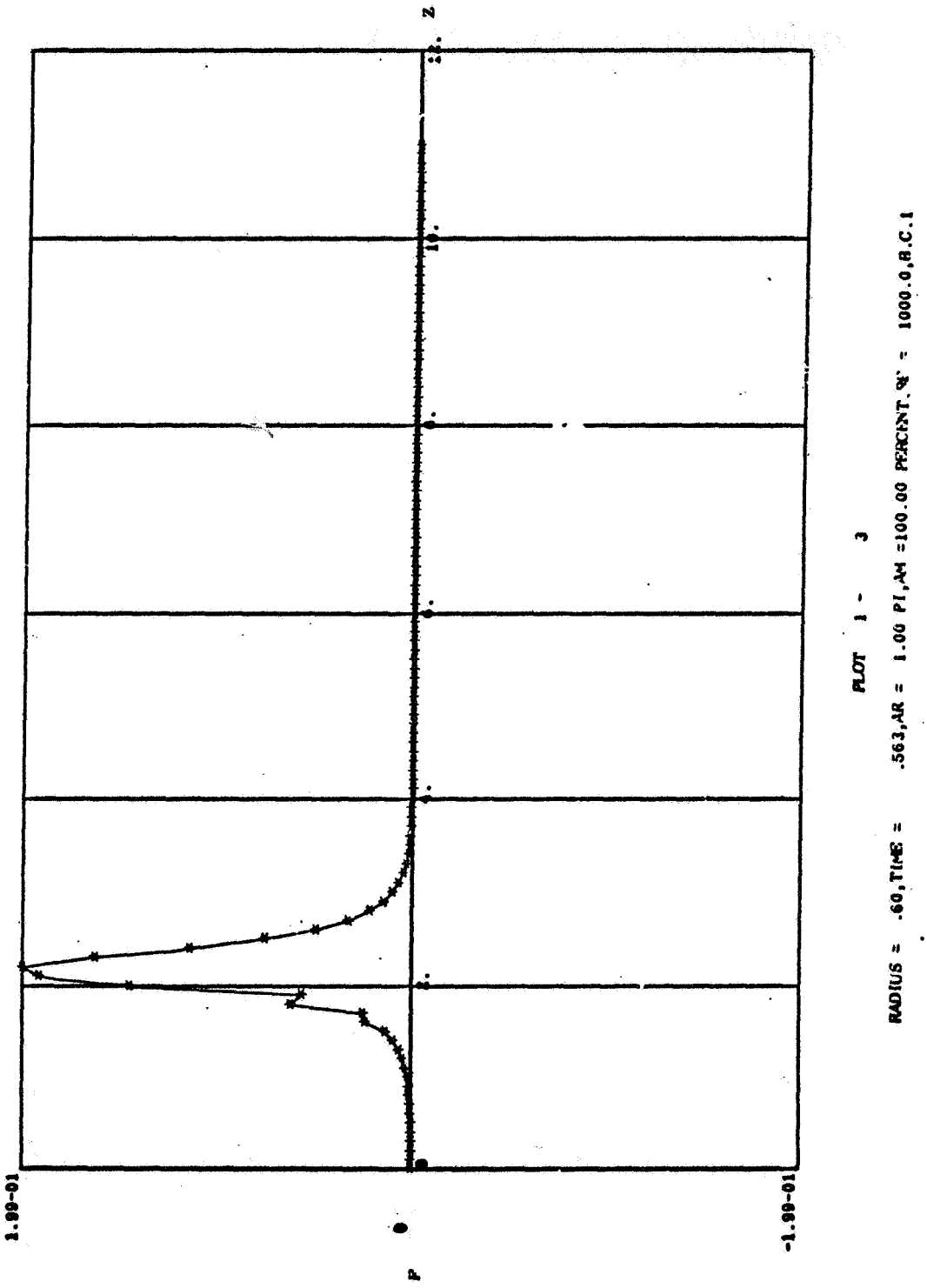

Figure 5a. Disturbance Stream Function

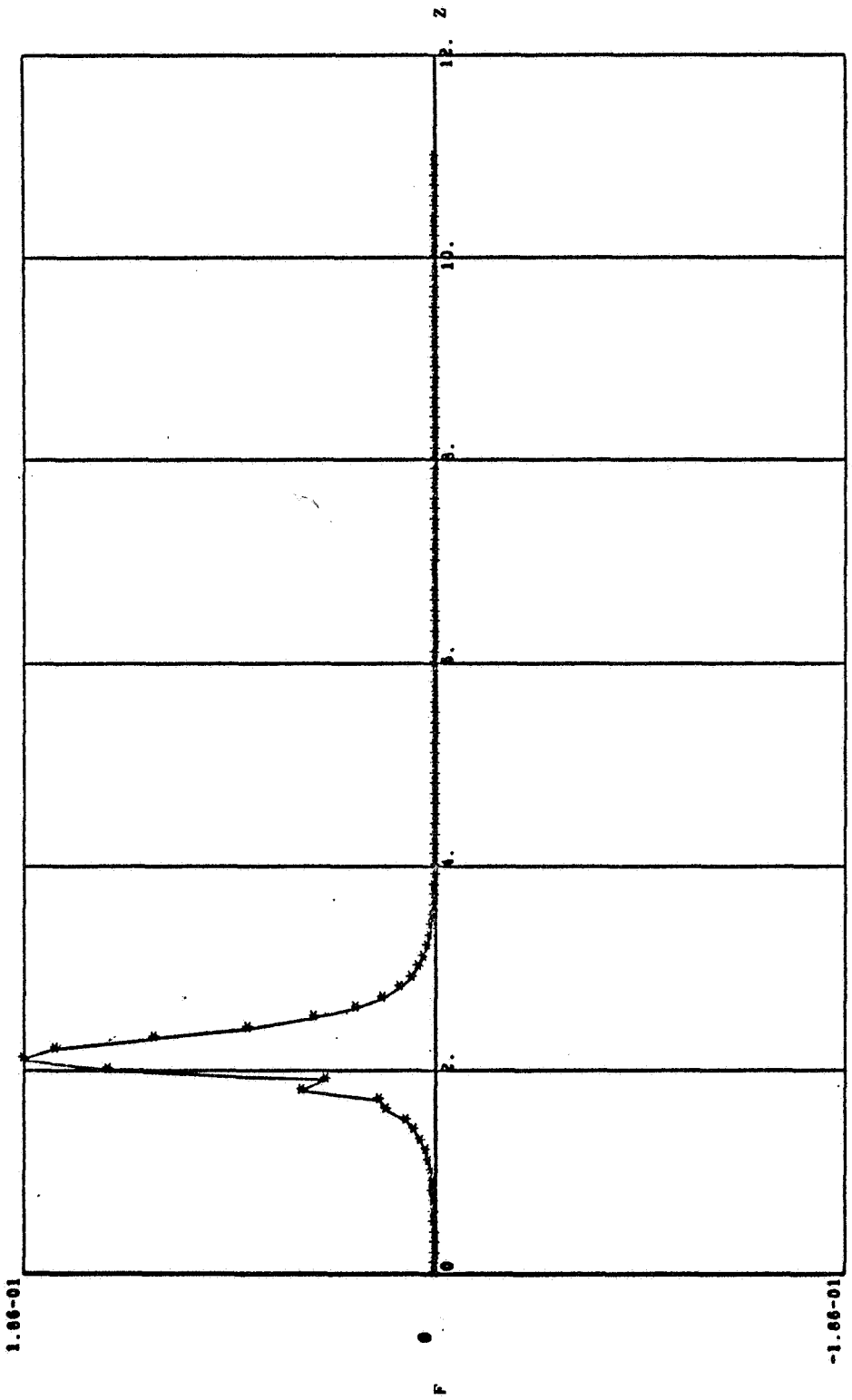

Figure 5b. Disturbance Stream Function

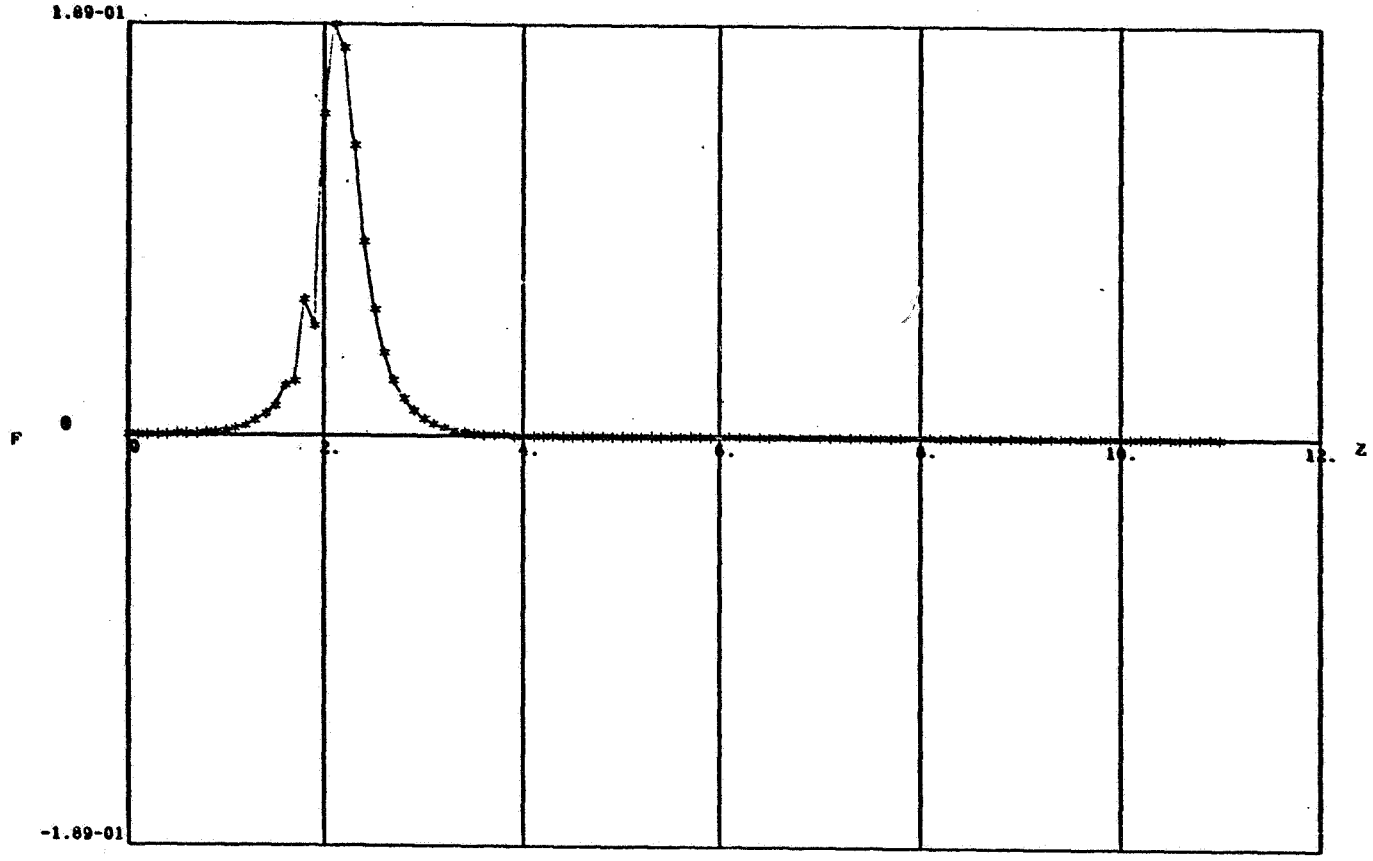

Figure 5c. Disturbance Stream Function

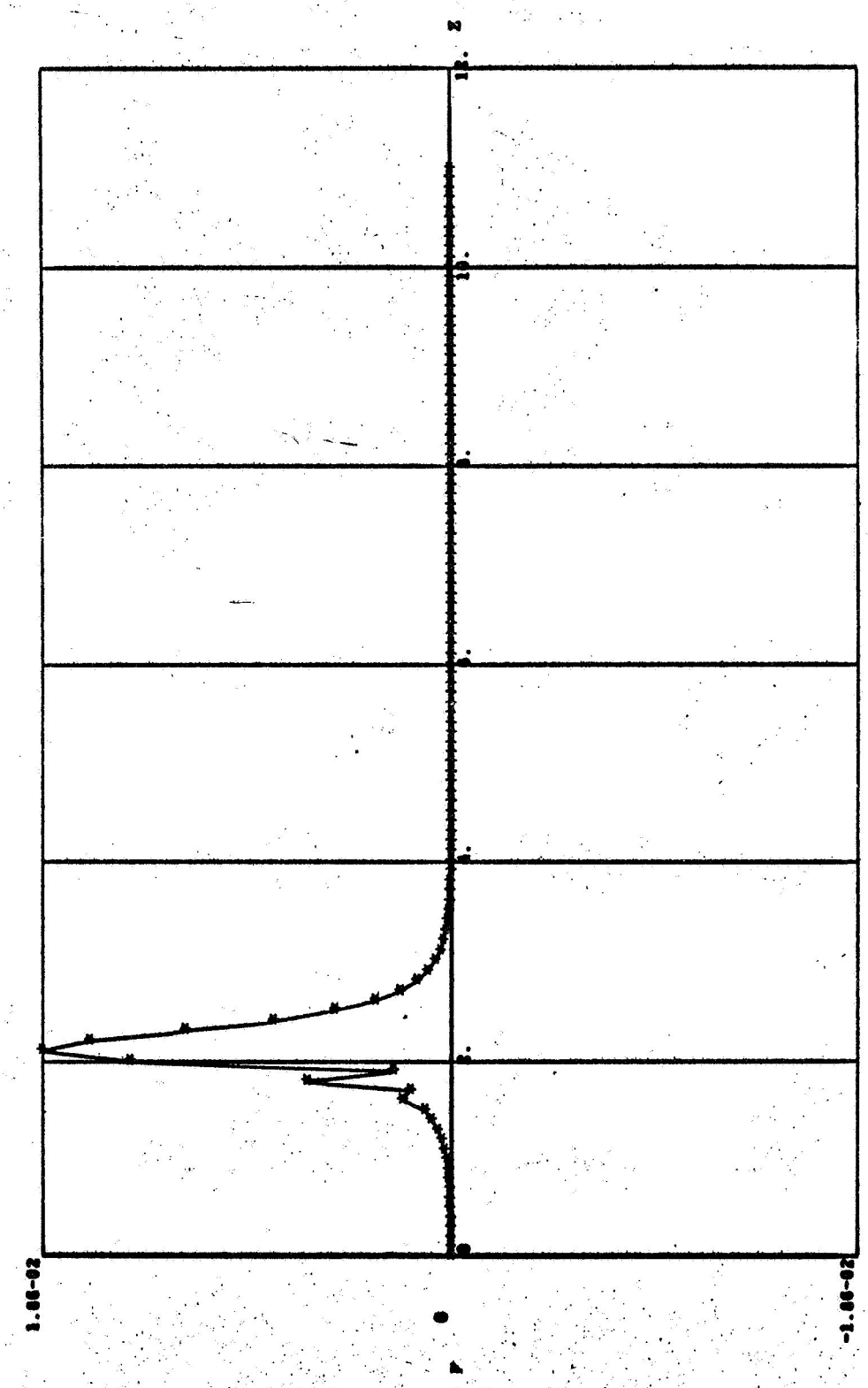

Figure 5d. Disturbance Stream Function

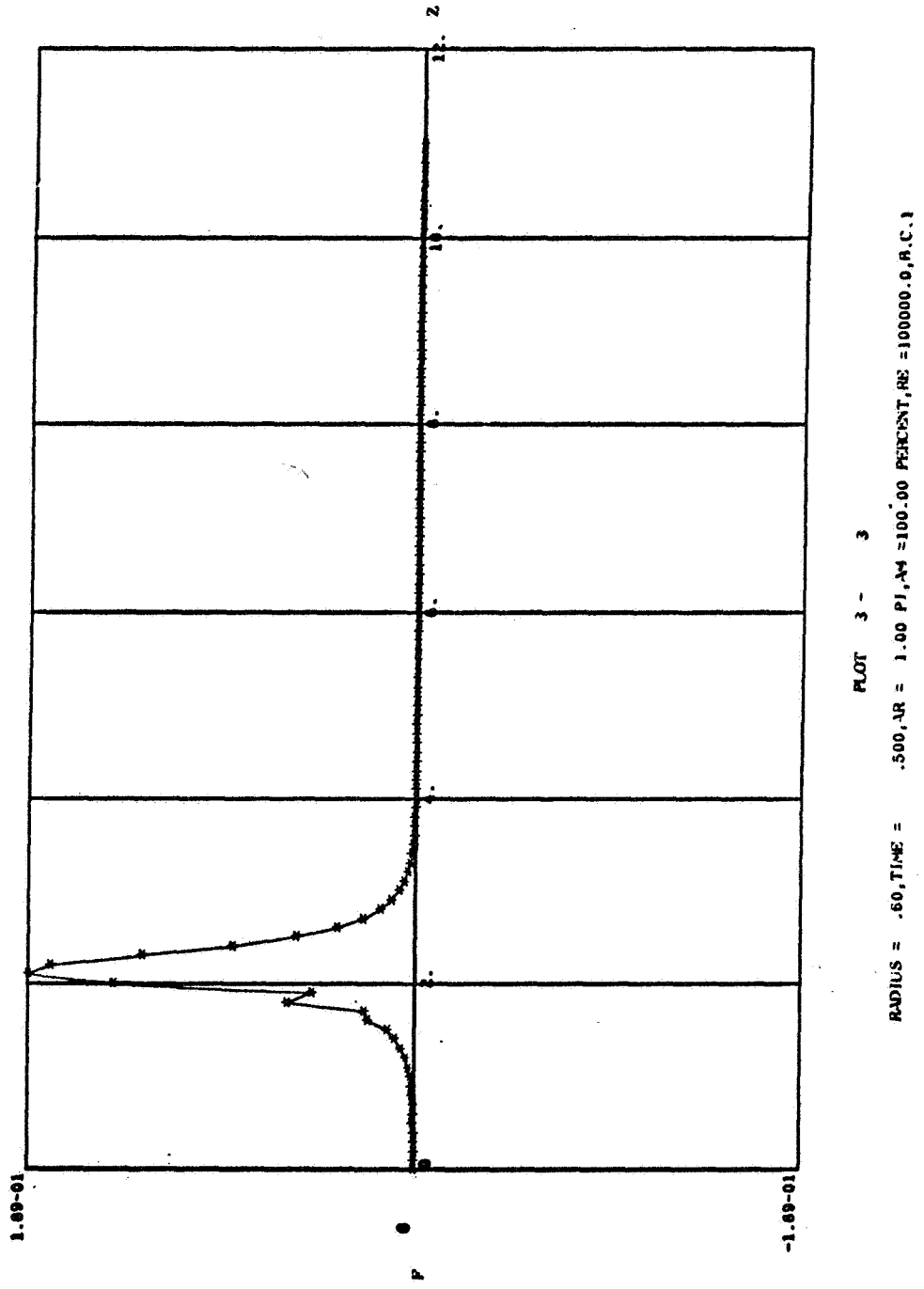

Figure 5e. Disturbance Stream Function

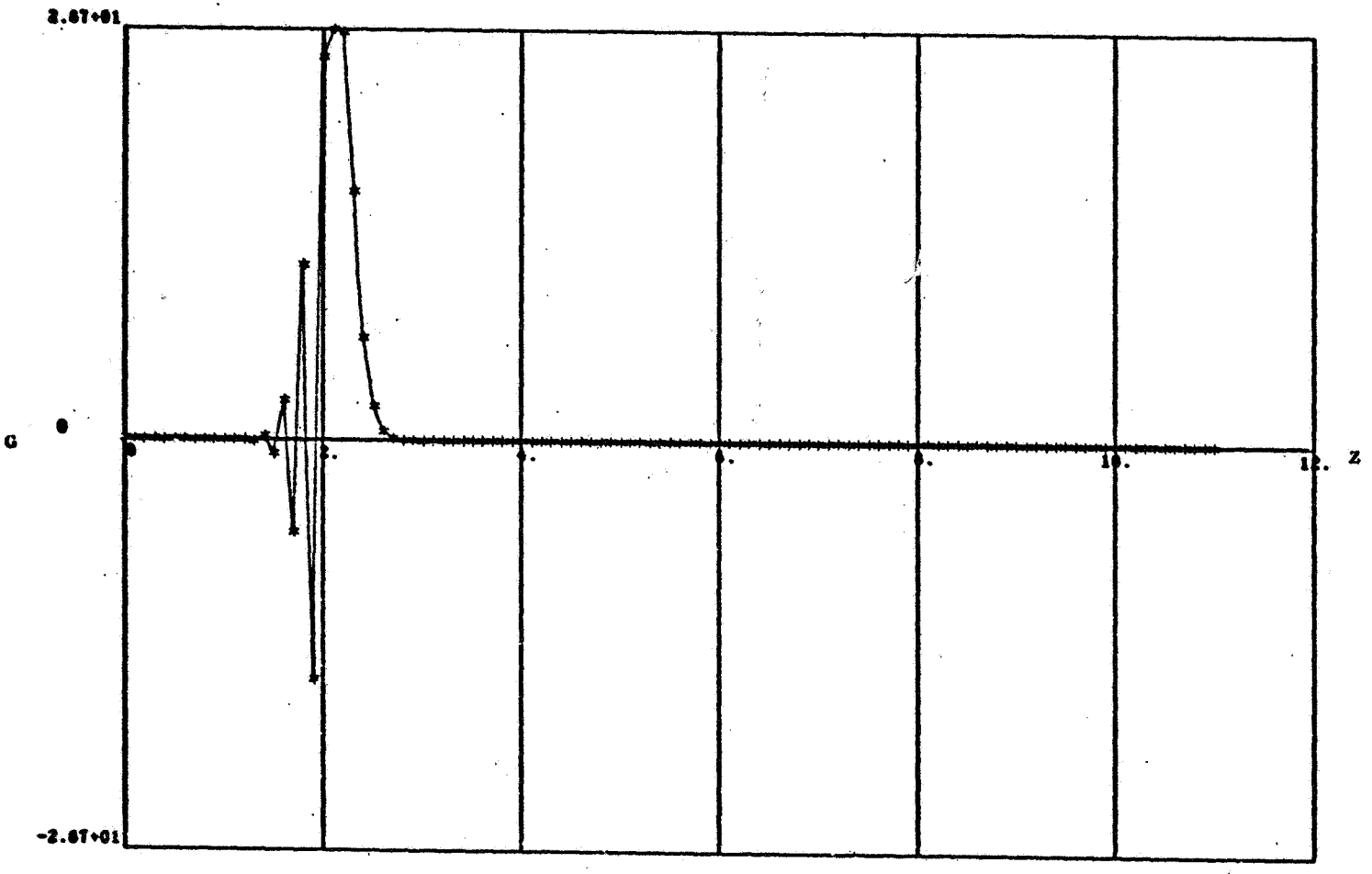

Figure 6a. Disturbance Vorticity

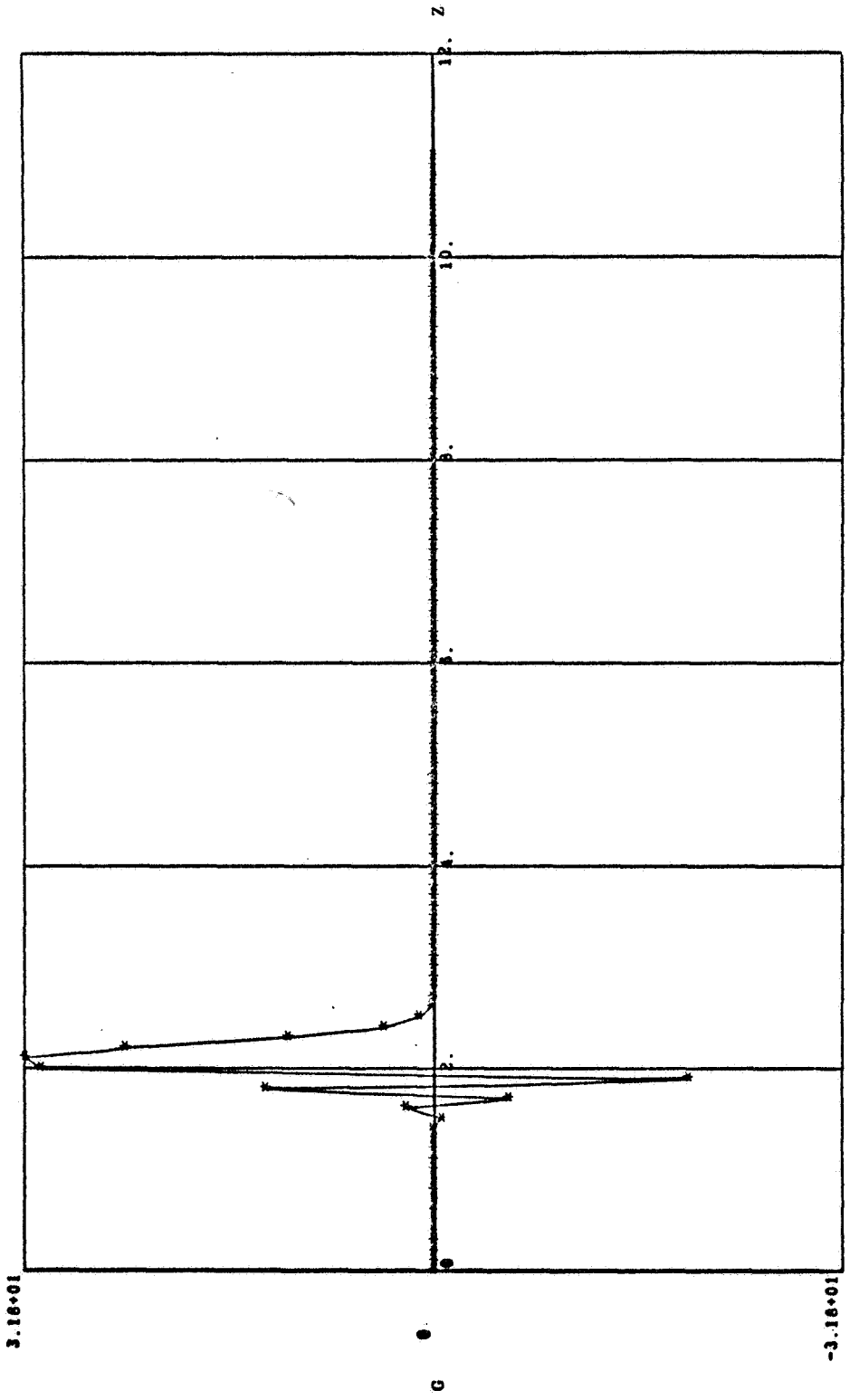

Figure 6b. Disturbance Vorticity

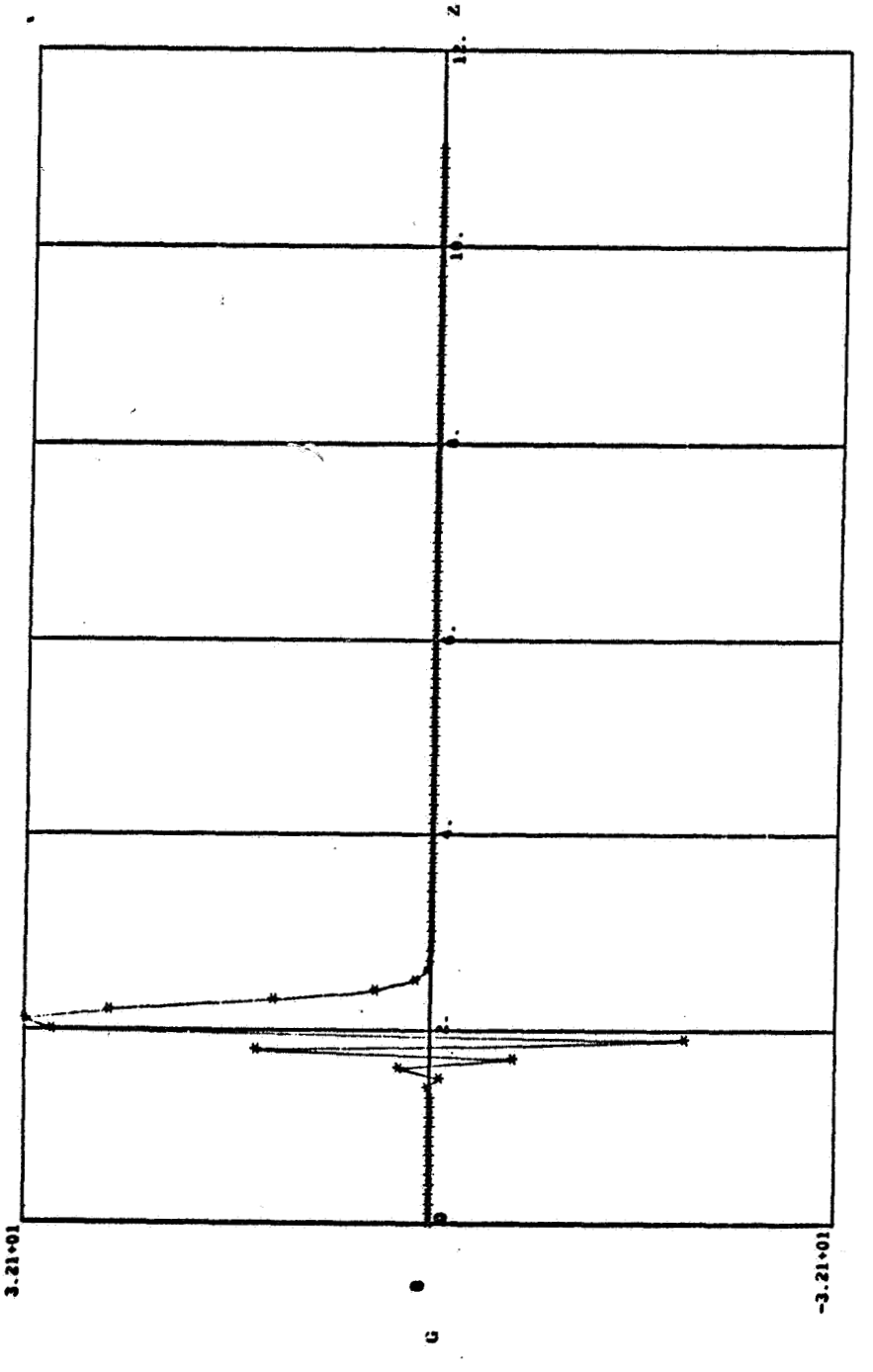

Figure 6c. Disturbance Vorticity

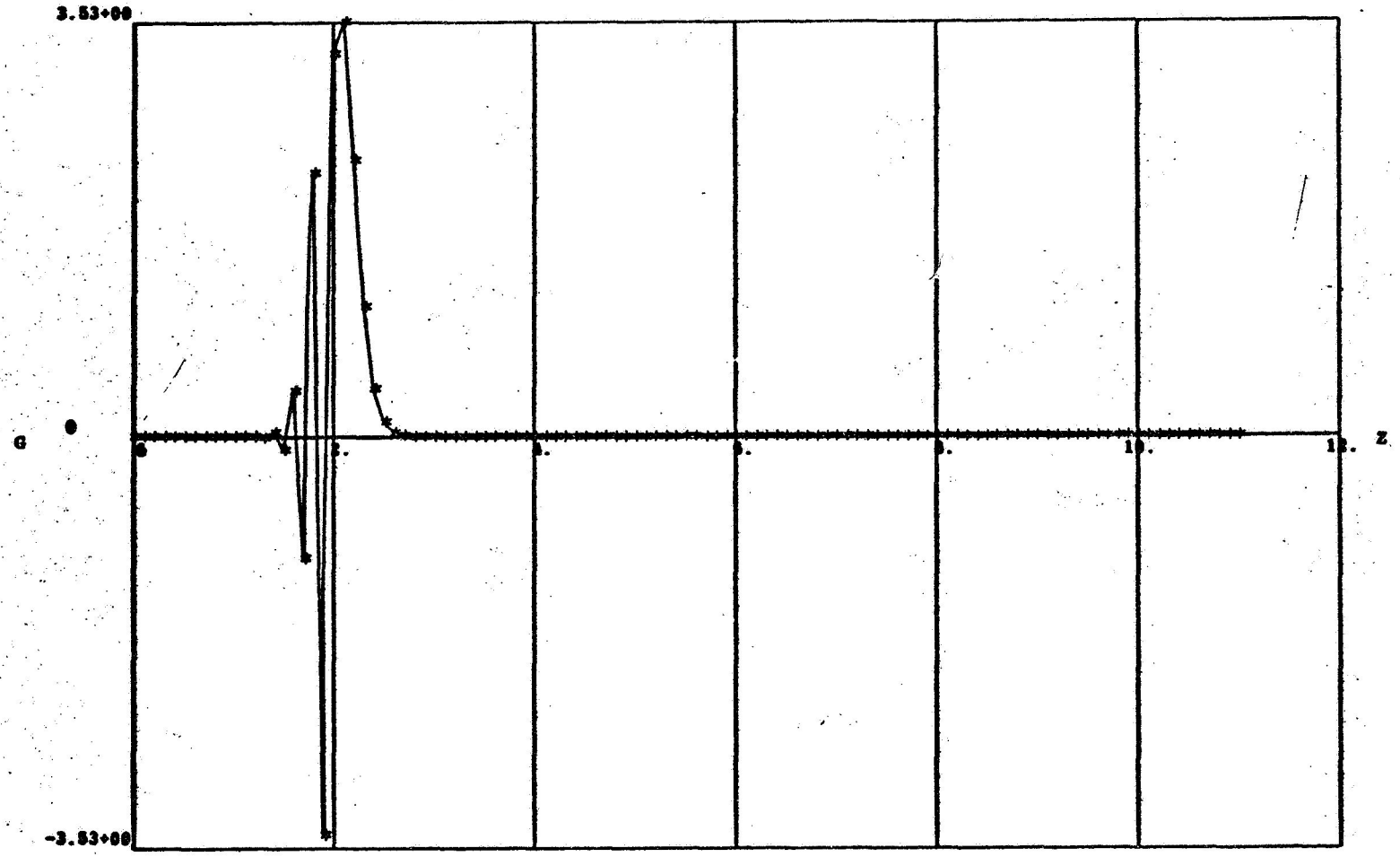

PLOT 5 - 4

RADIUS = .60,TIME = .535,AR = 1.00 PI,AM = 10.00 PERCENT,RE =100000.0,B.C.1

Figure 6d. Disturbance Vorticity

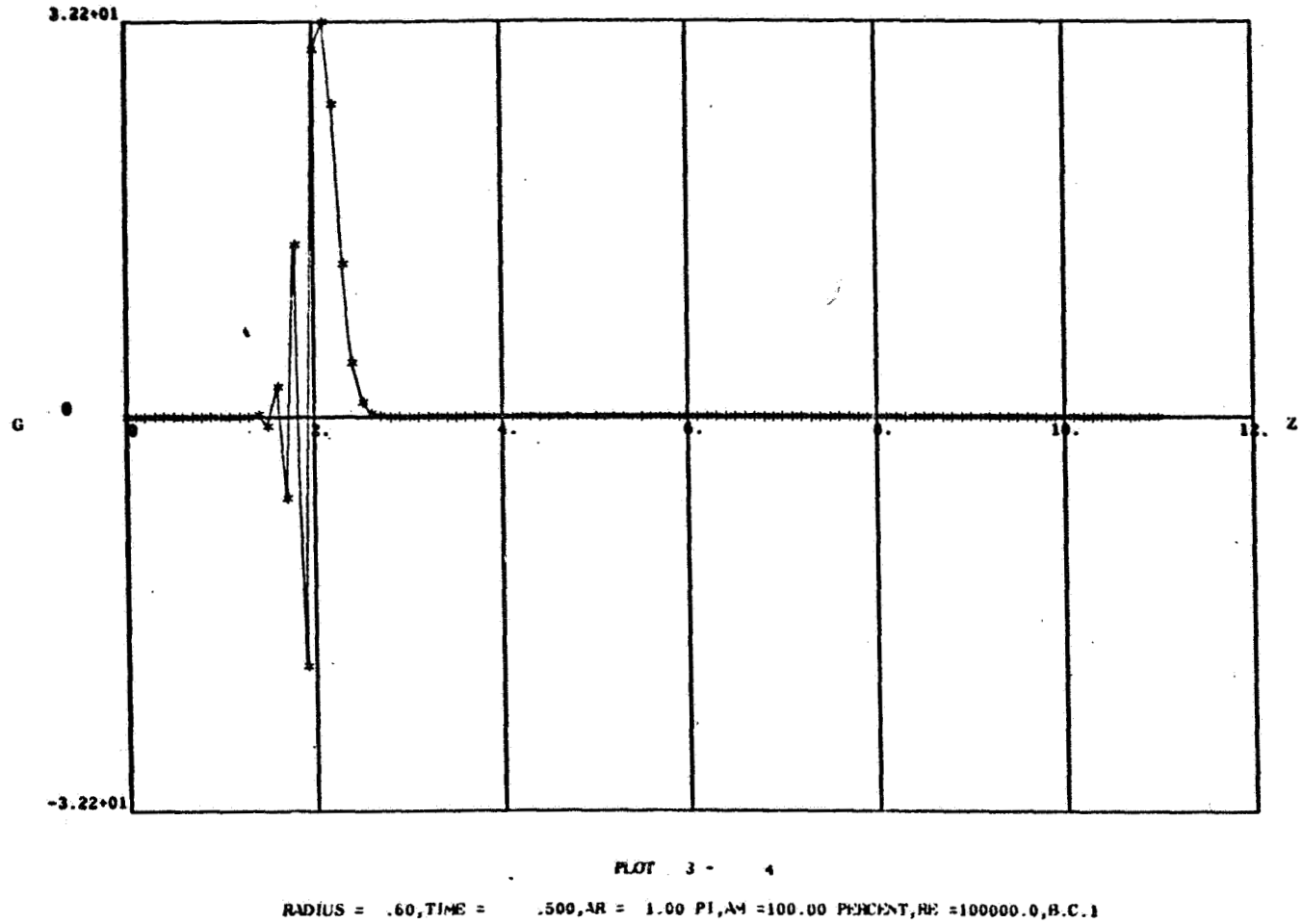

Figure 6e. Disturbance Vorticity

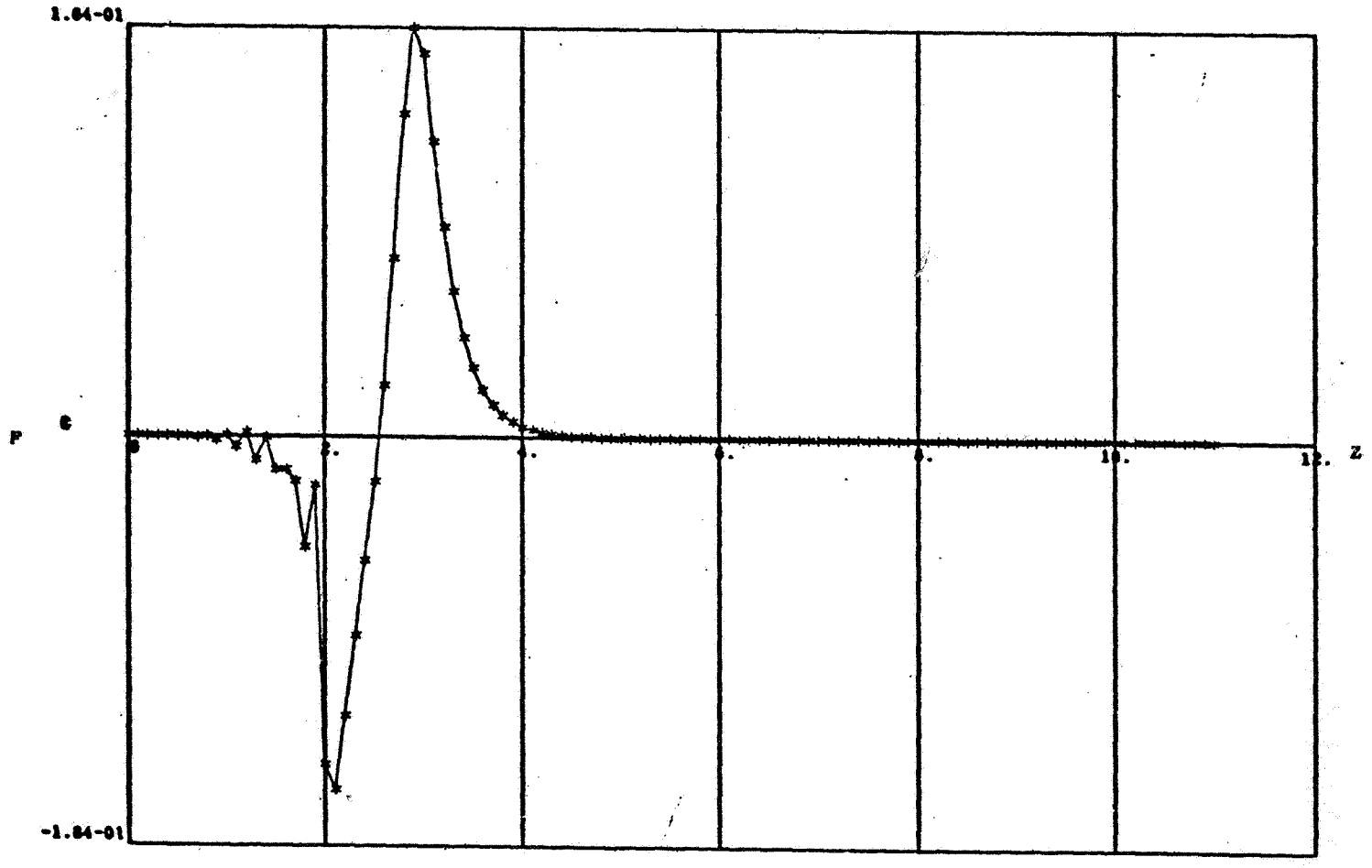

PLOT 1 - 15

RADIUS = .60,TIME = 1.483,AR = 1.00 PI,AH =100.00 PERCENT,RE = 1000.0,B.C.1

Figure 7a. Disturbance Stream Function

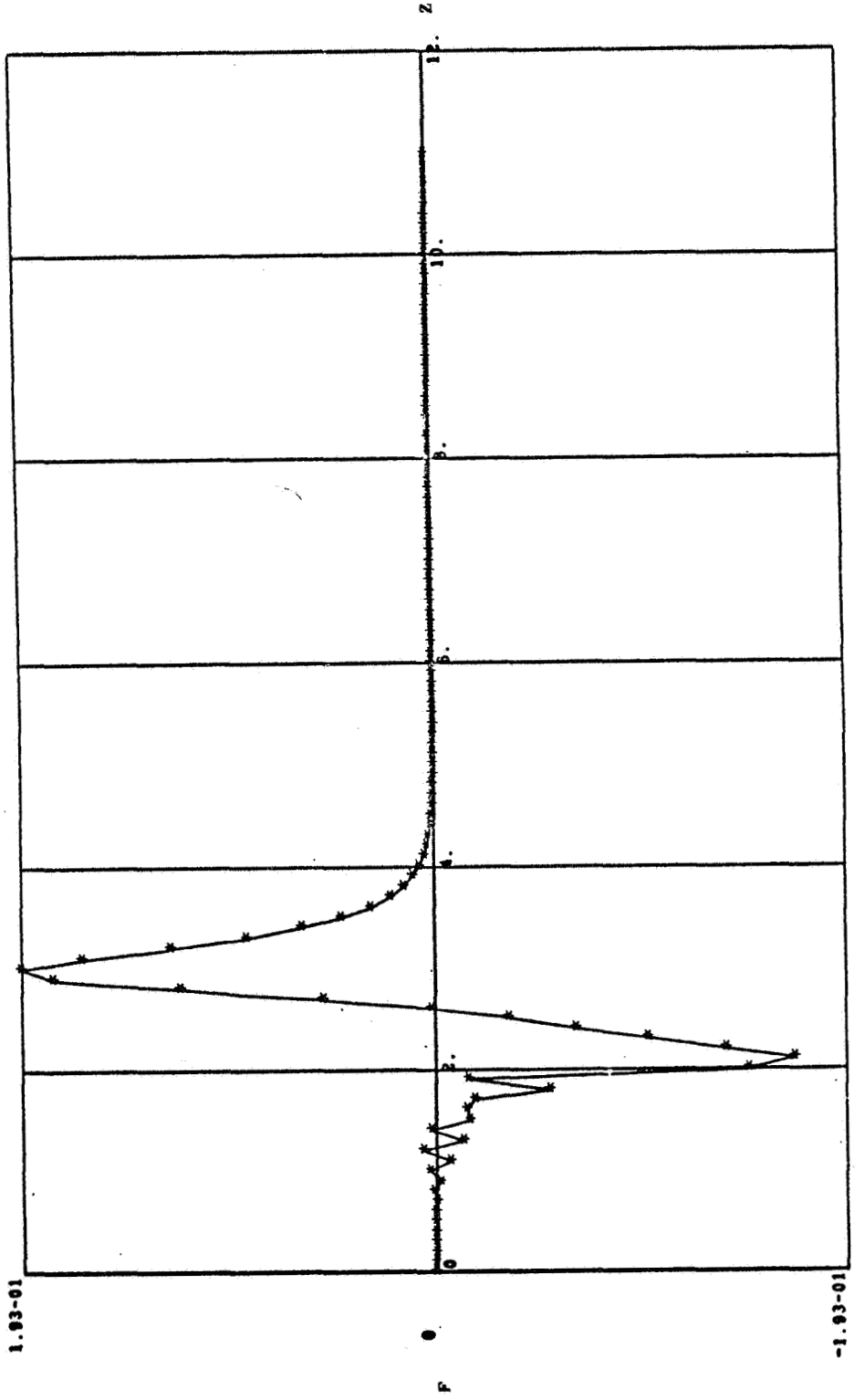

Figure 7b. Disturbance Stream Function

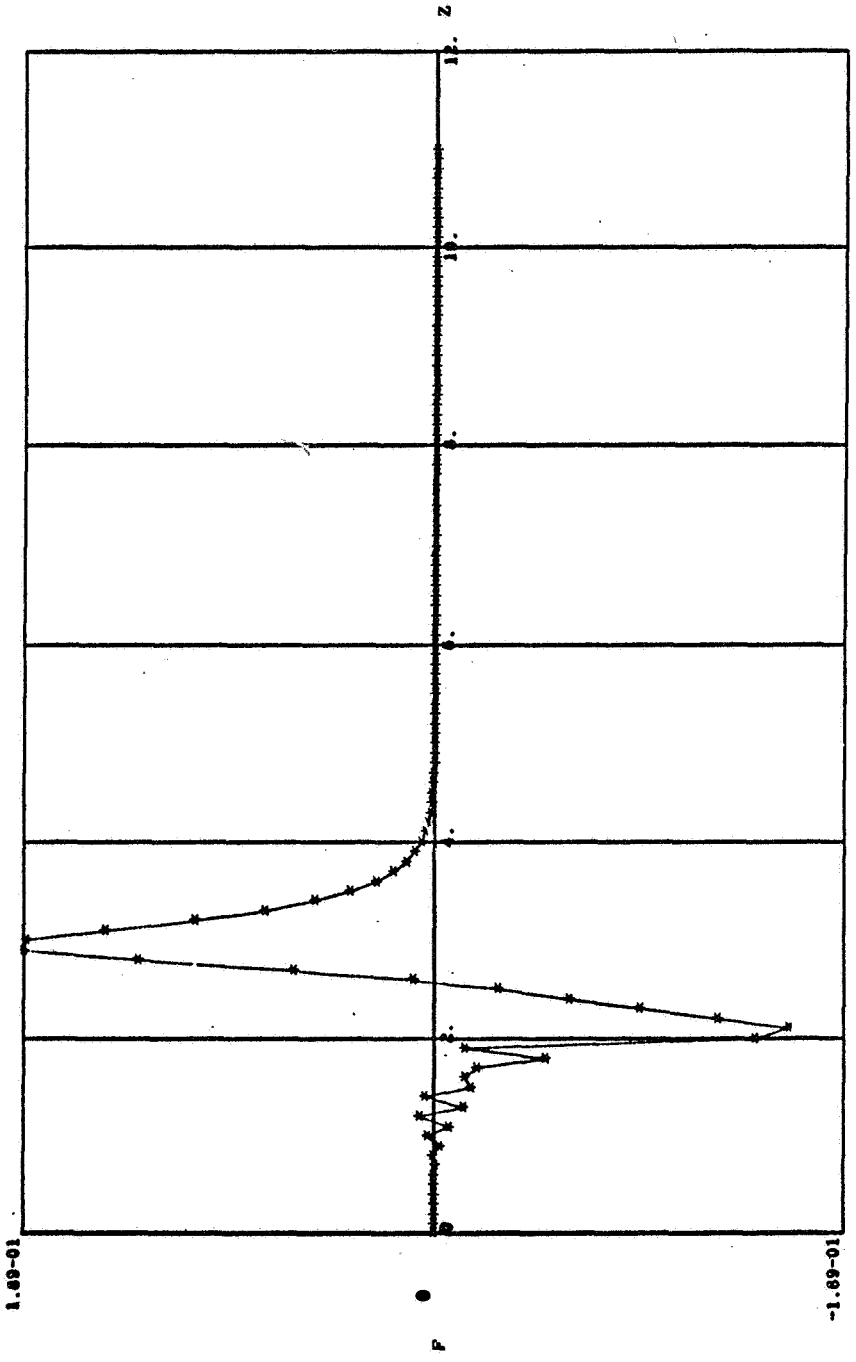

Figure 7c. Disturbance Stream Function

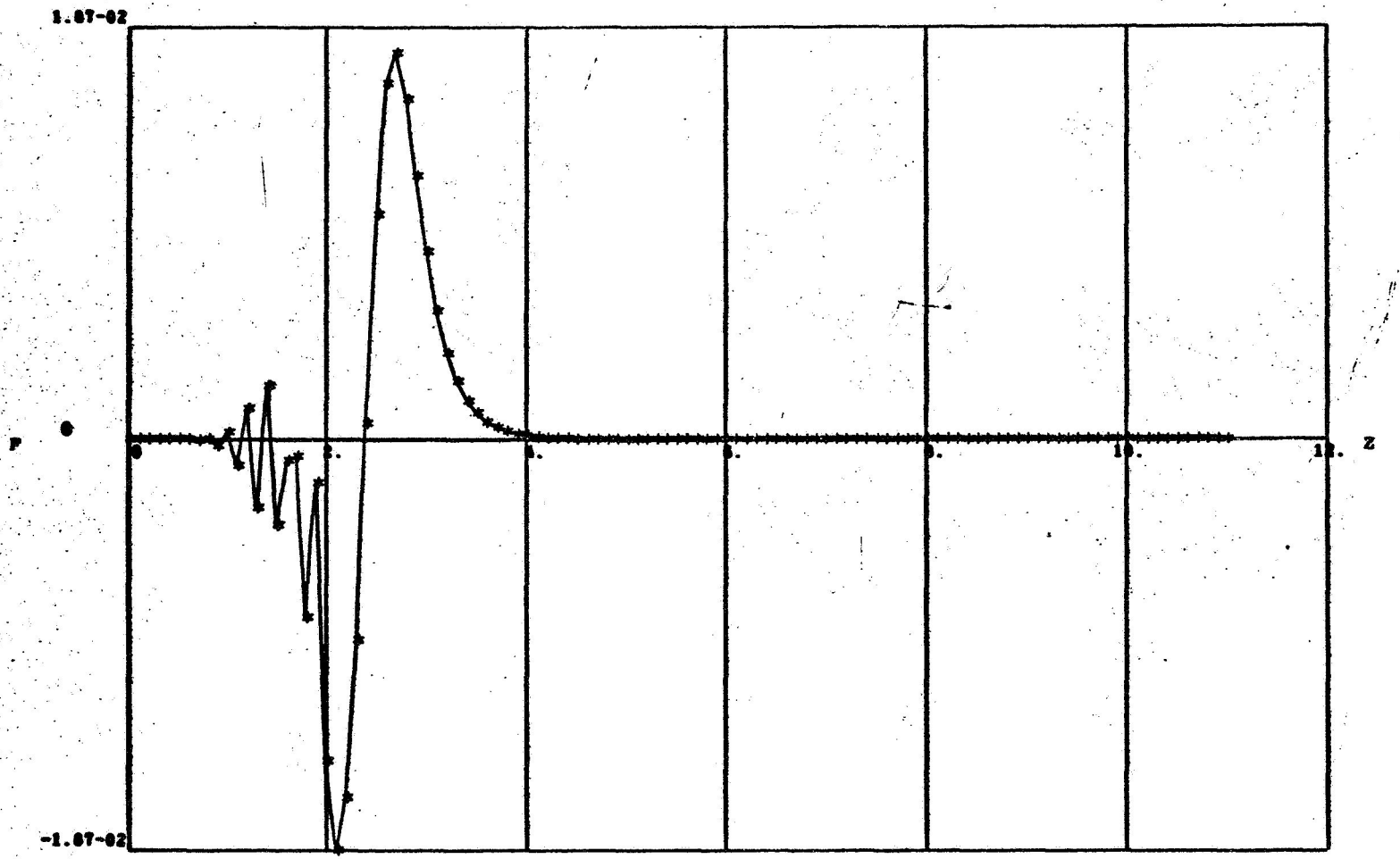

Figure 7d. Disturbance Stream Function

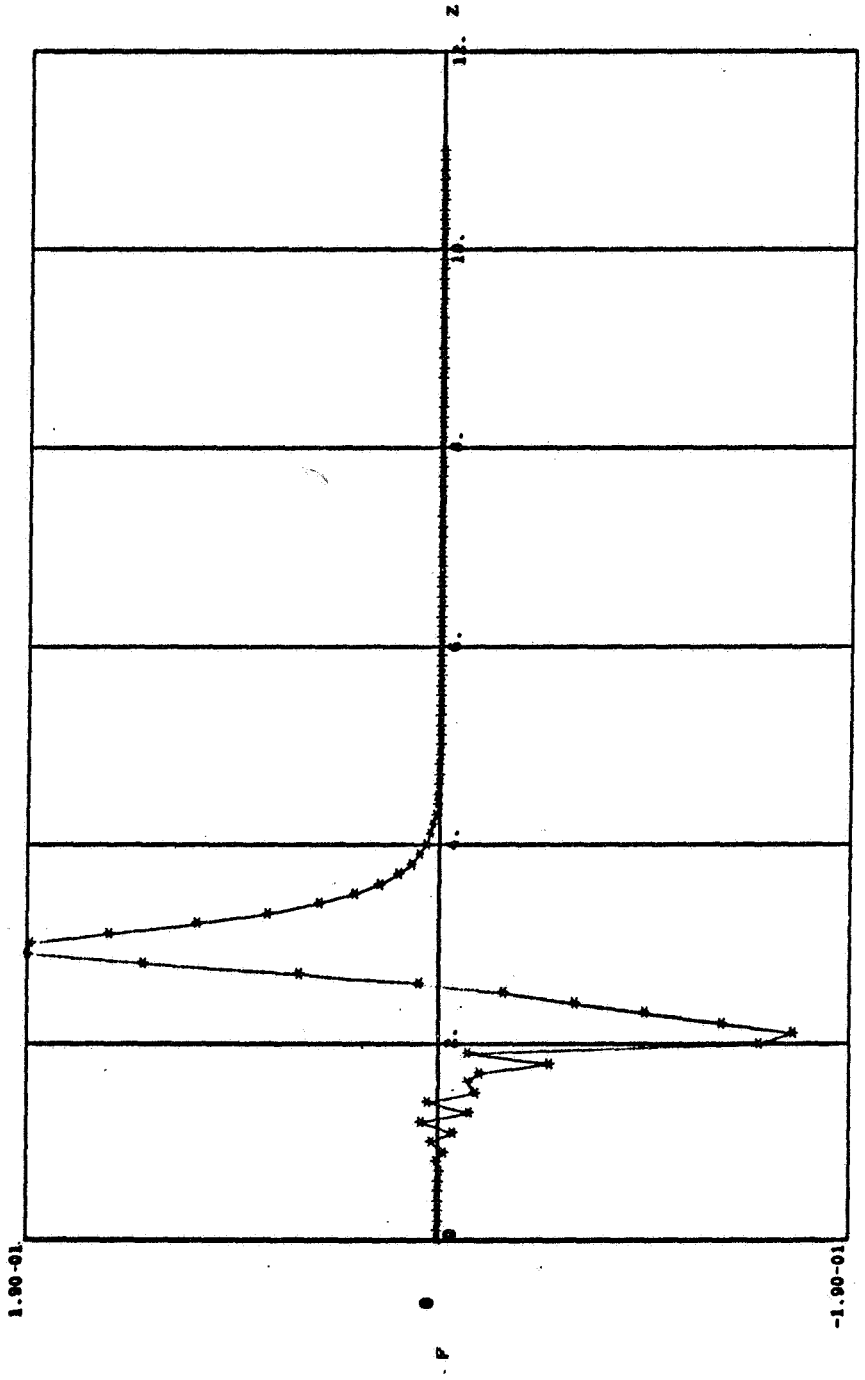

Figure 7e. Disturbance Vorticity

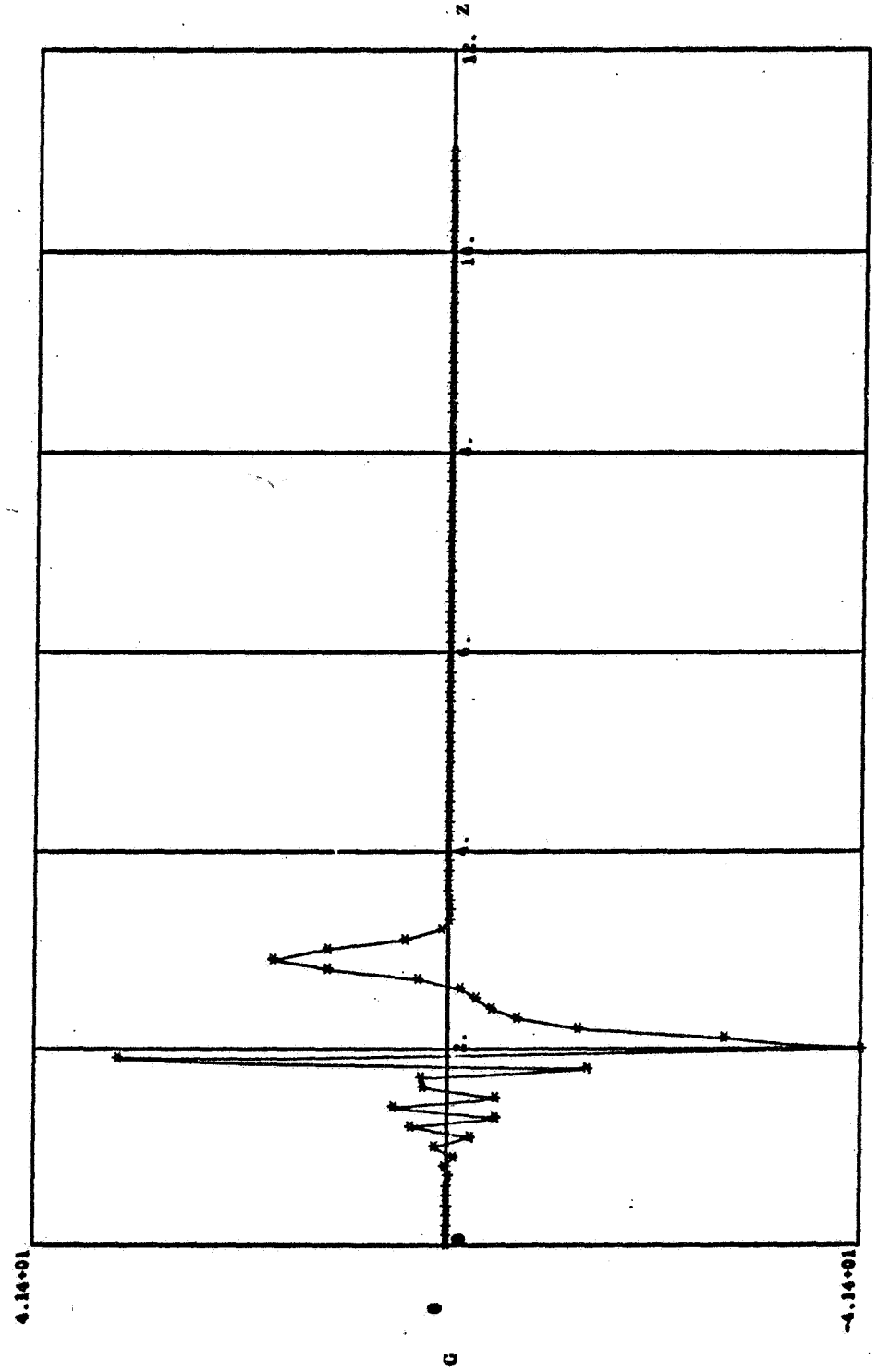

Figure 8a. Disturbance Vorticity

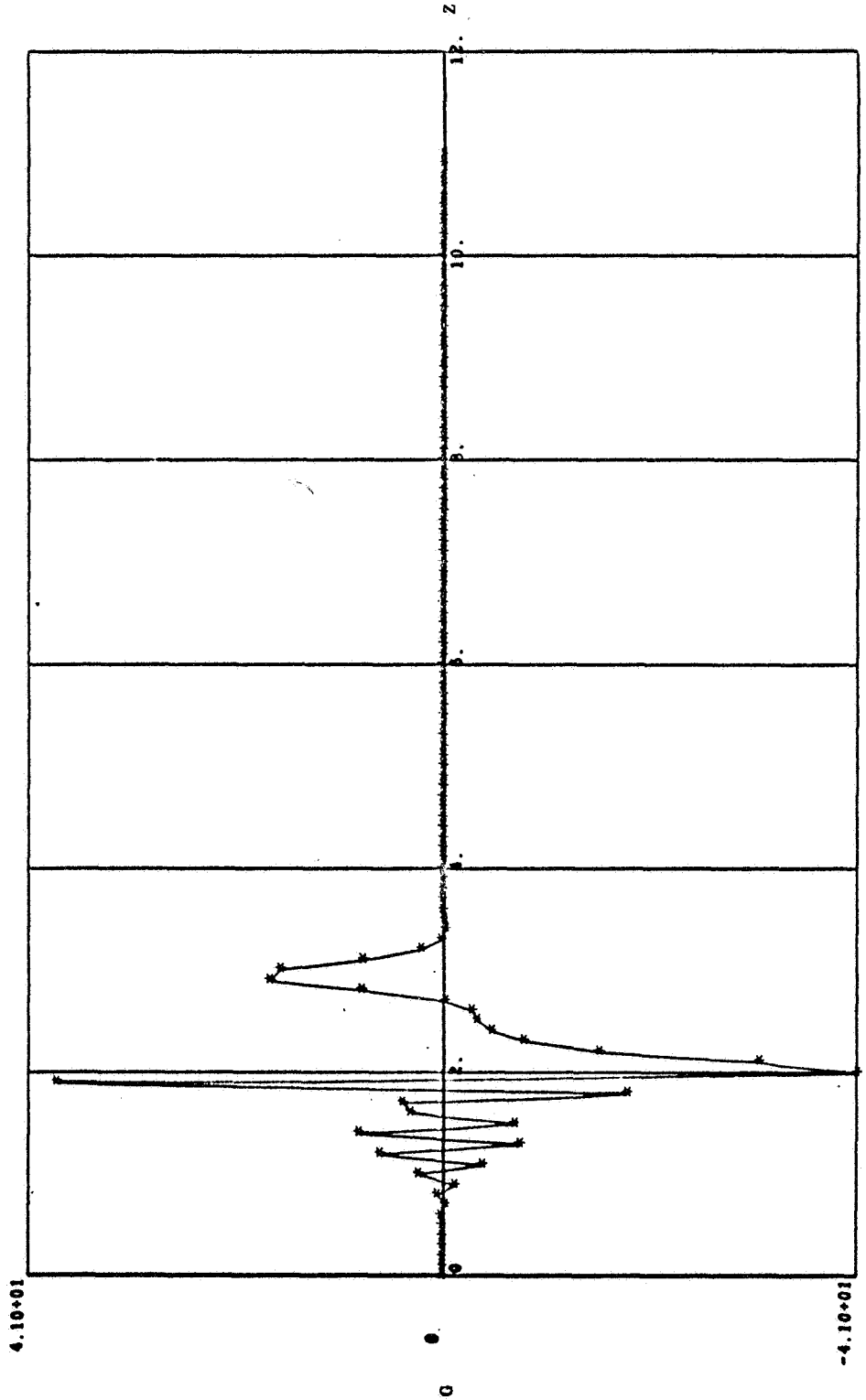

Figure 8b. Disturbance Vorticity

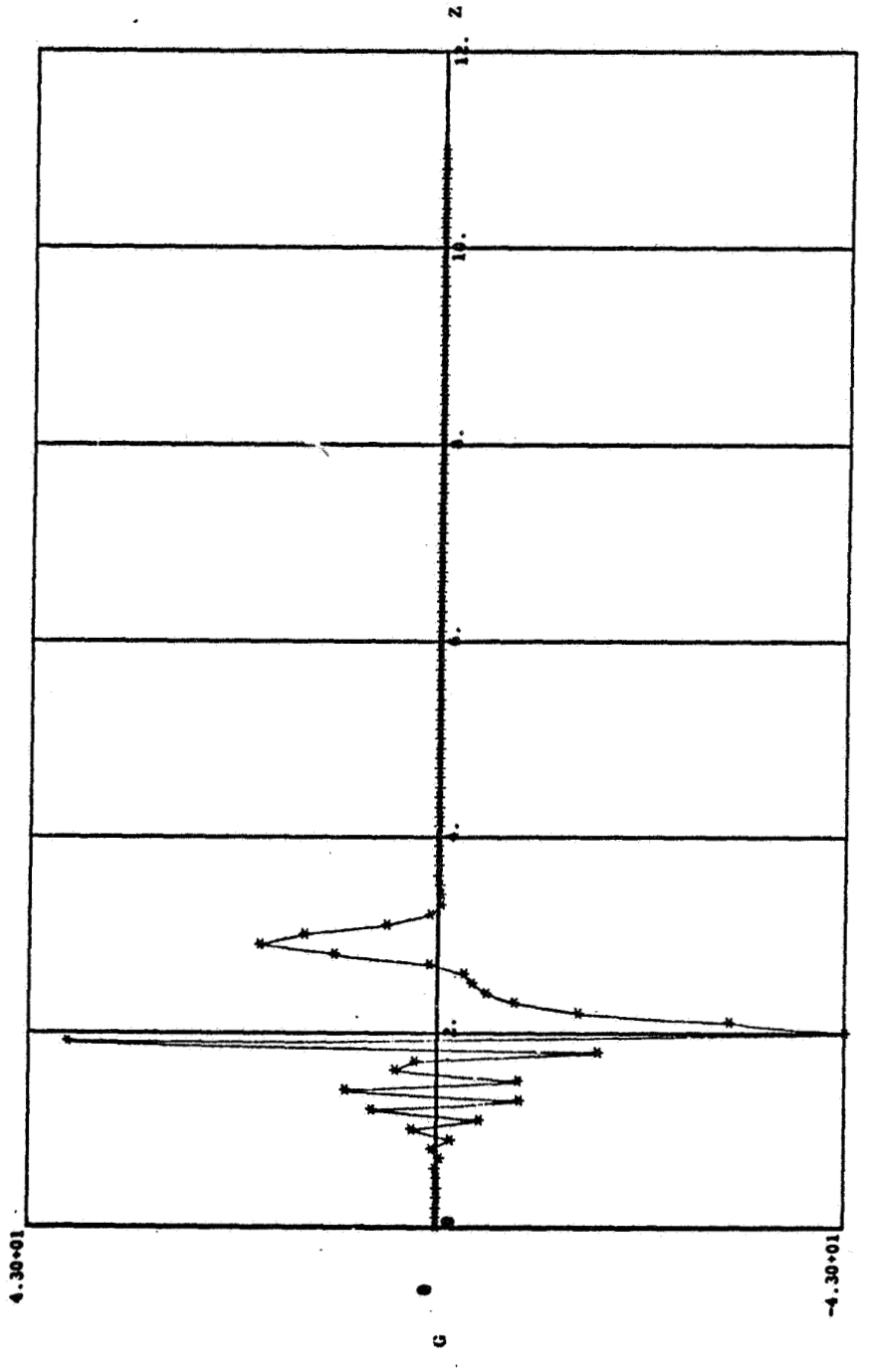

Figure 8c. Disturbance Vorticity

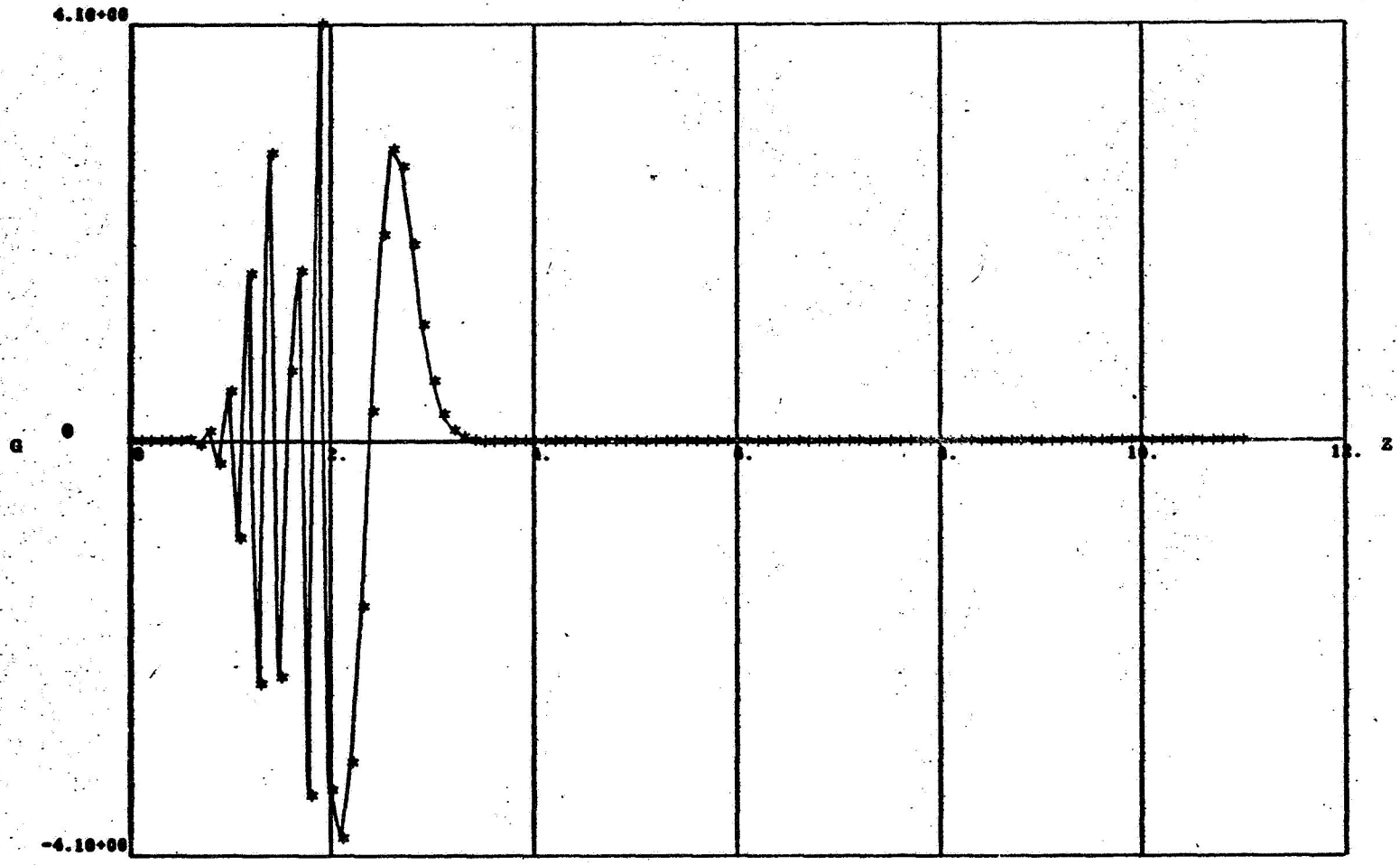

Figure 8d. Disturbance Vorticity

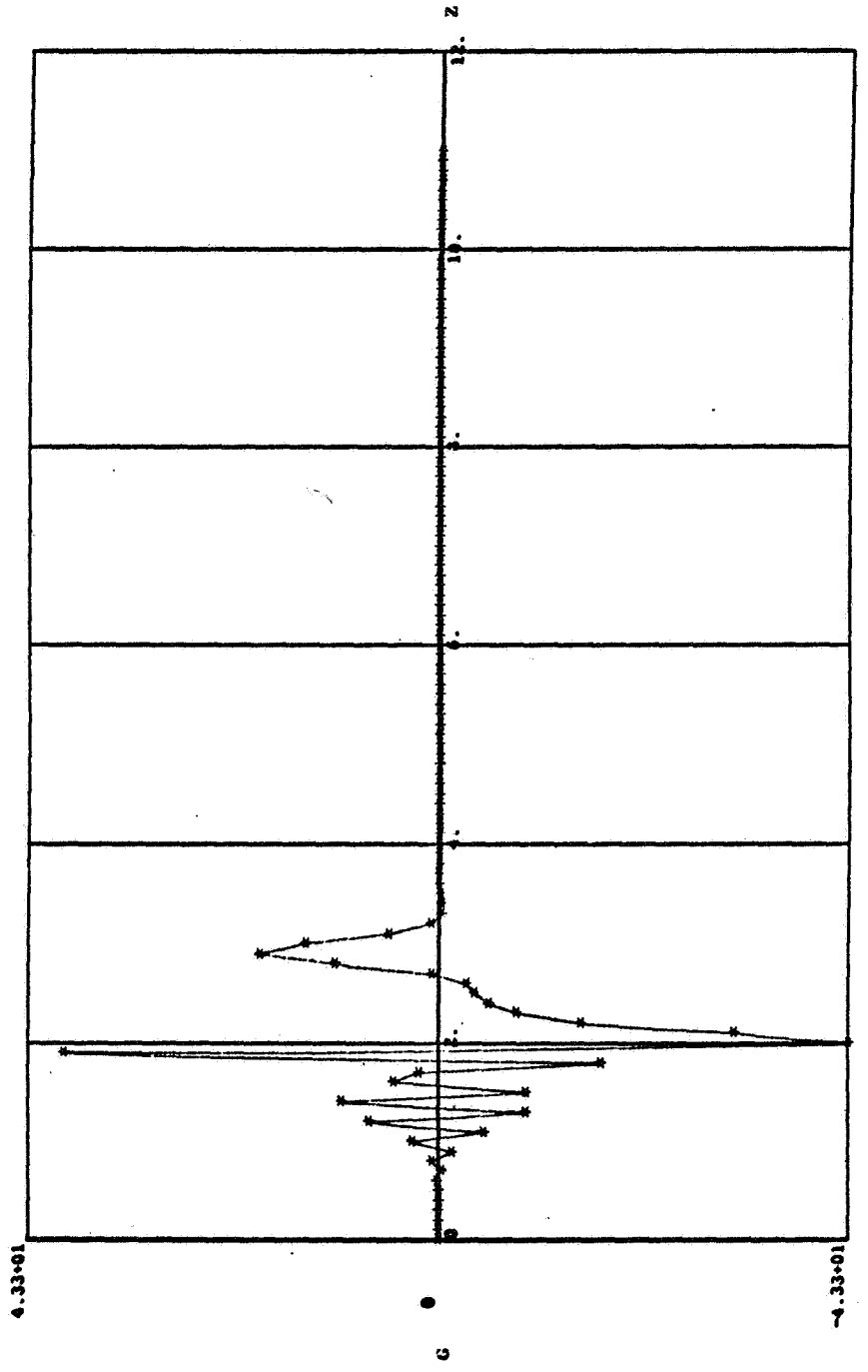

Figure 8e. Disturbance Vorticity

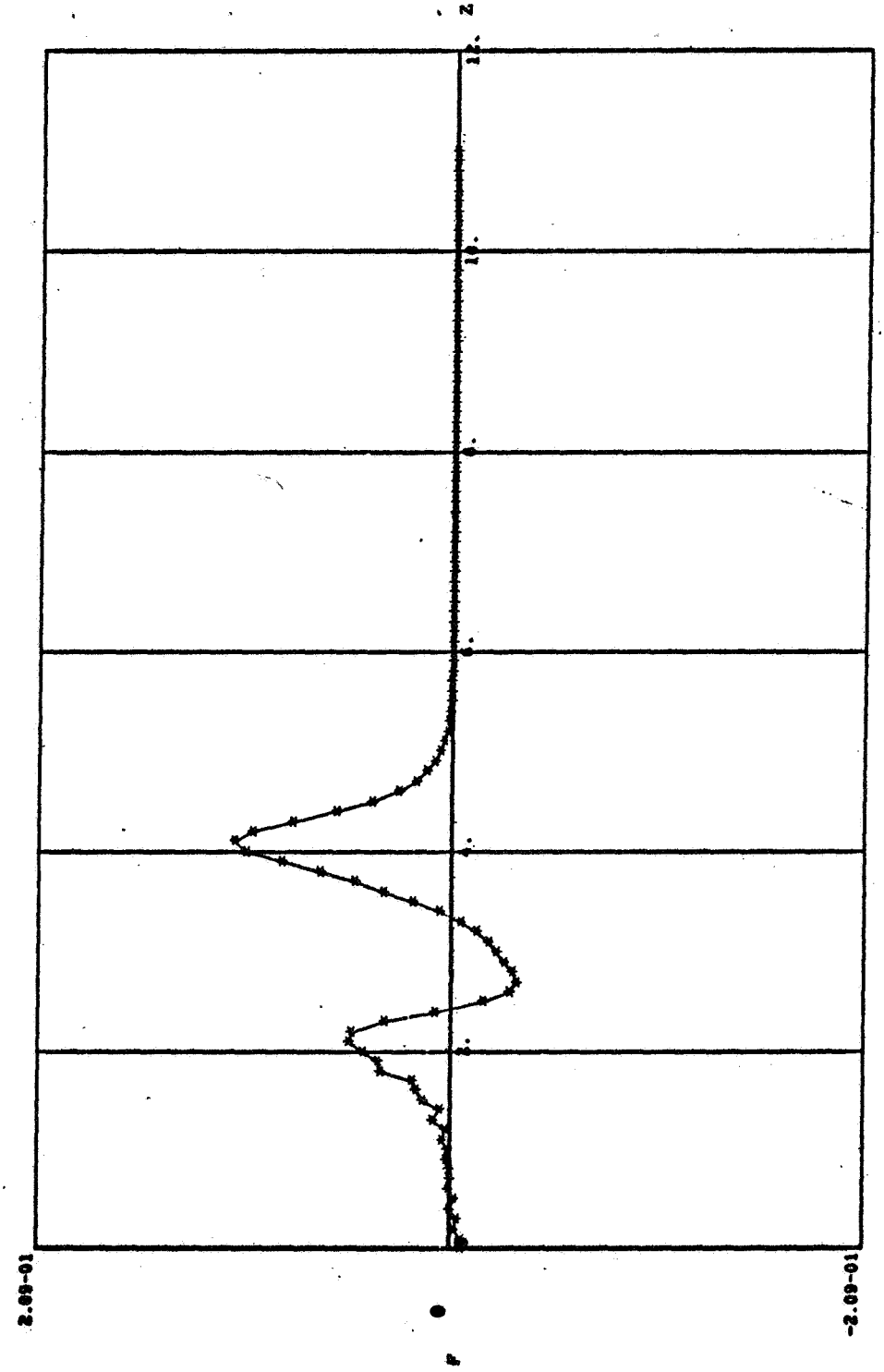

Figure 9a. Disturbance Stream Function

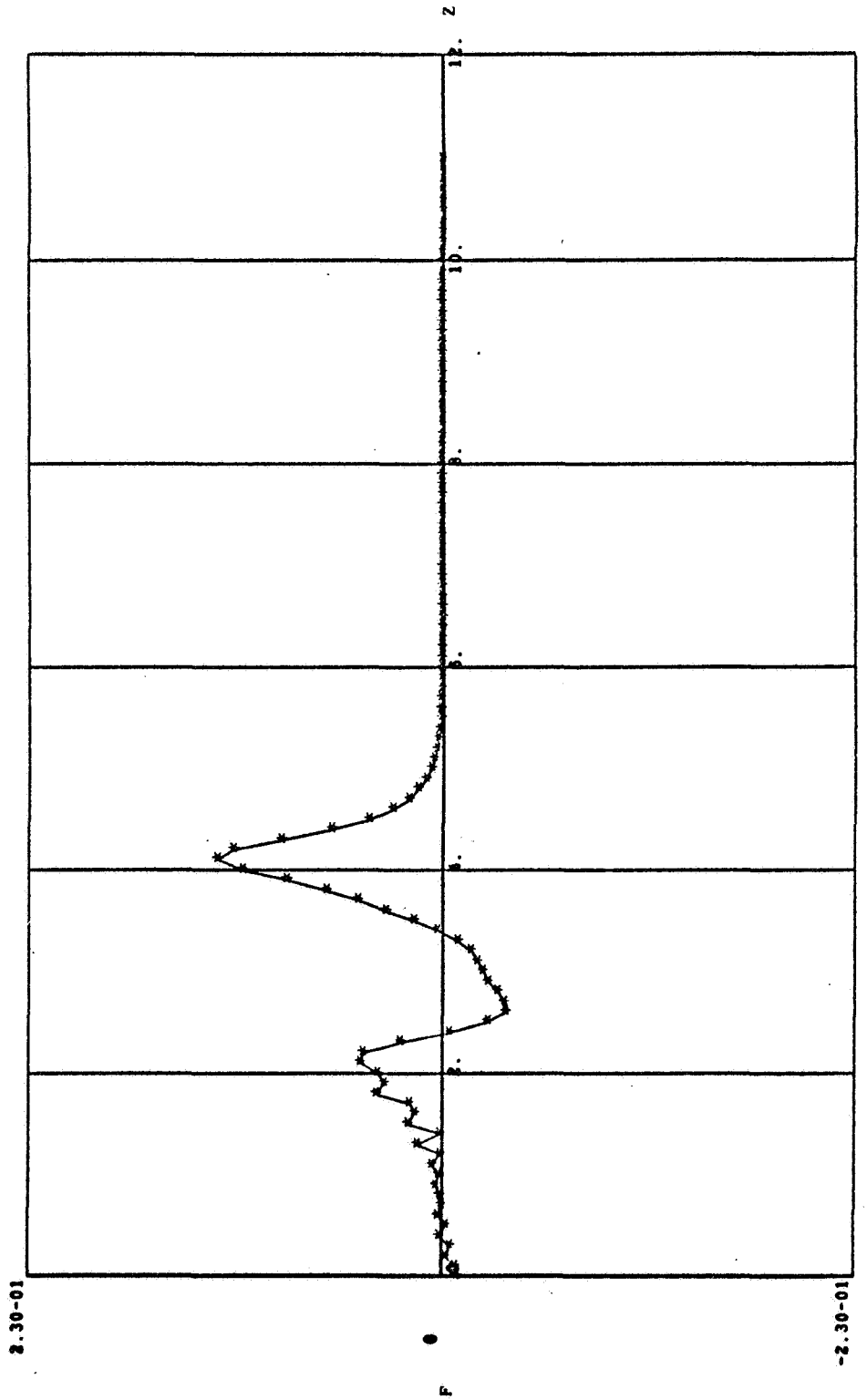

Figure 9b. Disturbance Stream Function

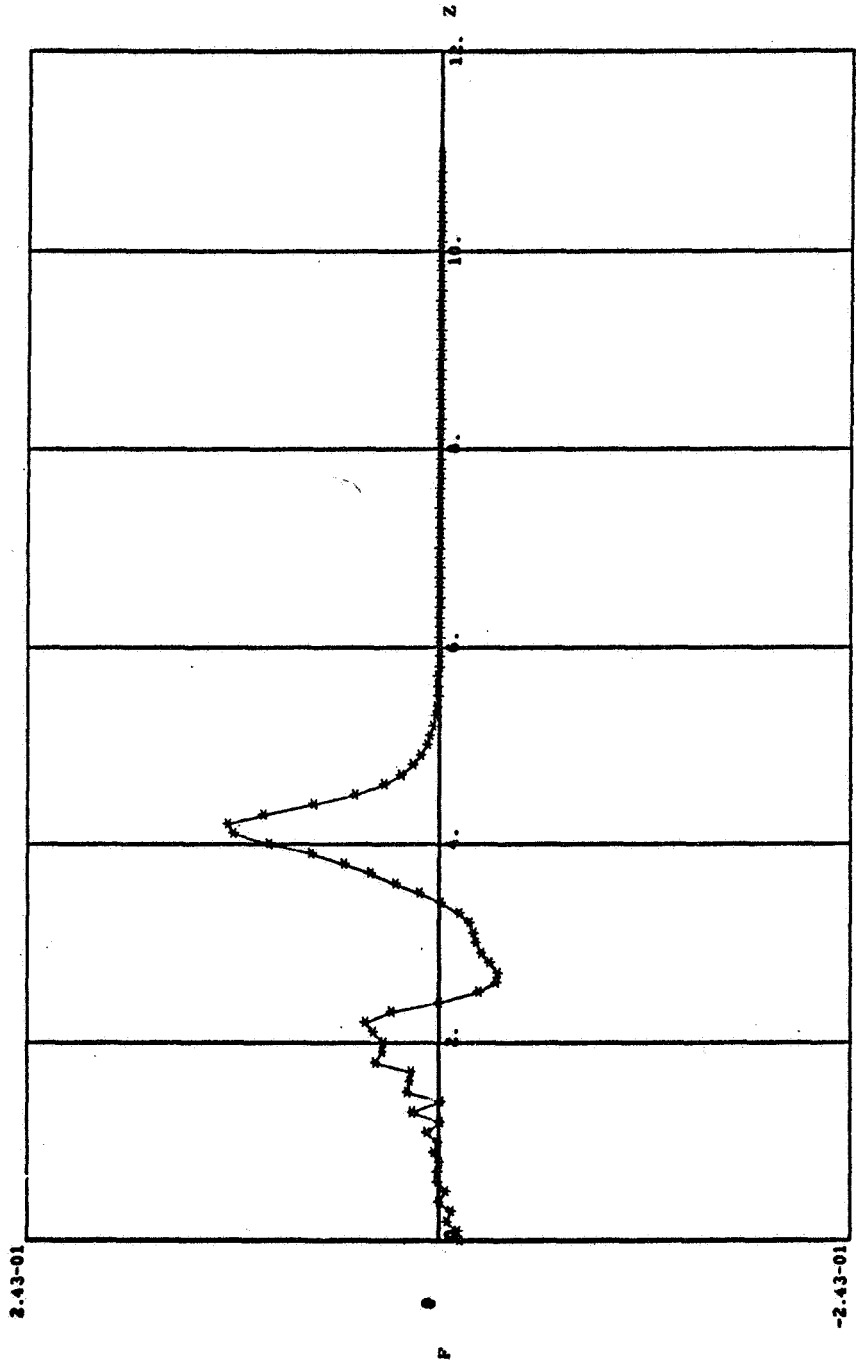

Figure 9c. Disturbance Stream Function

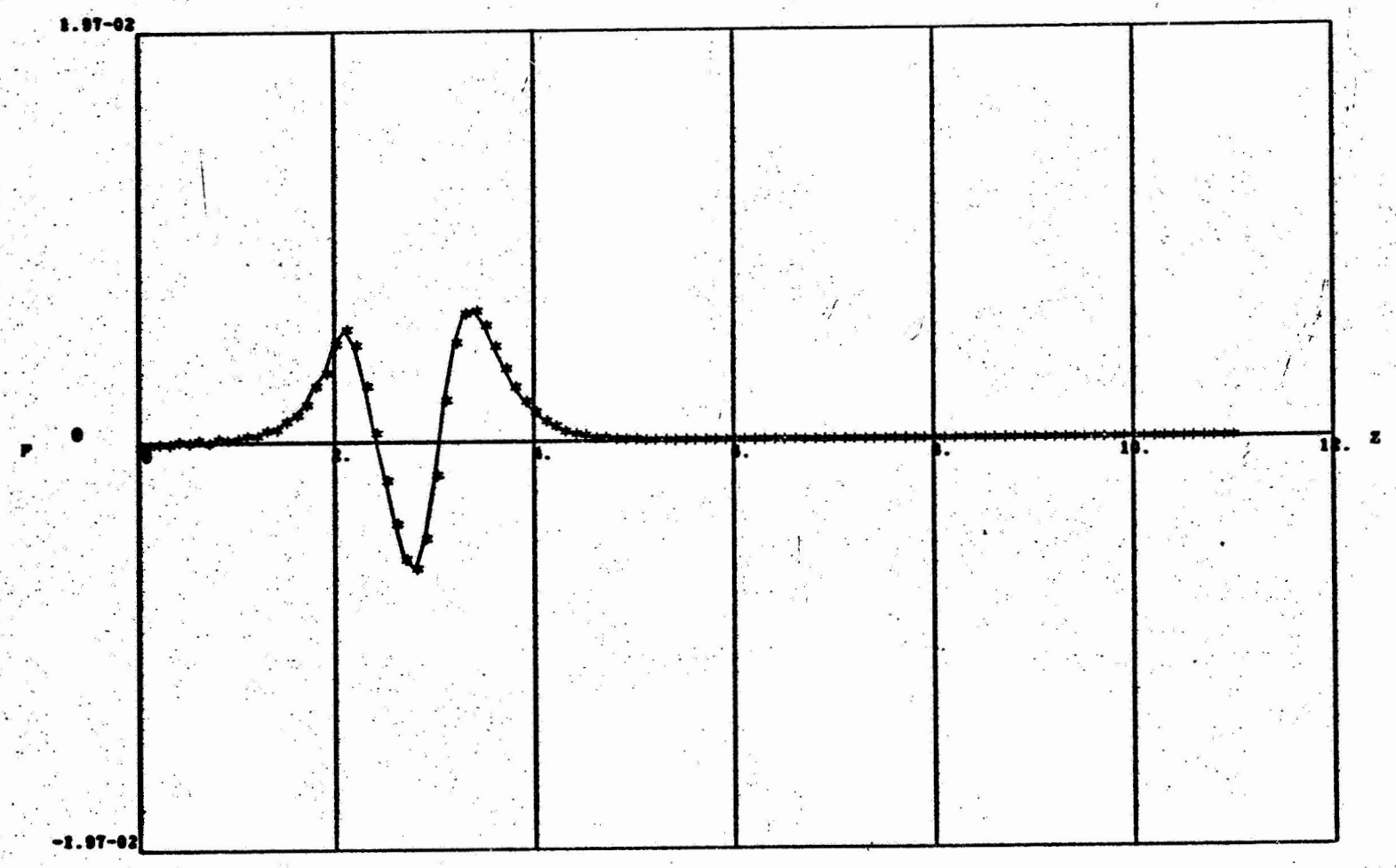

PLOT 5 - 25

RADIUS = .40,TIME = 2.499,AR = 1.00 PI,AM = 10.00 PERCENT,RE =100000.0,B.C.1

Figure 9d. Disturbance Stream Function

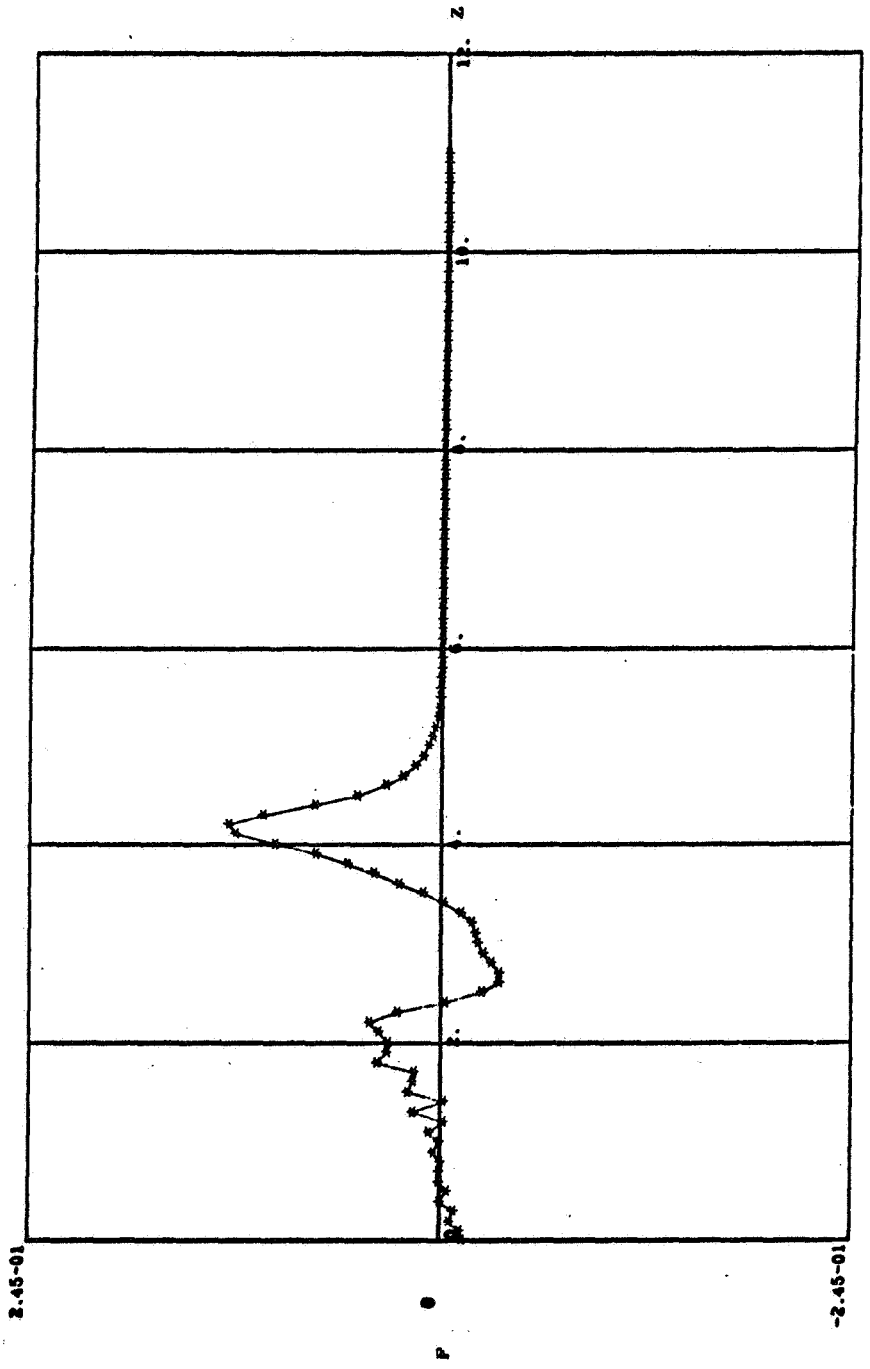

Figure 9e. Disturbance Stream Function

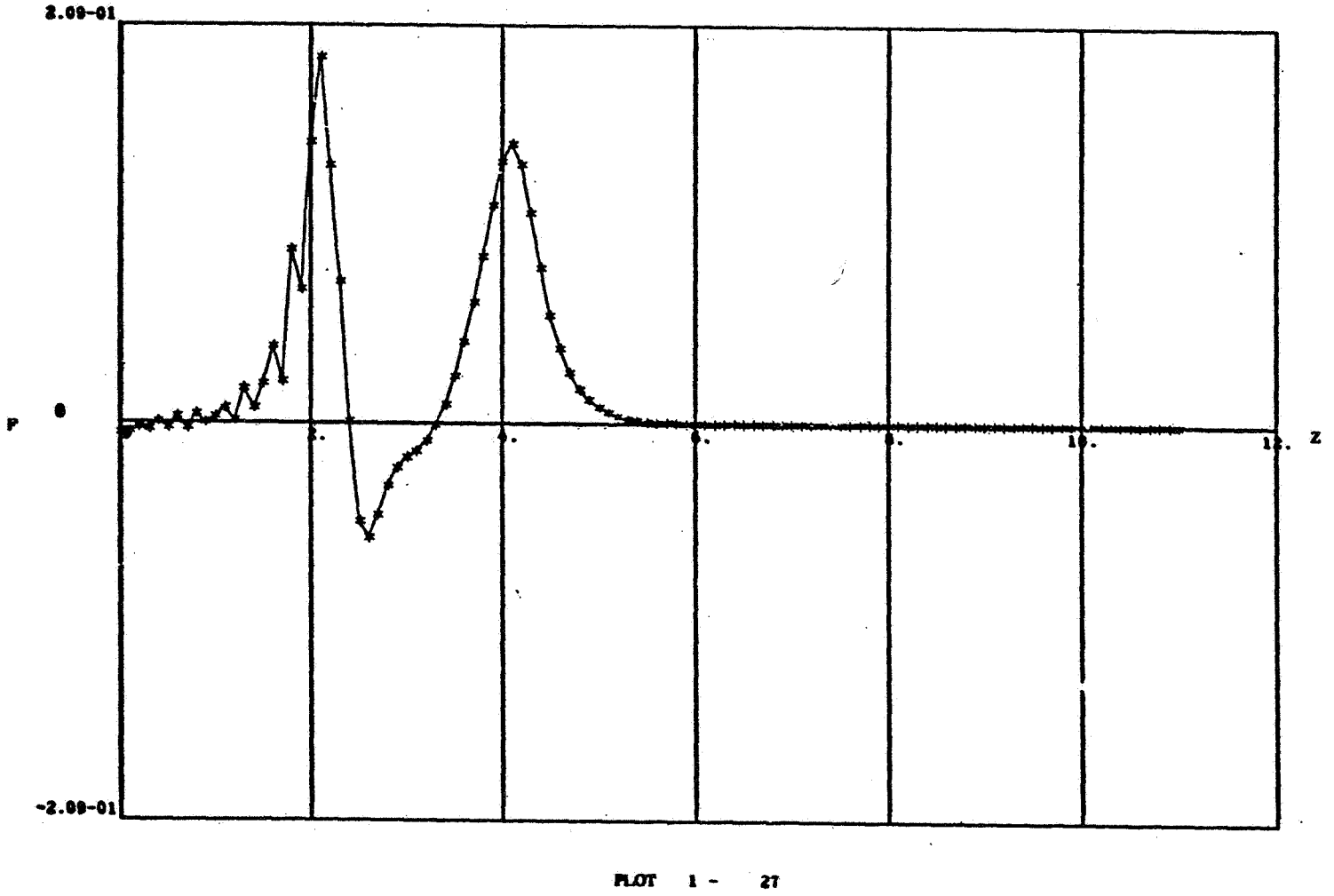

Figure 10a. Disturbance Stream Function

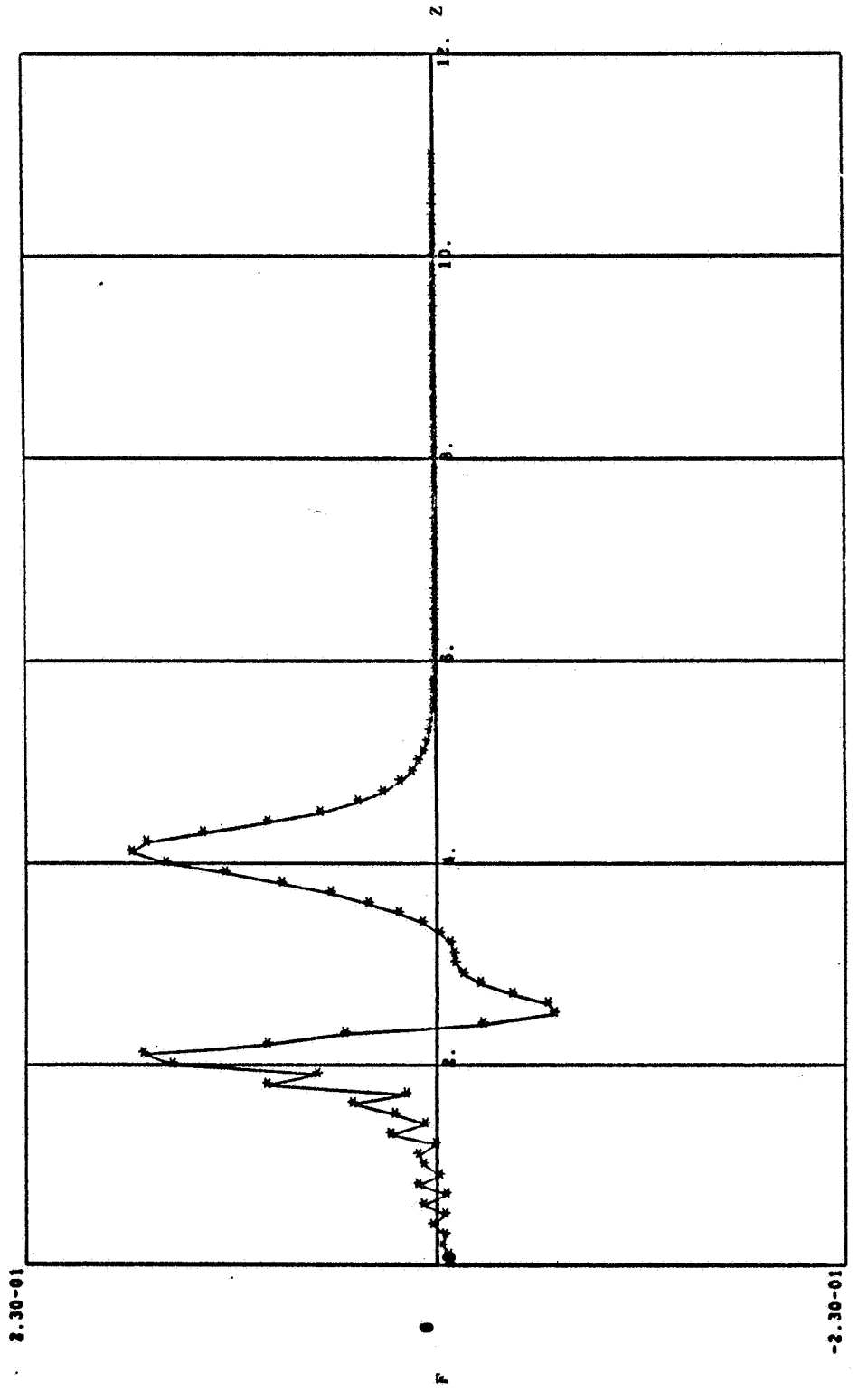

Figure 10b. Disturbance Stream Function

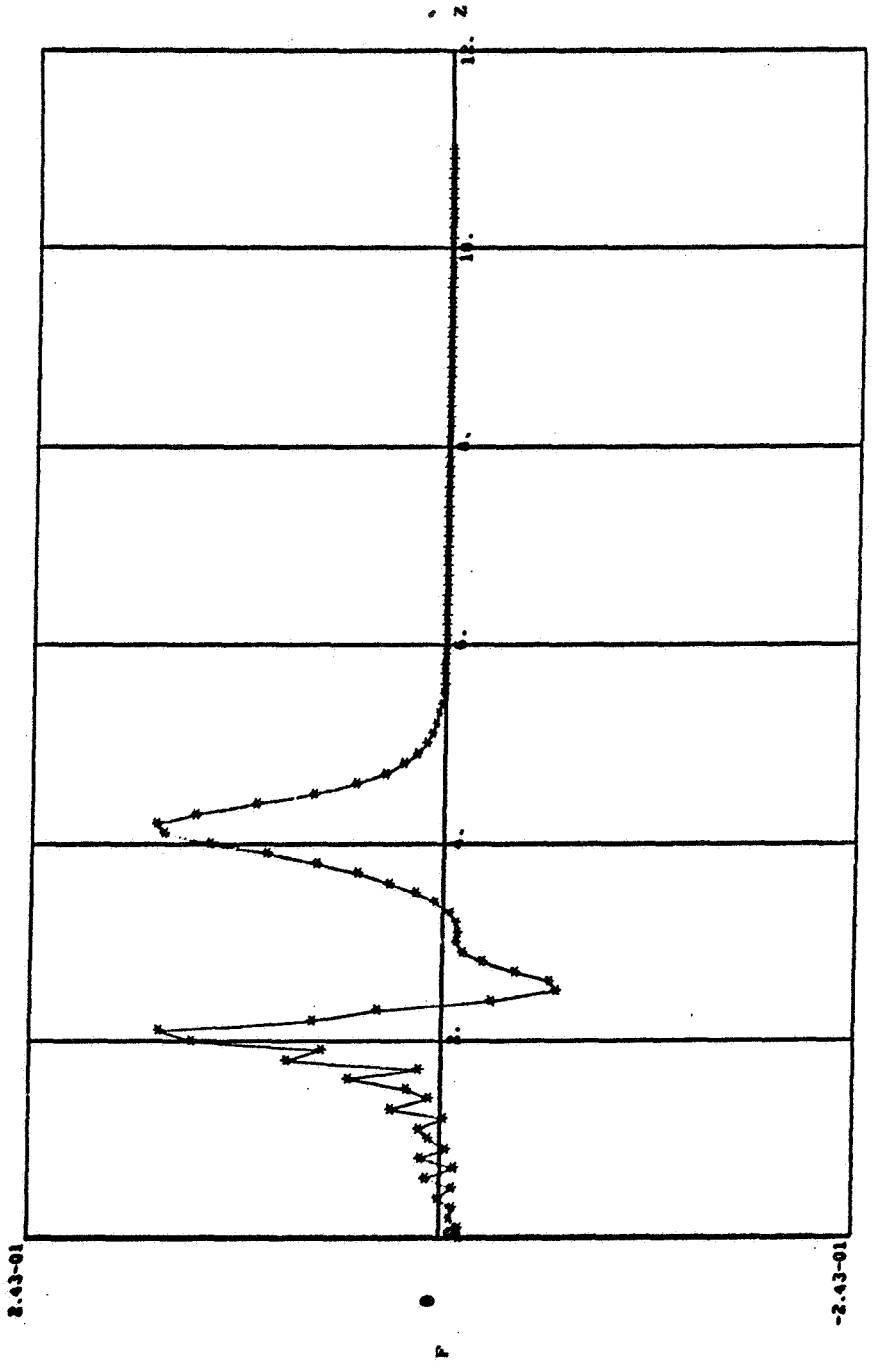

Figure 10c. Disturbance Stream Function

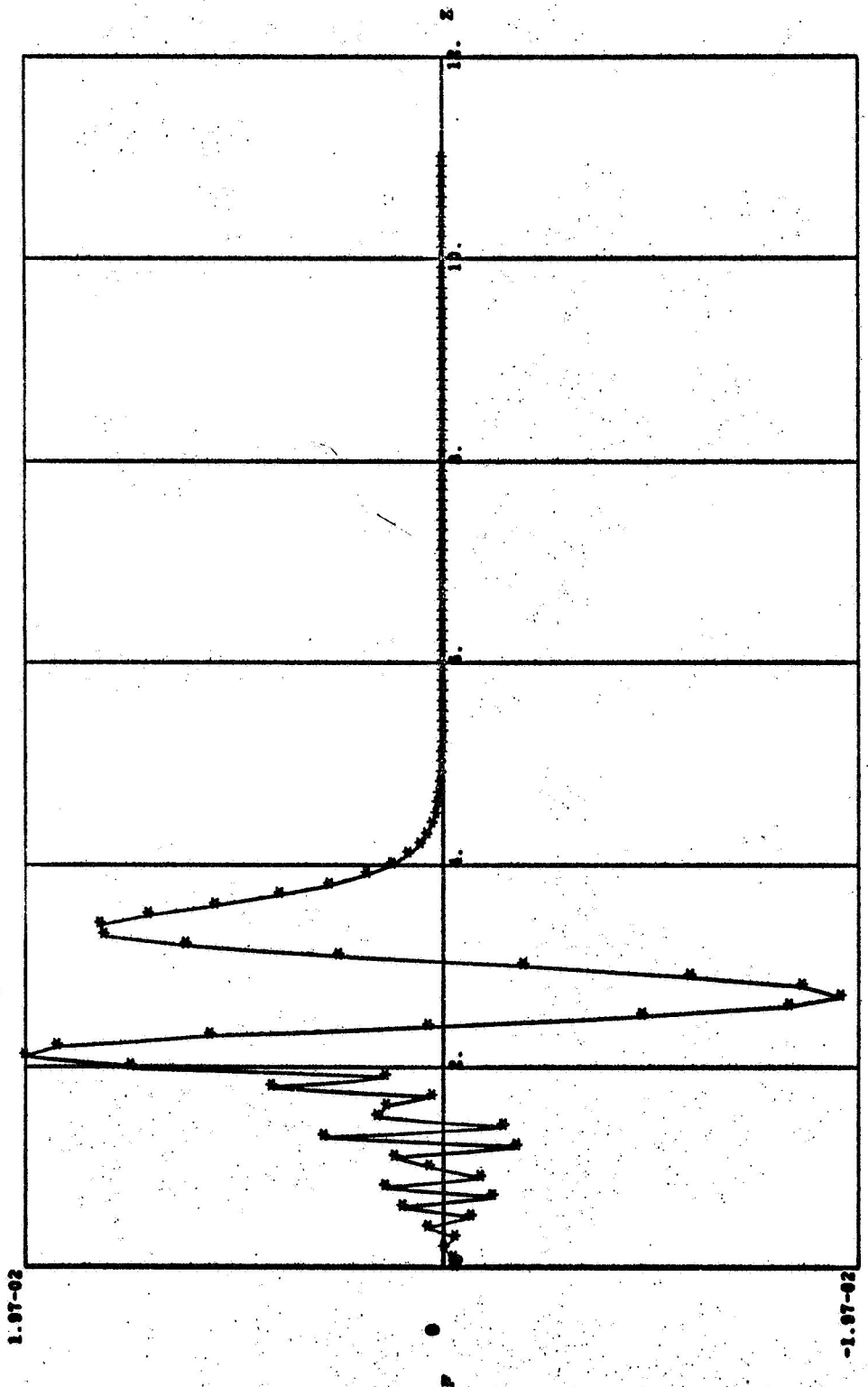

Figure 10d. Disturbance Stream Function

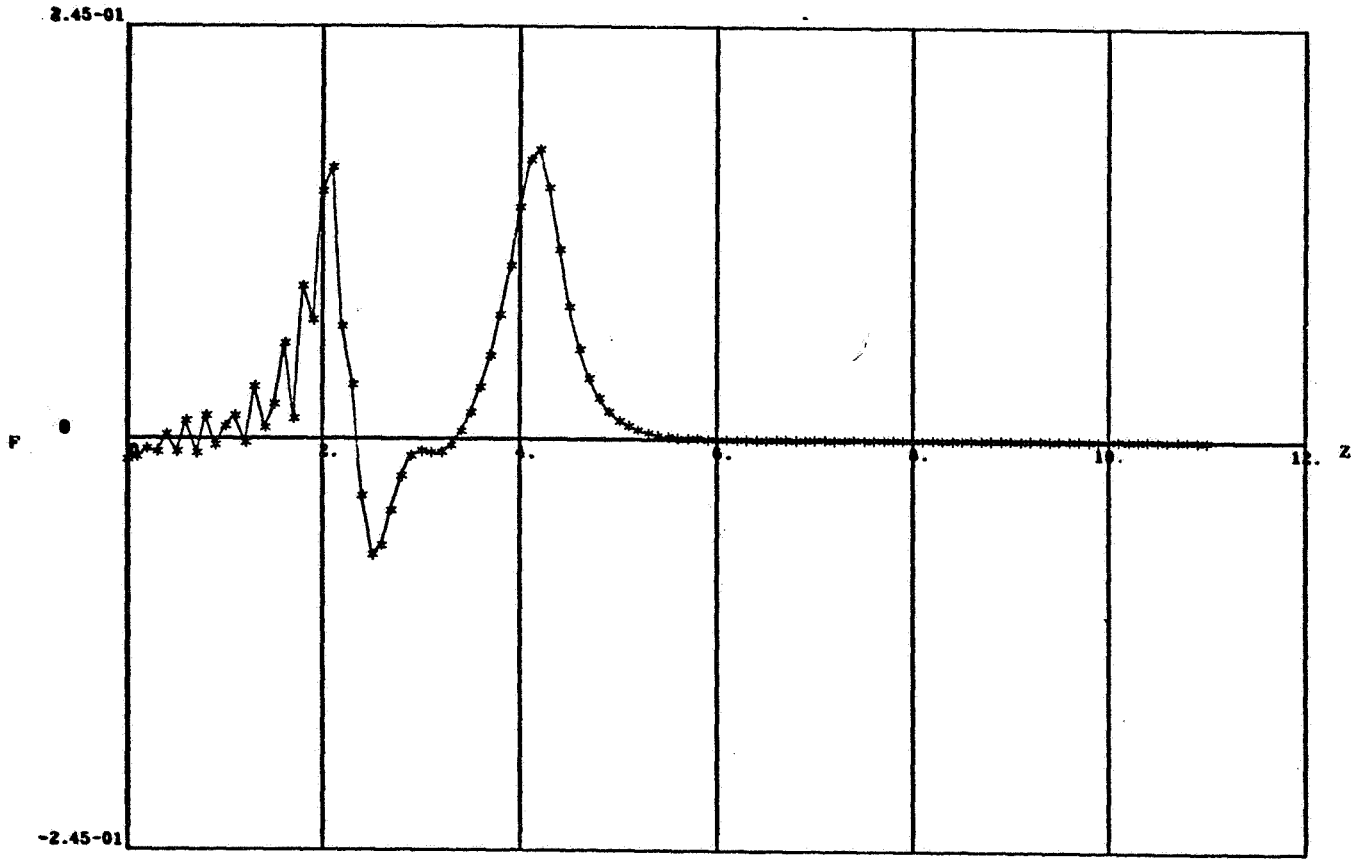

Figure 10e. Disturbance Stream Function

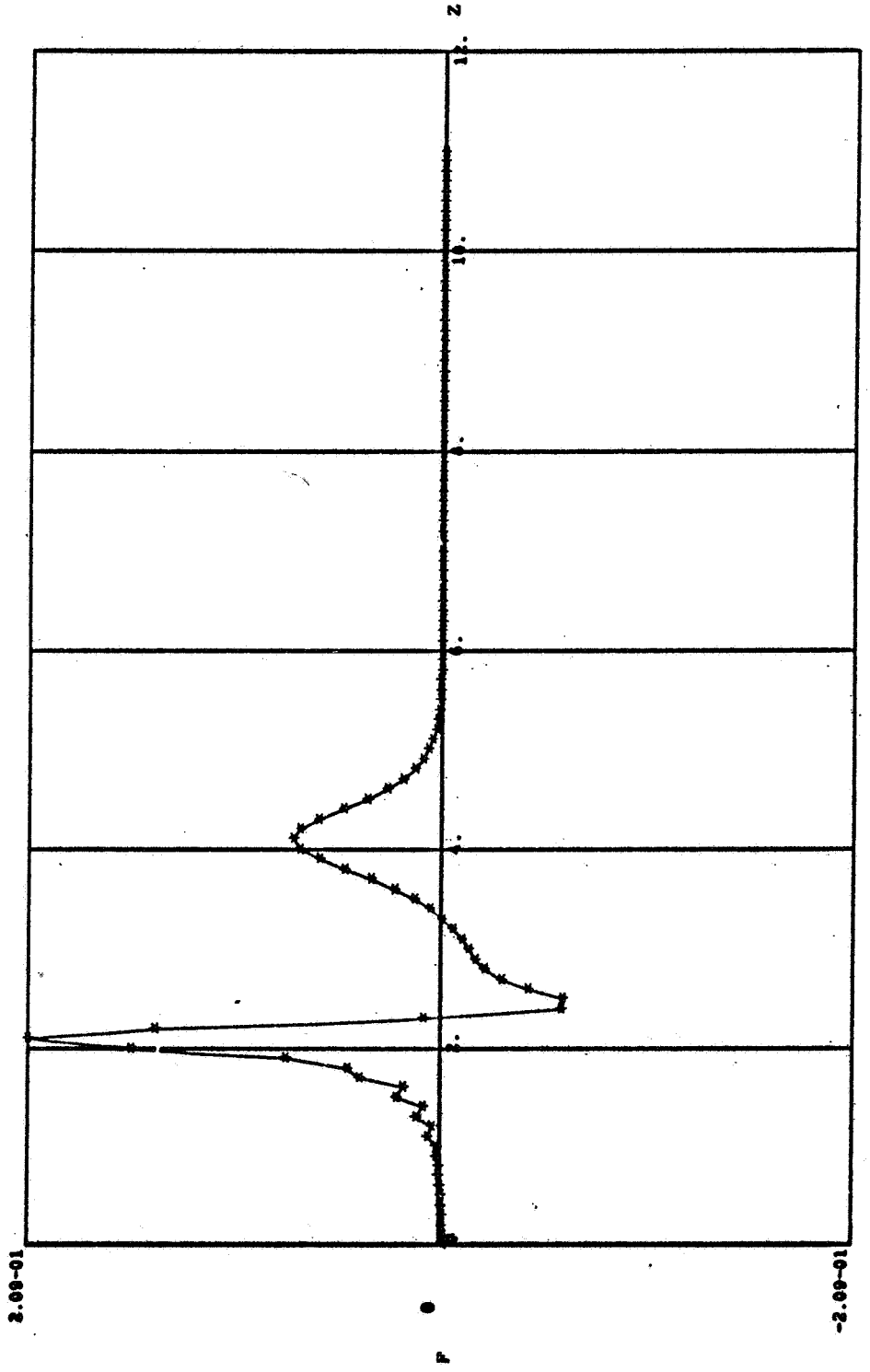

Figure 11a. Disturbance Stream Function

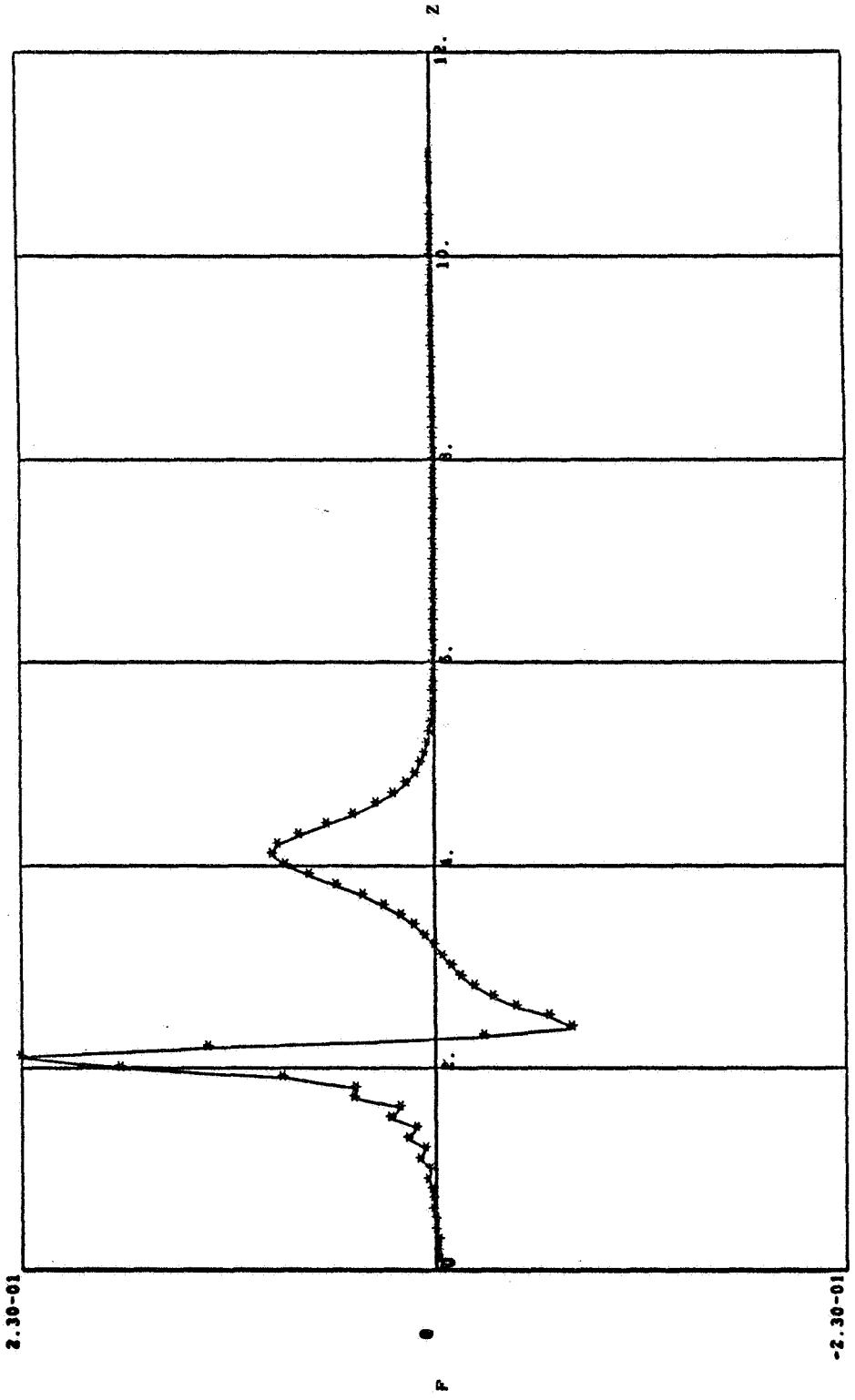

Figure 11b. Disturbance Stream Function

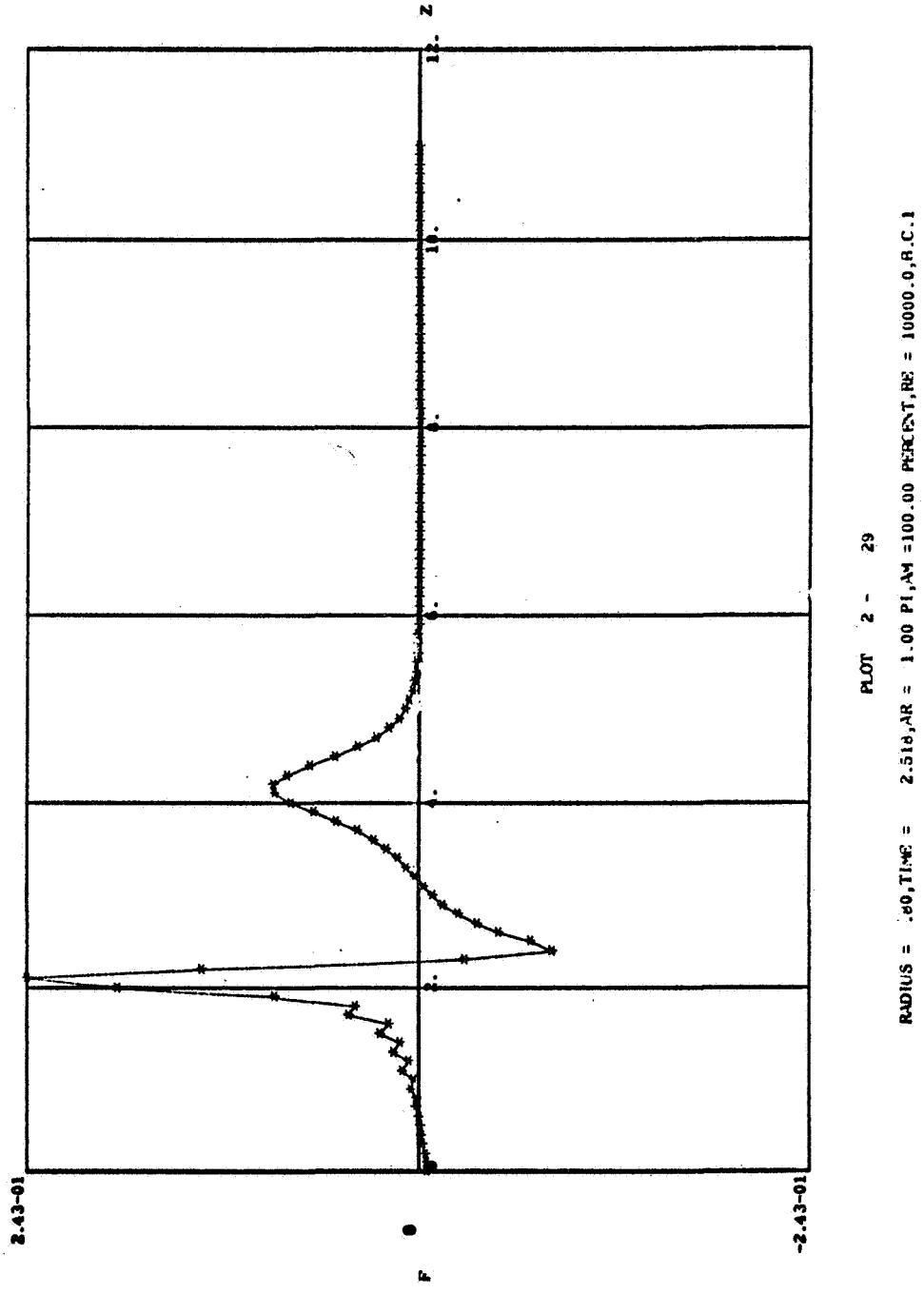

Figure 11c. Disturbance Stream Function

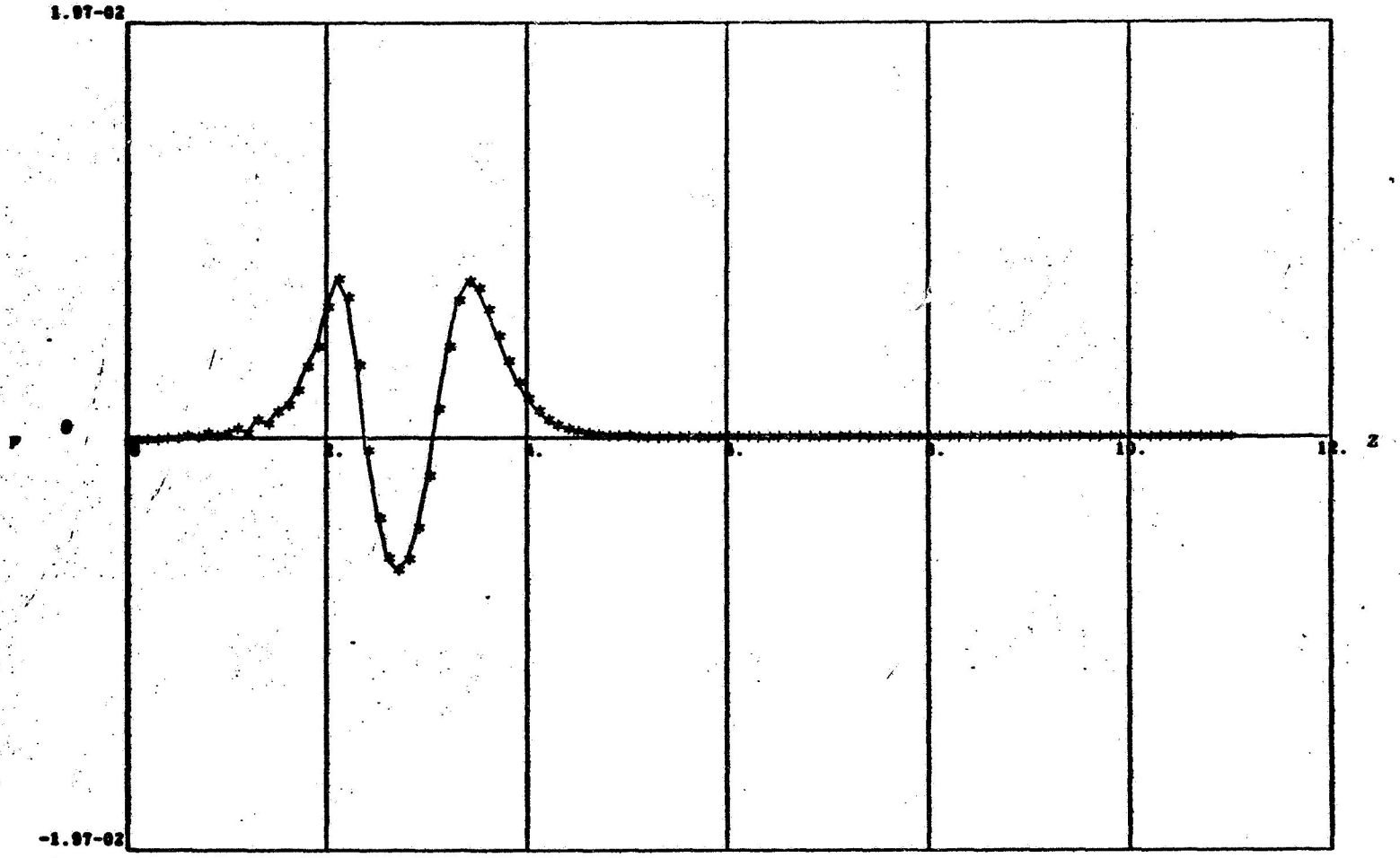

Figure 11d. Disturbance Stream Function

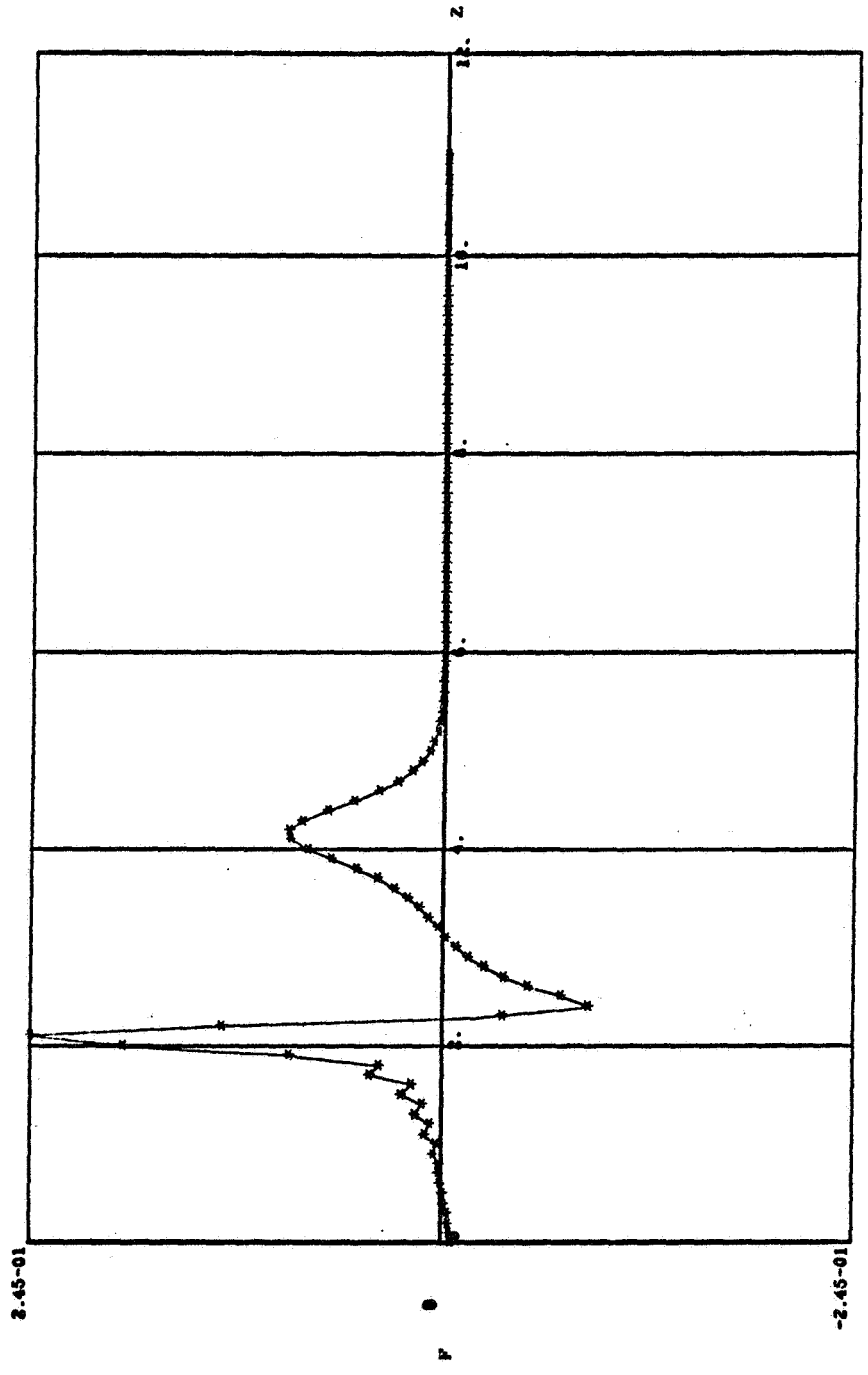

Figure 11e. Disturbance Stream Function

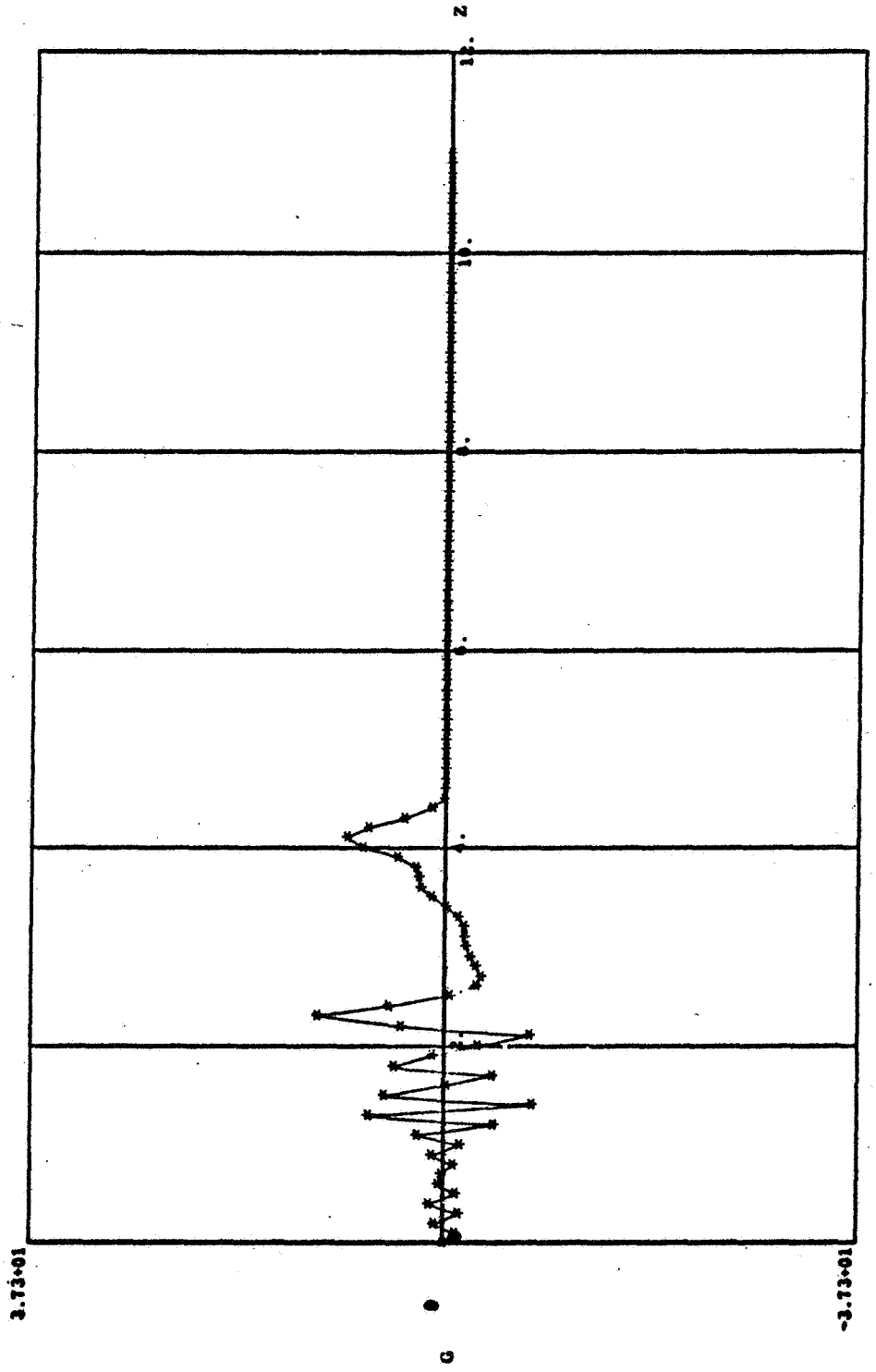

Figure 12a. Disturbance Vorticity

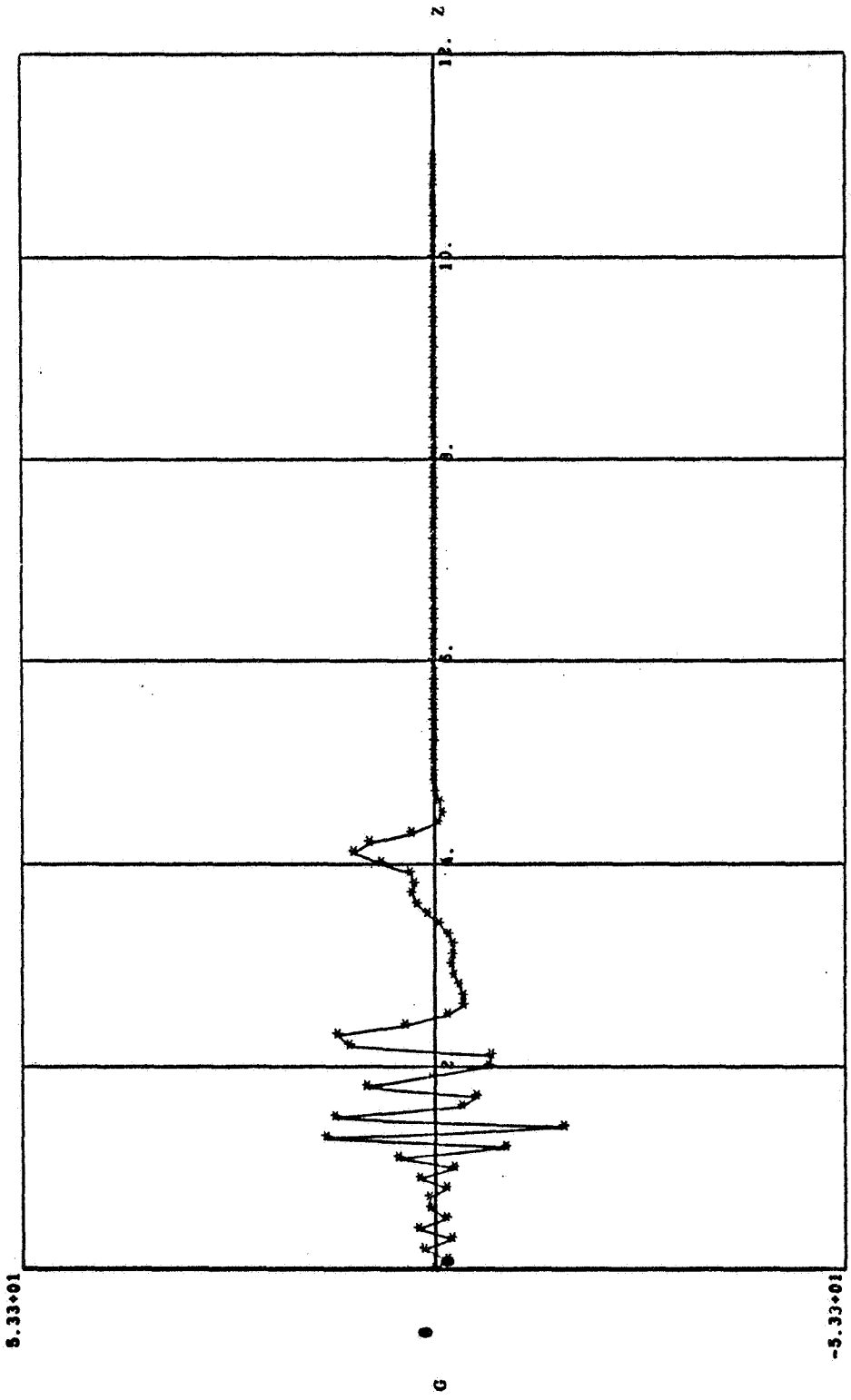

Figure 12b. Disturbance Vorticity

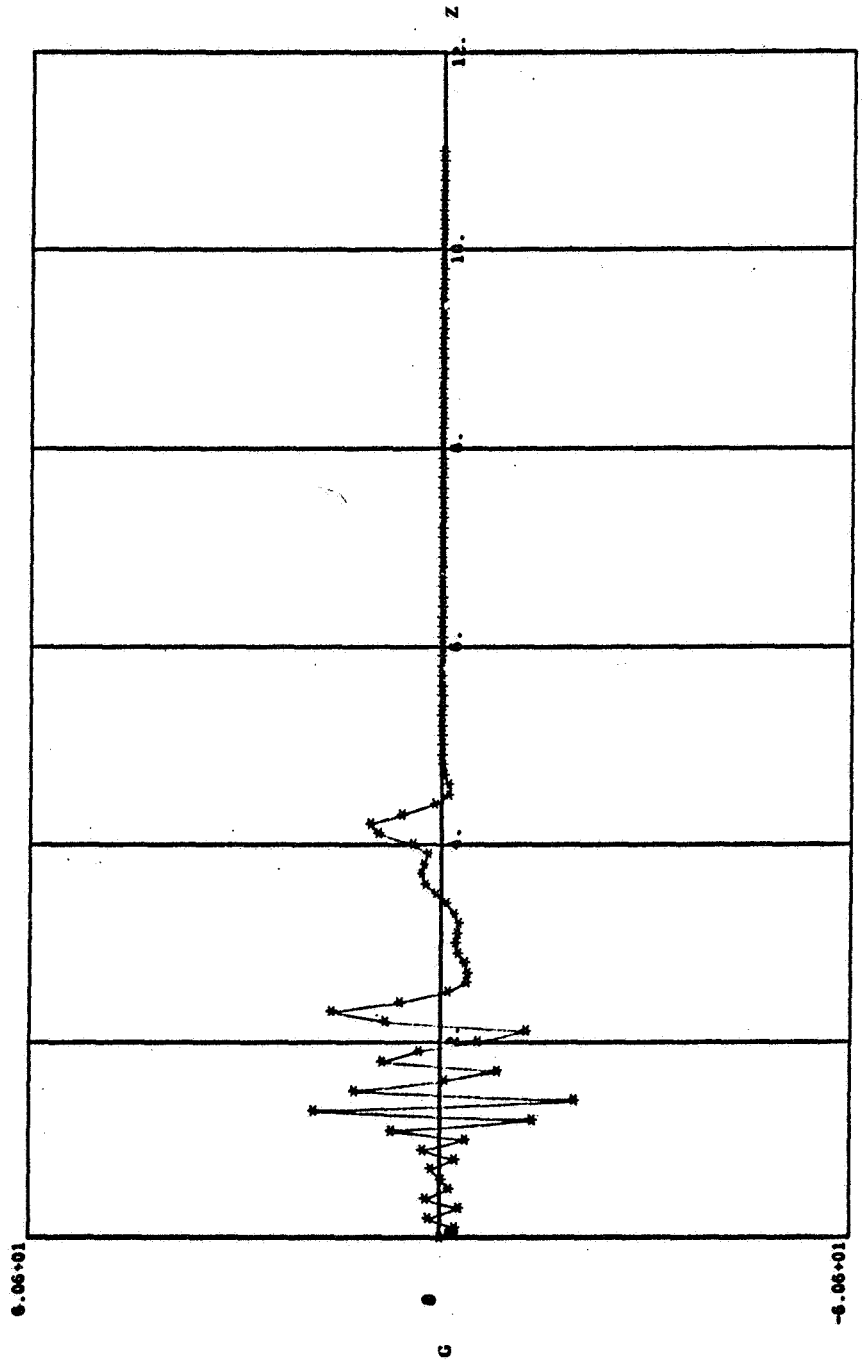

Figure 12c. Disturbance Vorticity

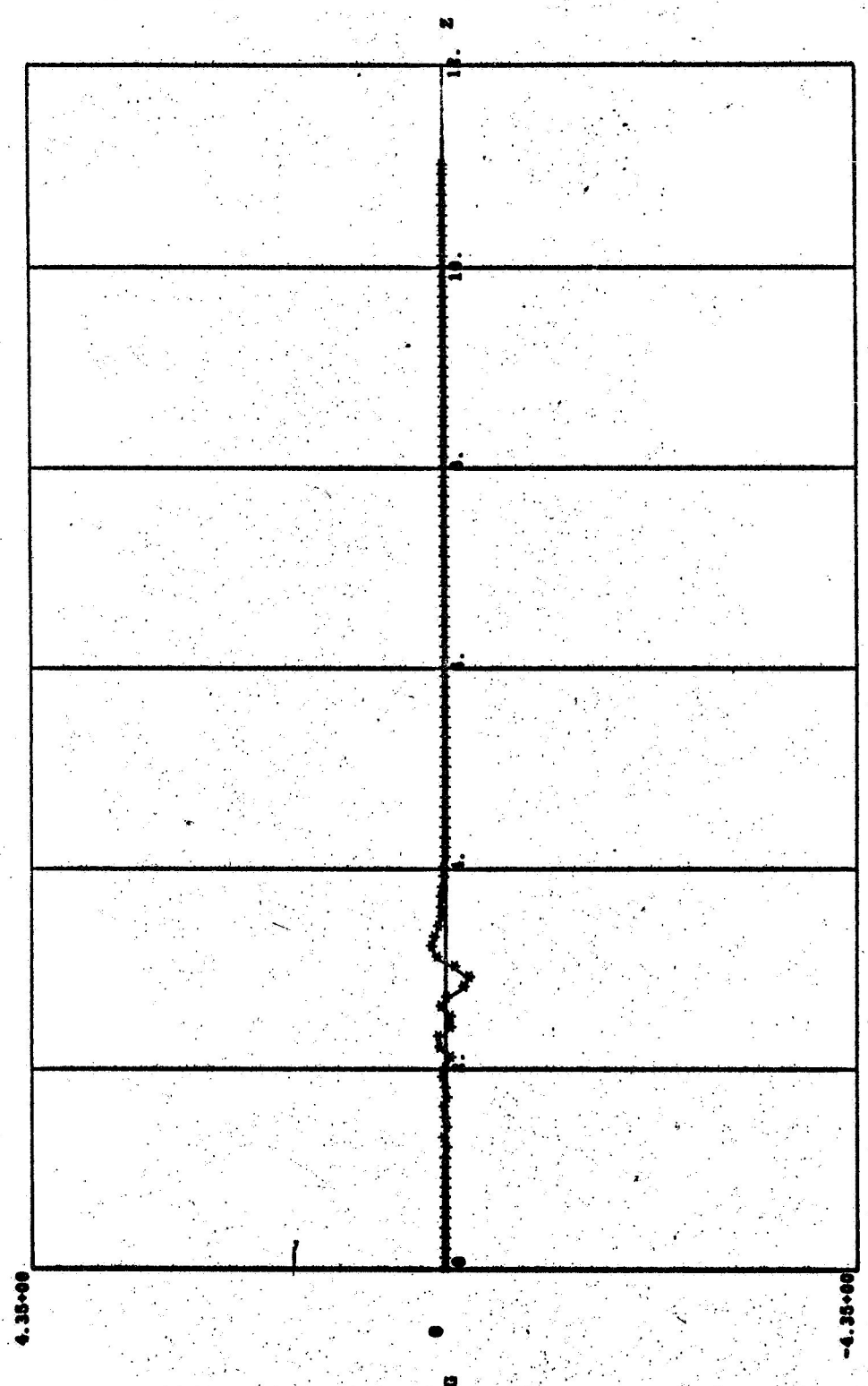

Figure 12d. Disturbance Vorticity

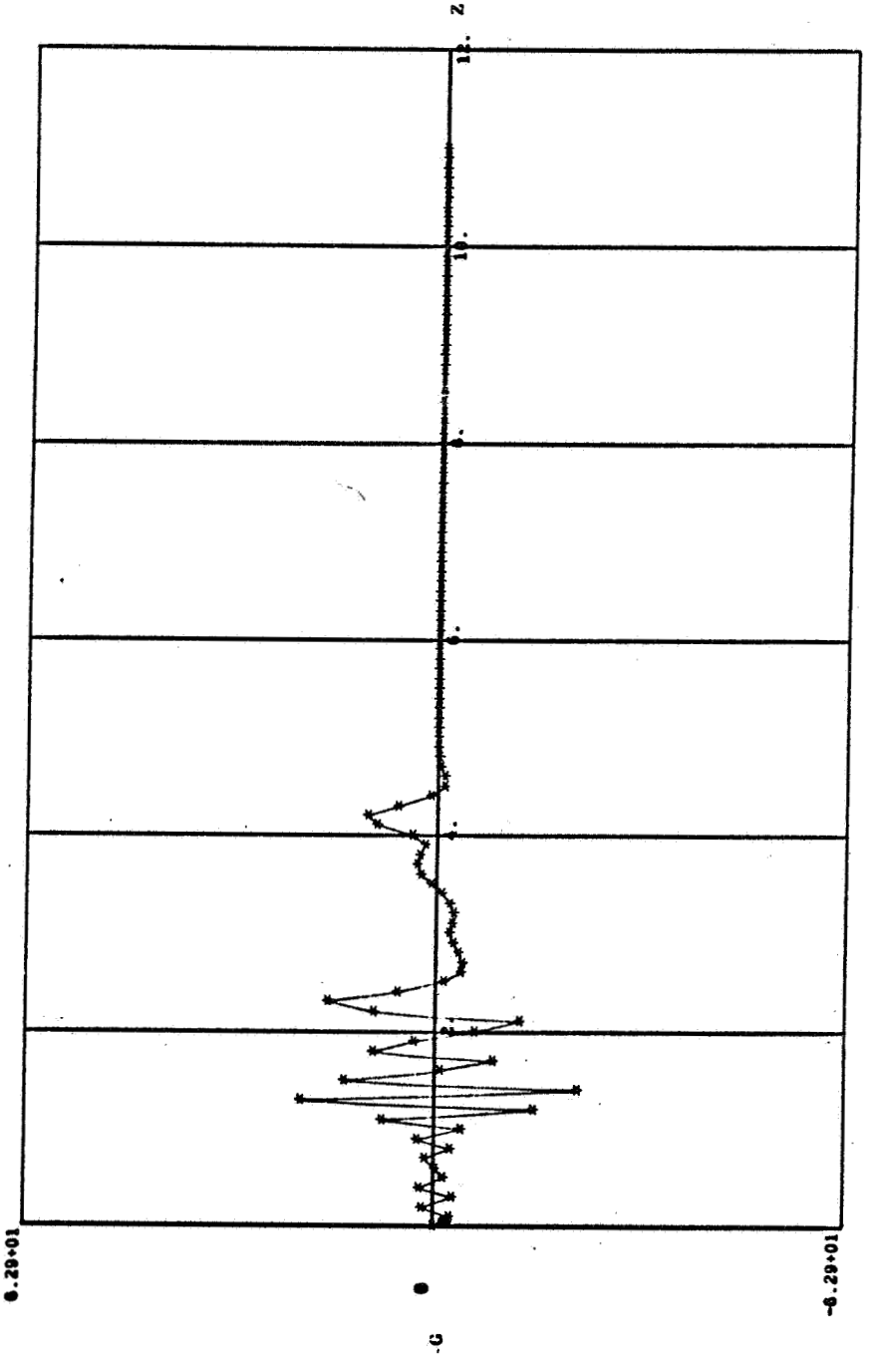

Figure 12e. Disturbance Vorticity

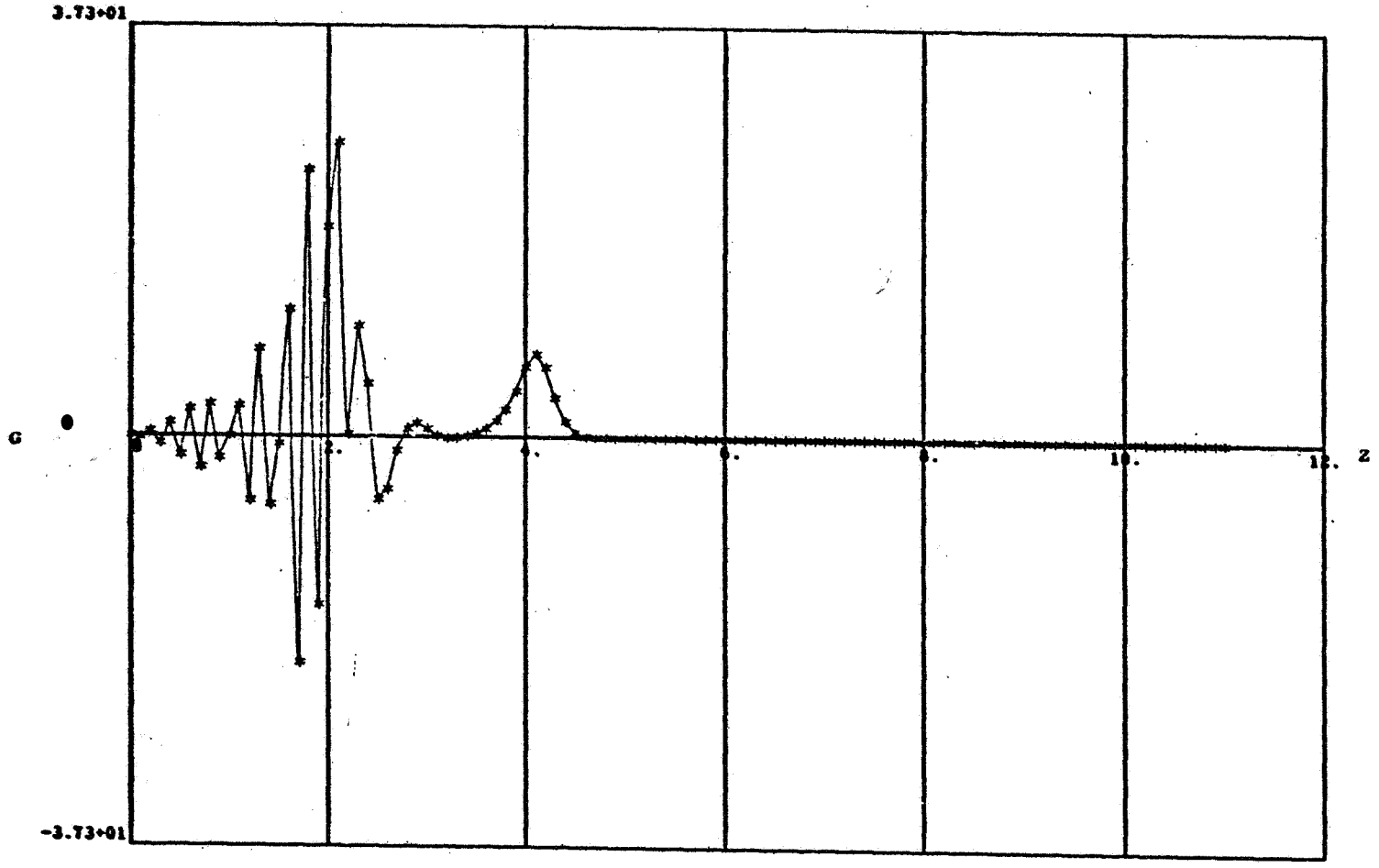

PLOT 1 - 28

RADIUS = .60,TIME = 2.521,AR = 1.00 PI,AM =100.00 PERCENT,RE = 1000.0,B.C.1

Figure 13a. Disturbance Vorticity

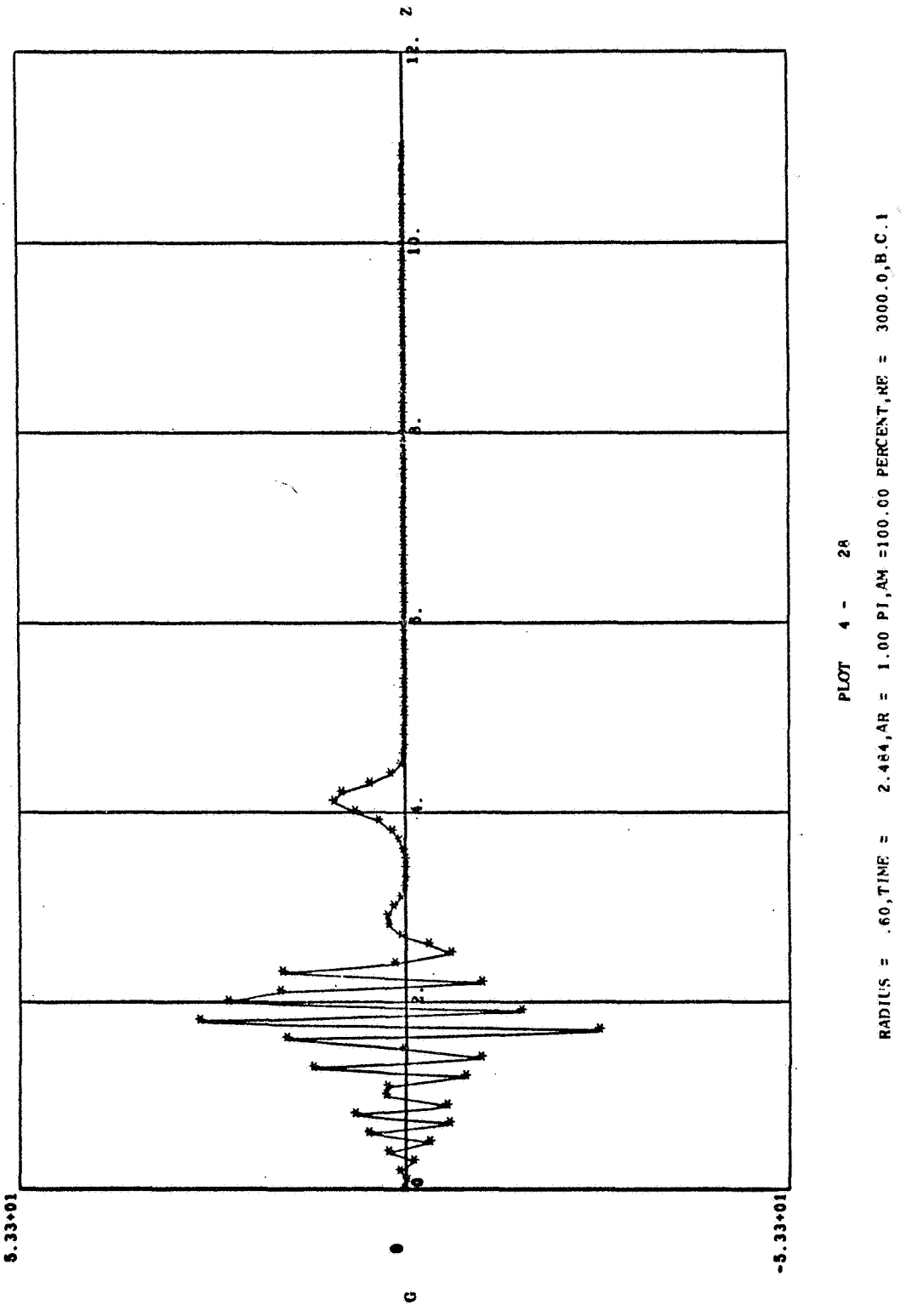

Figure 13b. Disturbance Vorticity

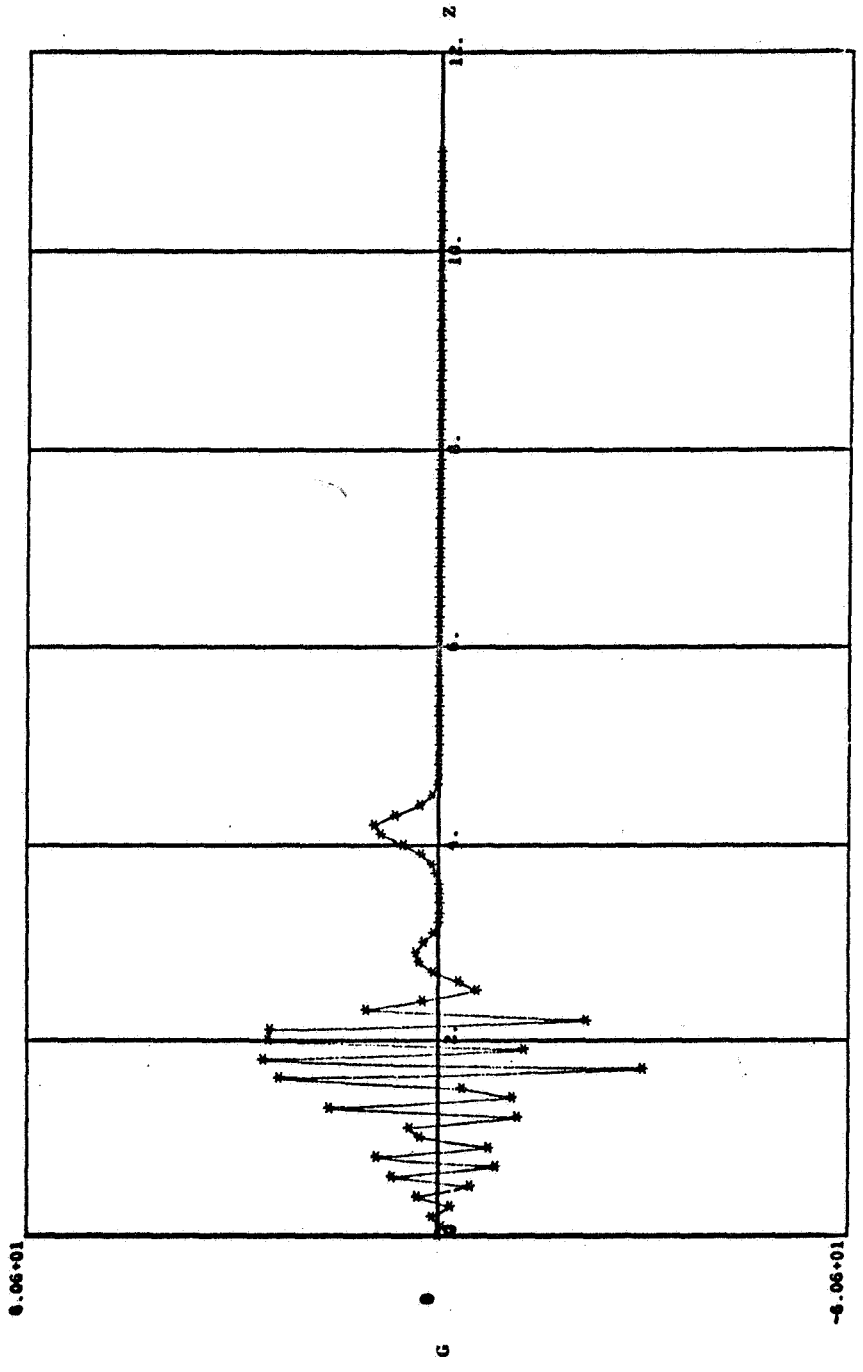

Figure 13c. Disturbance Vorticity

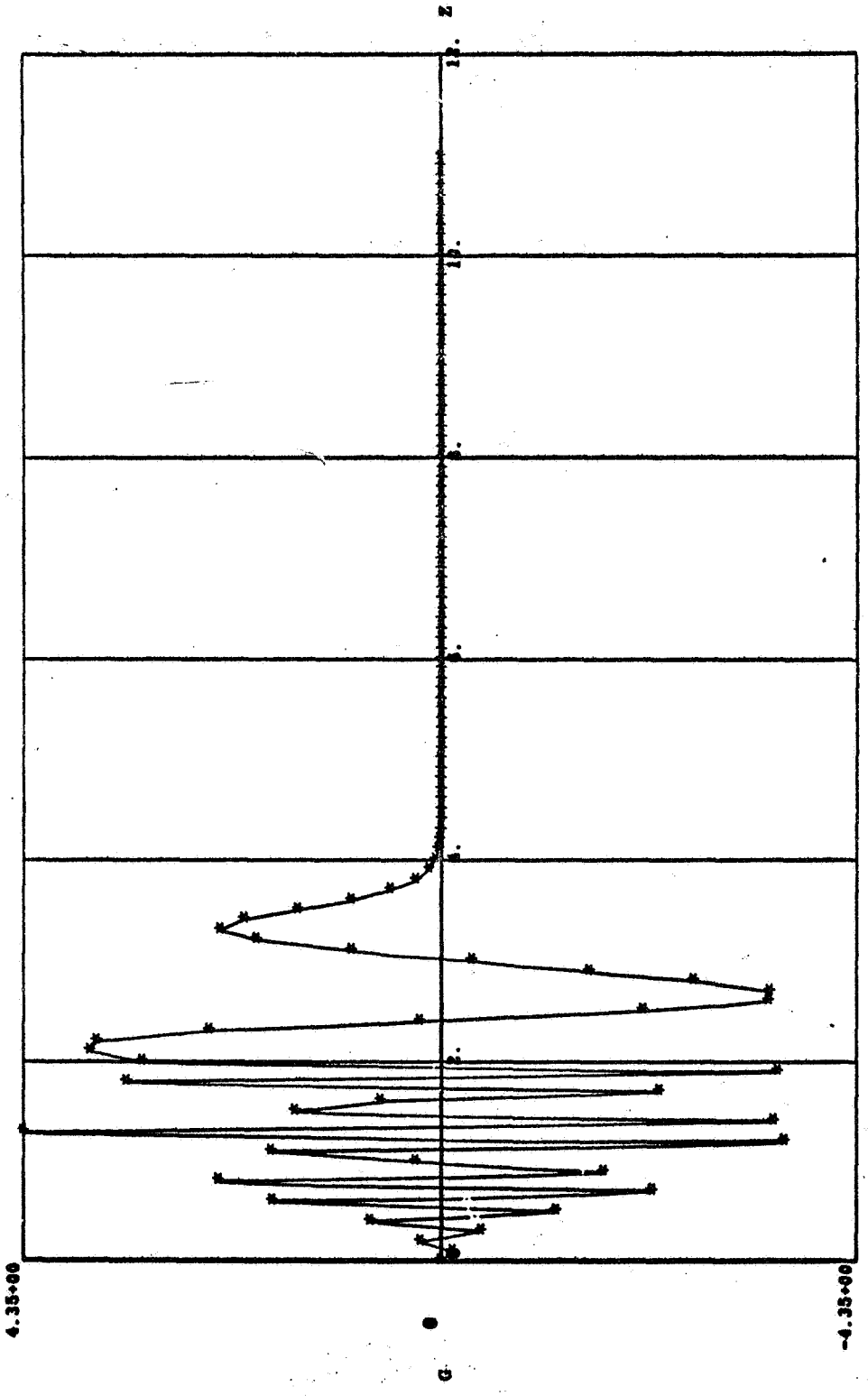

Figure 13d. Disturbance Vorticity

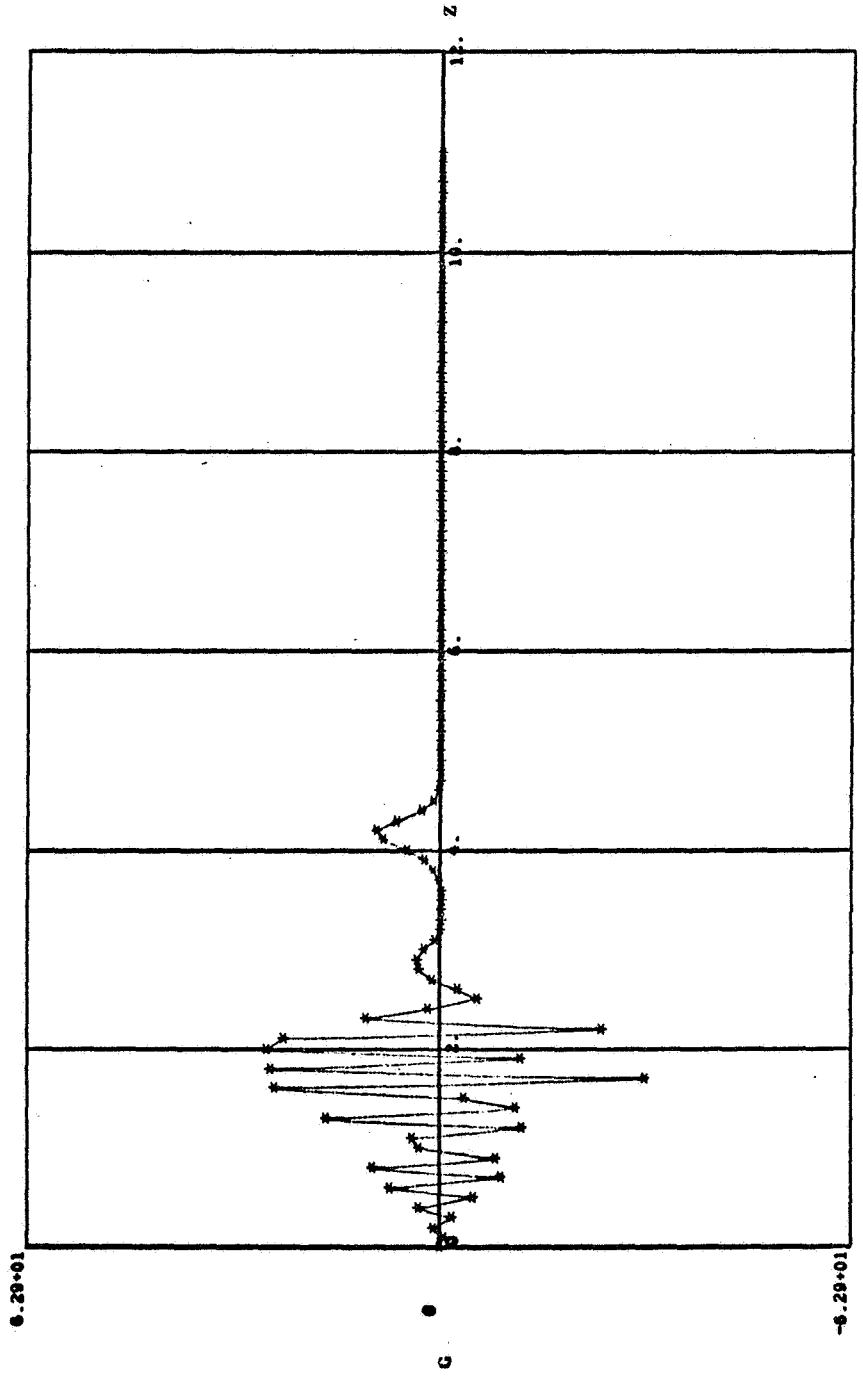

Figure 13e. Disturbance Vorticity

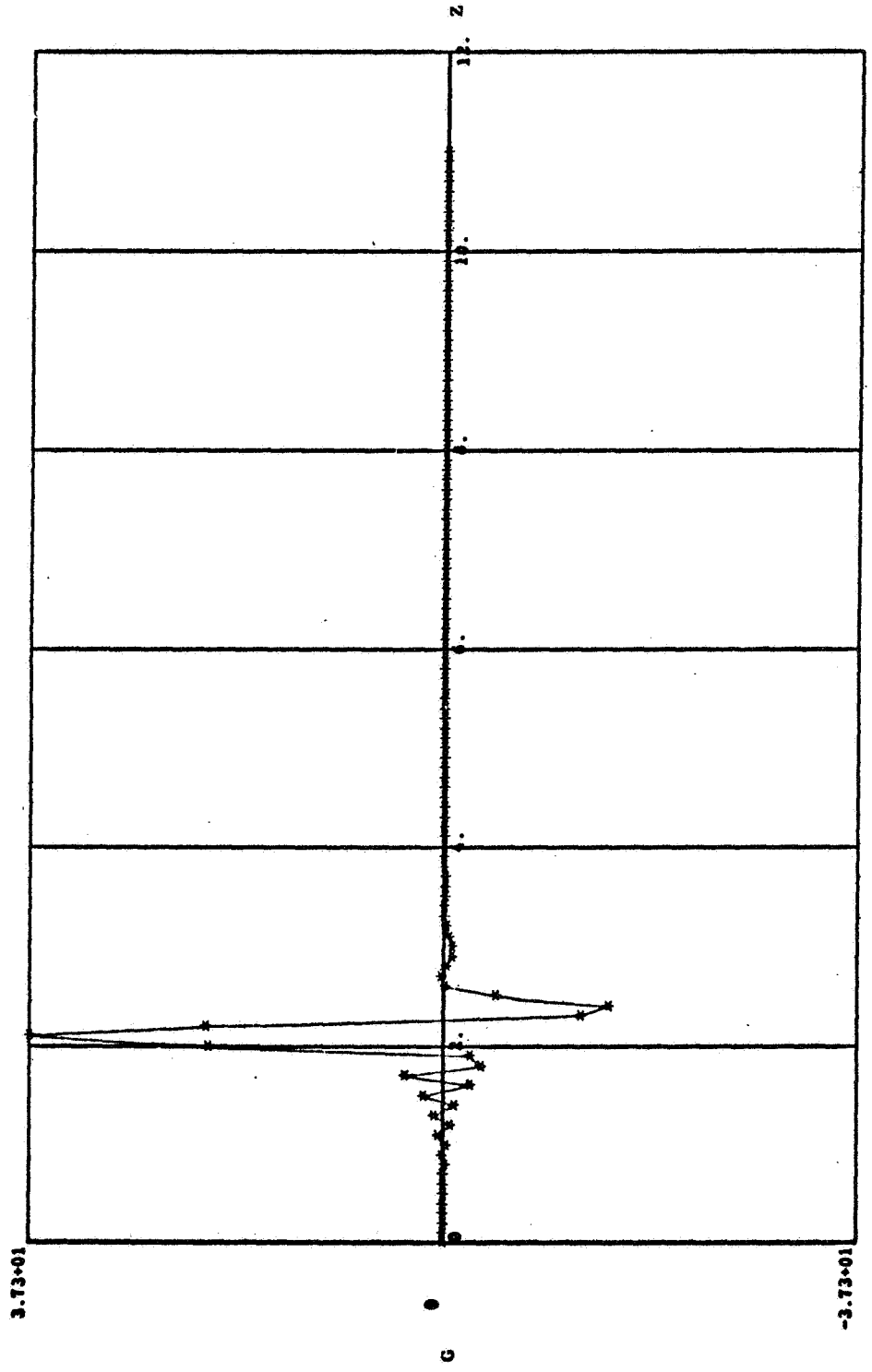

Figure 14a. Disturbance Vorticity

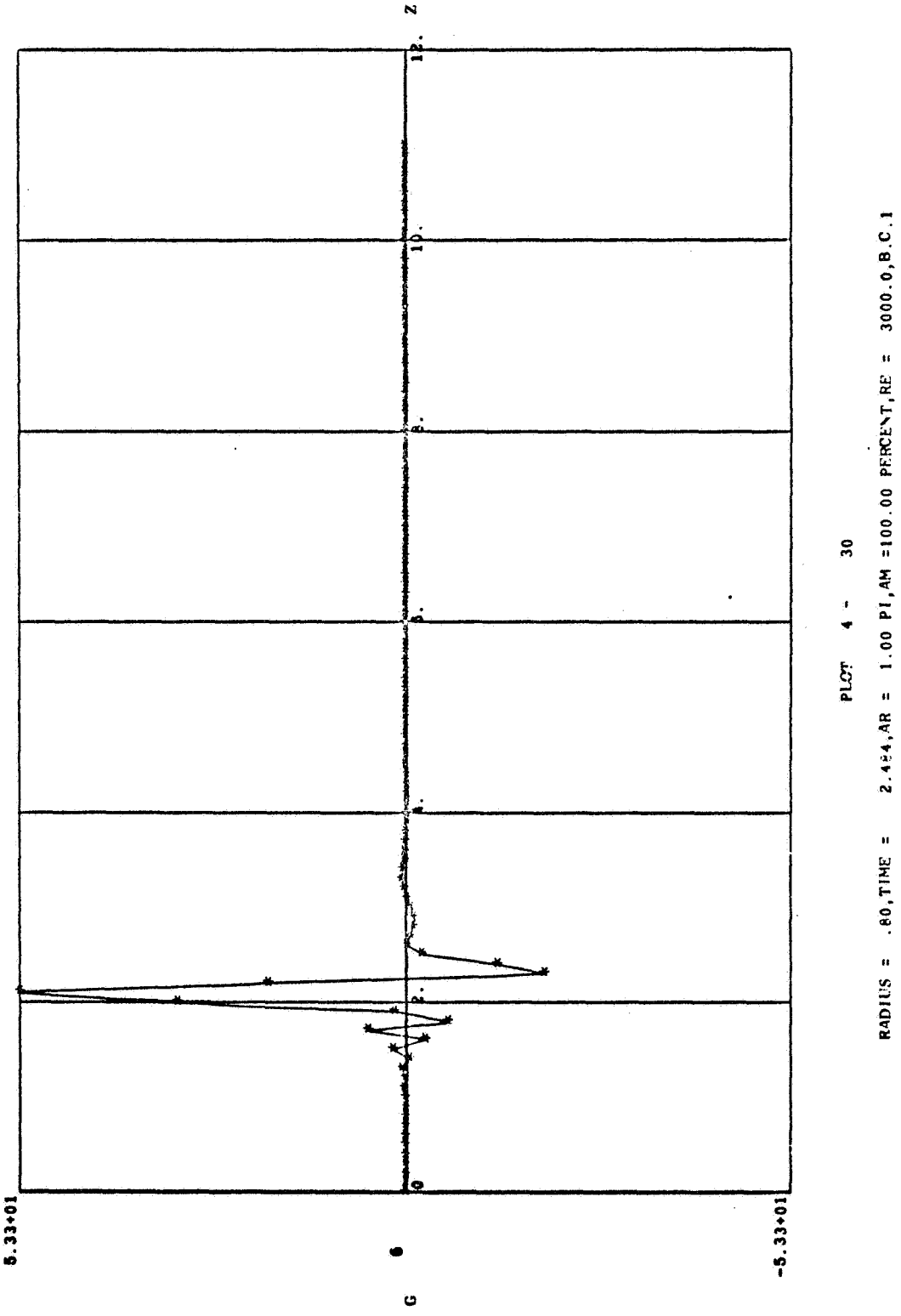

Figure 14b. Disturbance Vorticity

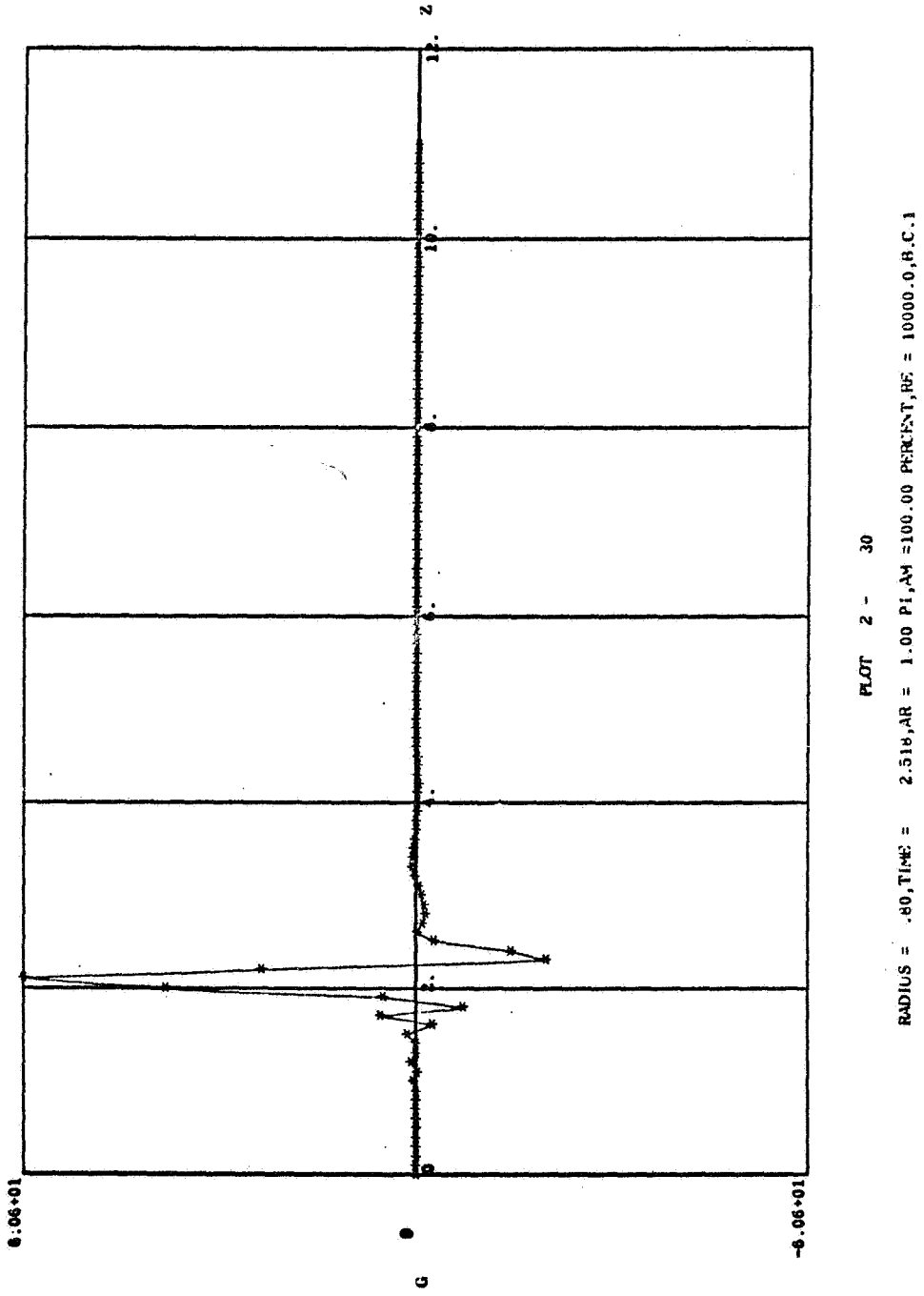

Figure 14c. Disturbance Vorticity

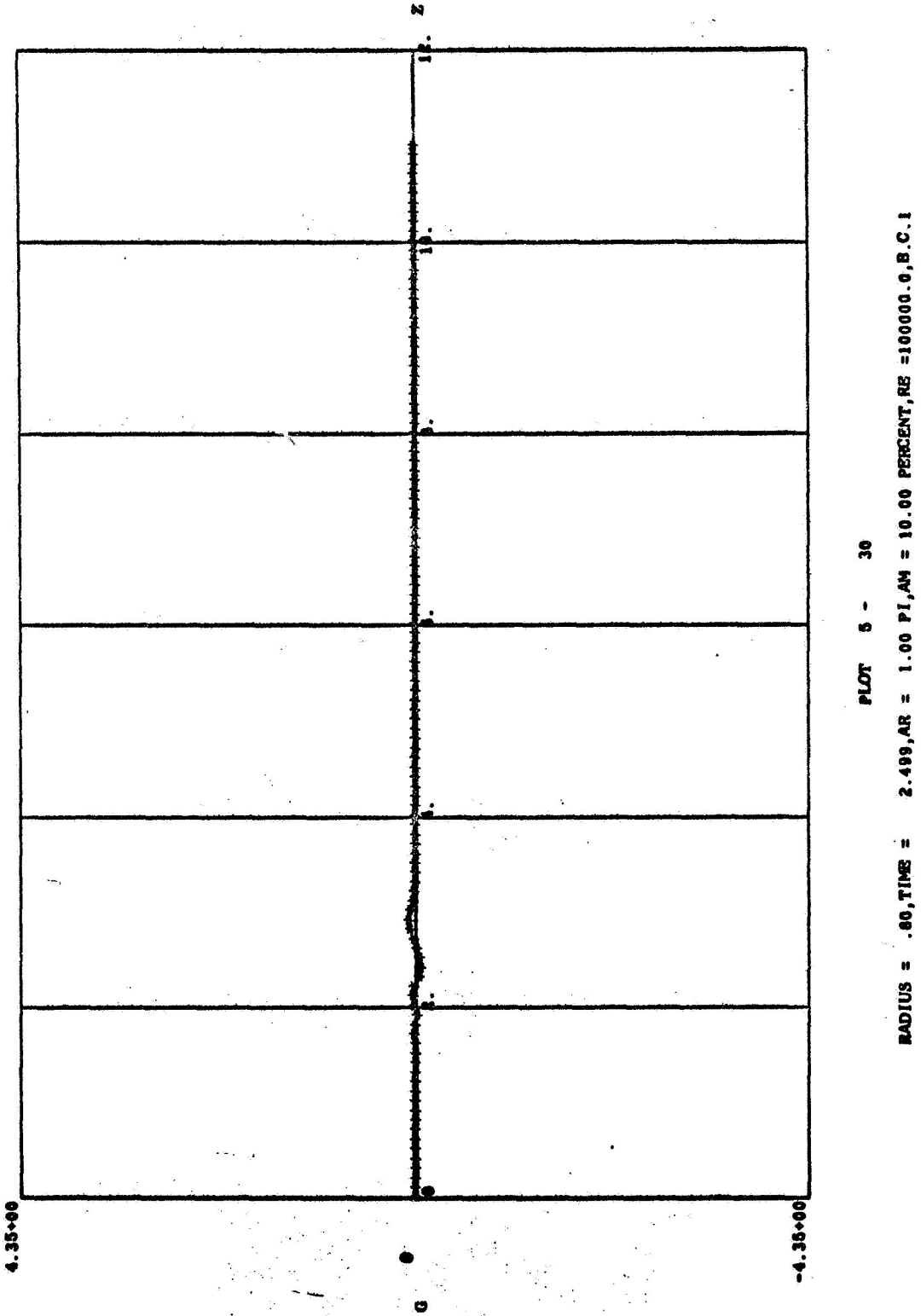

Figure 14d. Disturbance Vorticity

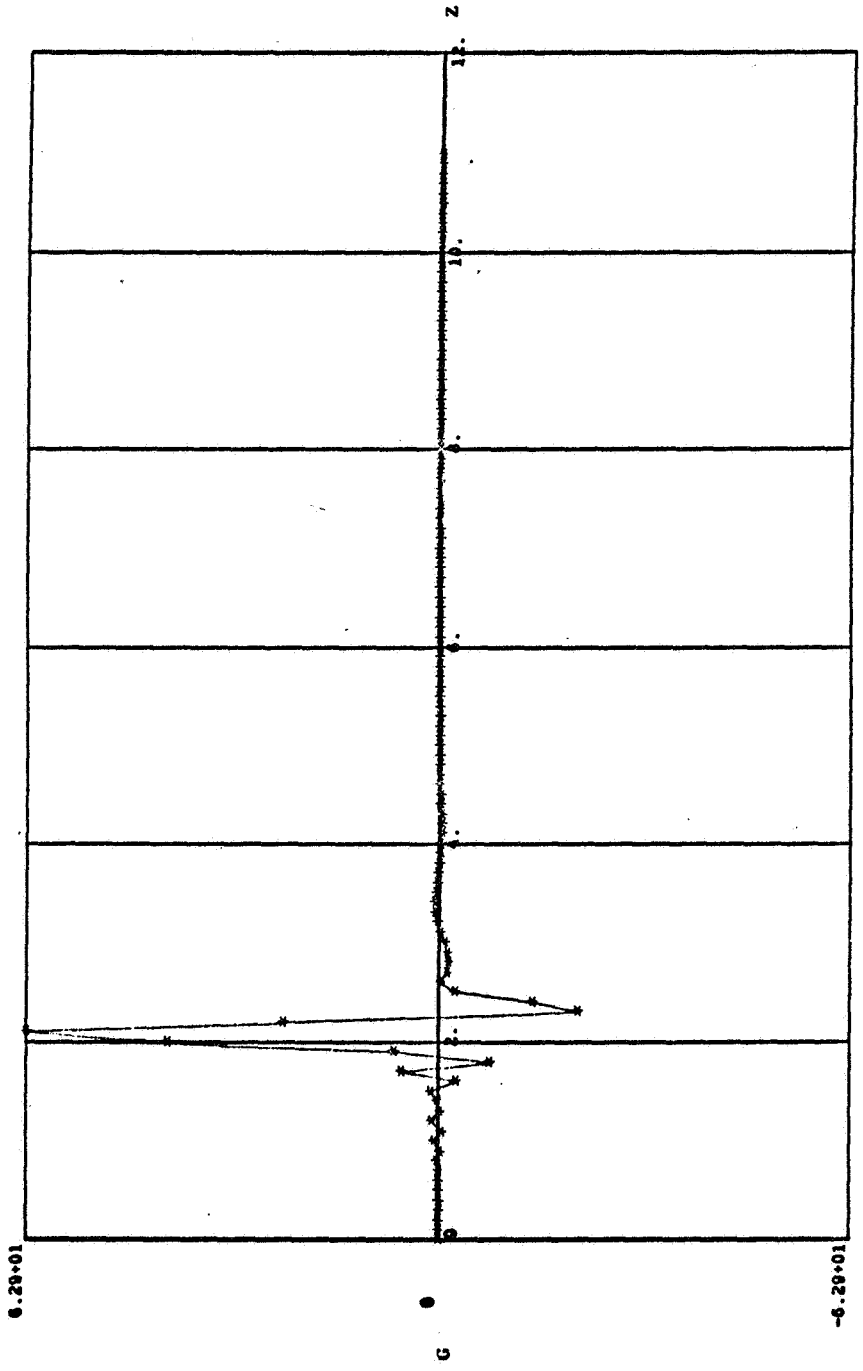

Figure 14e. Disturbance Vorticity

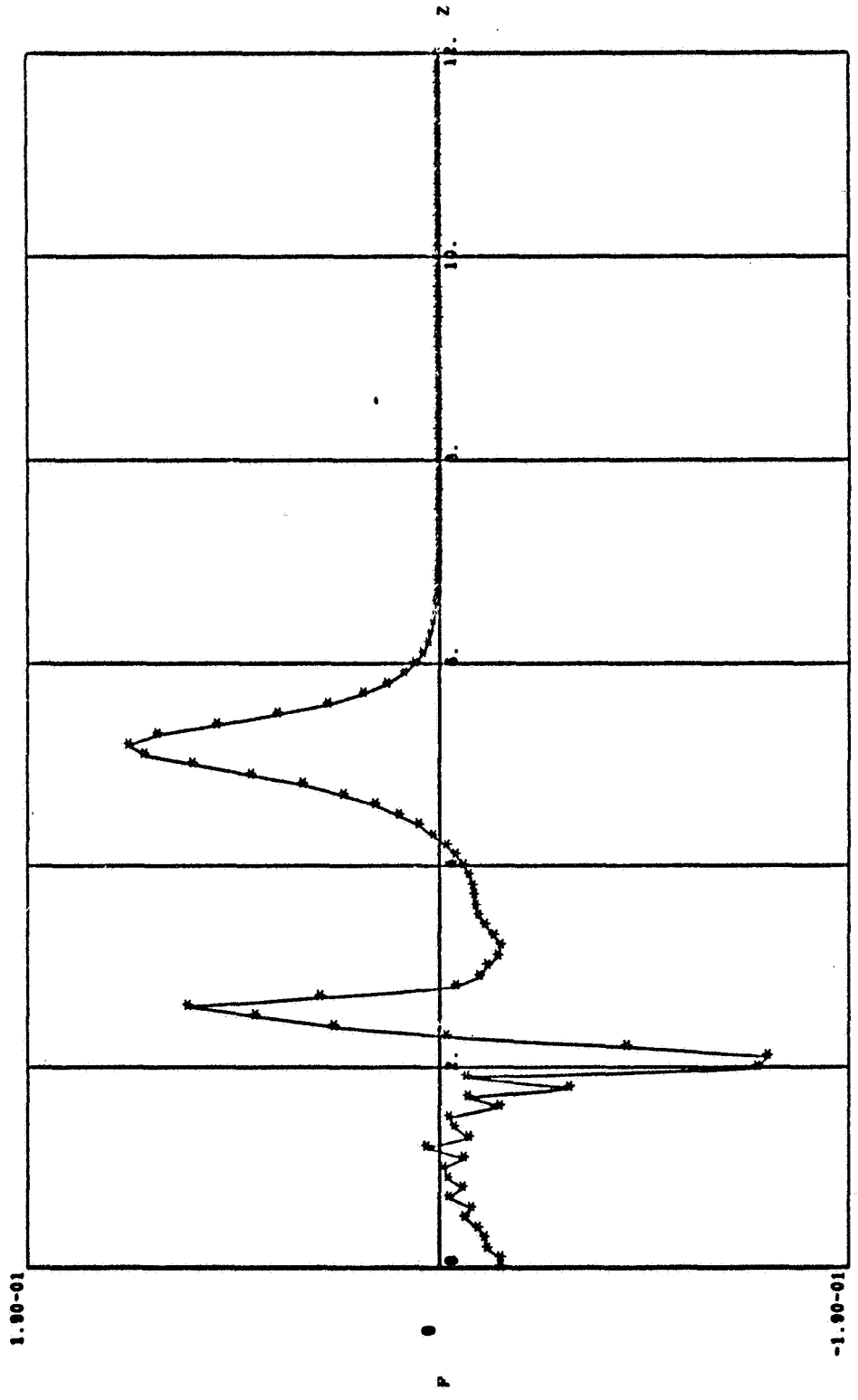

Figure 15a. Disturbance Stream Function

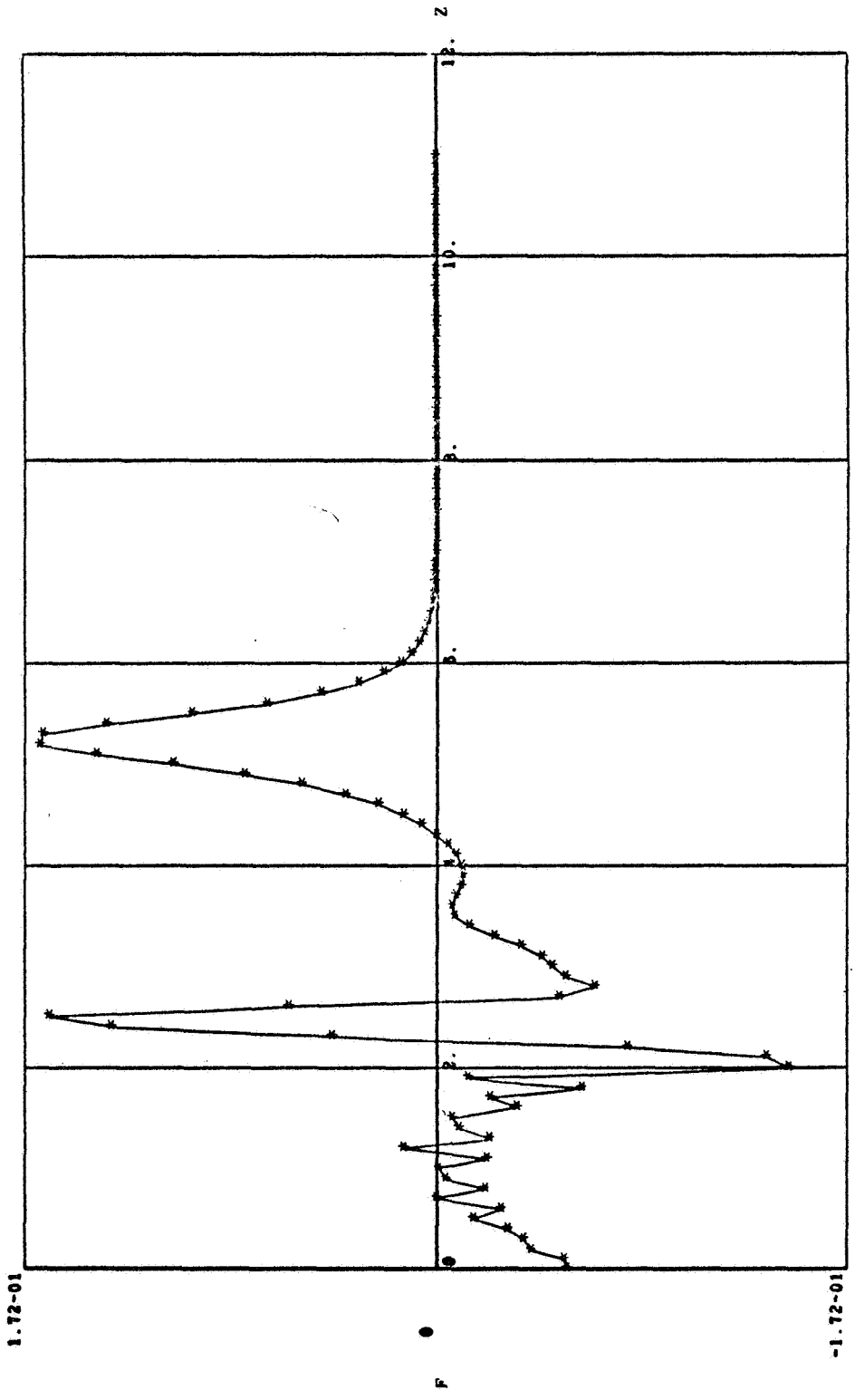

Figure 15b. Disturbance Stream Function

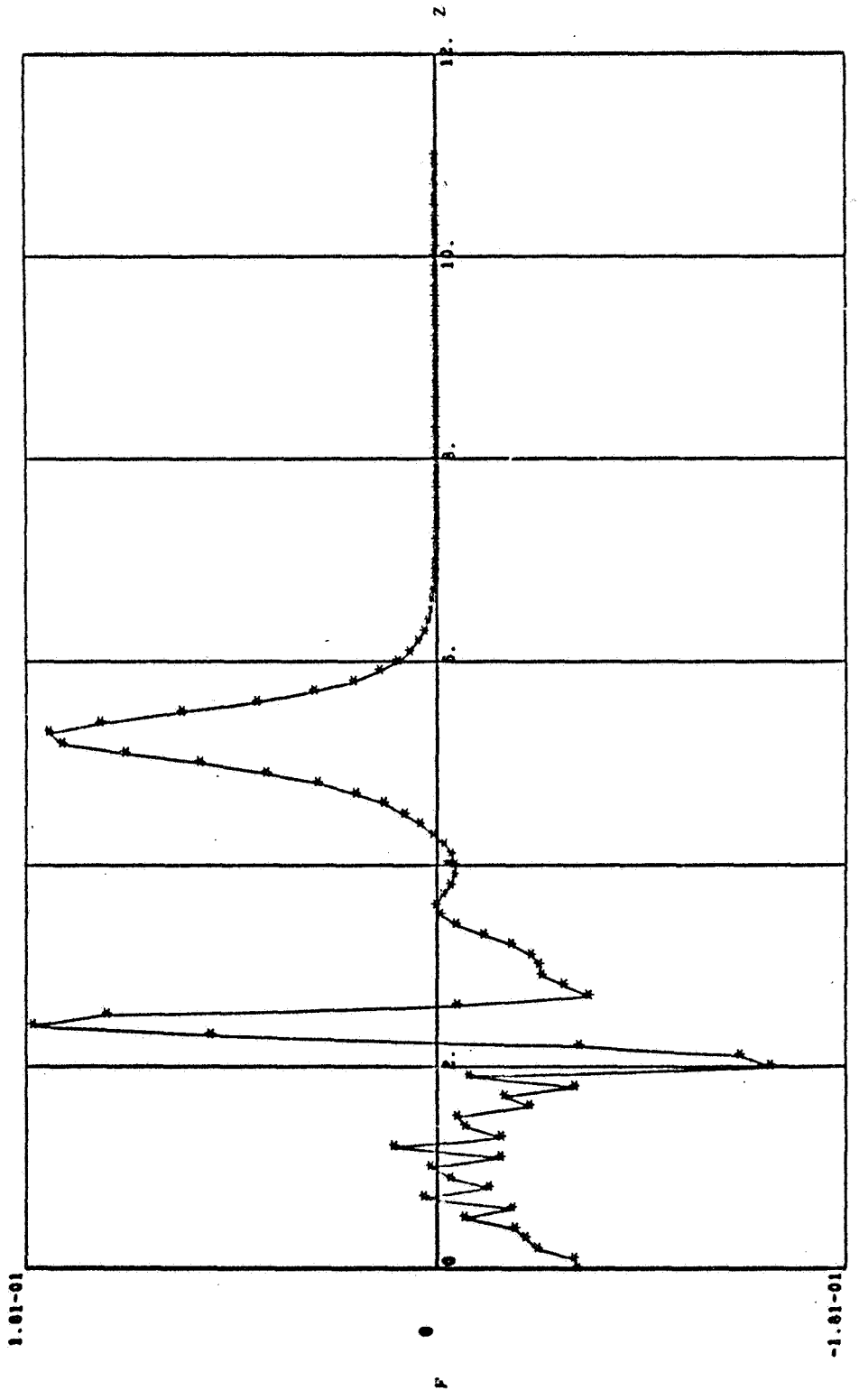

Figure 15c. Disturbance Stream Function

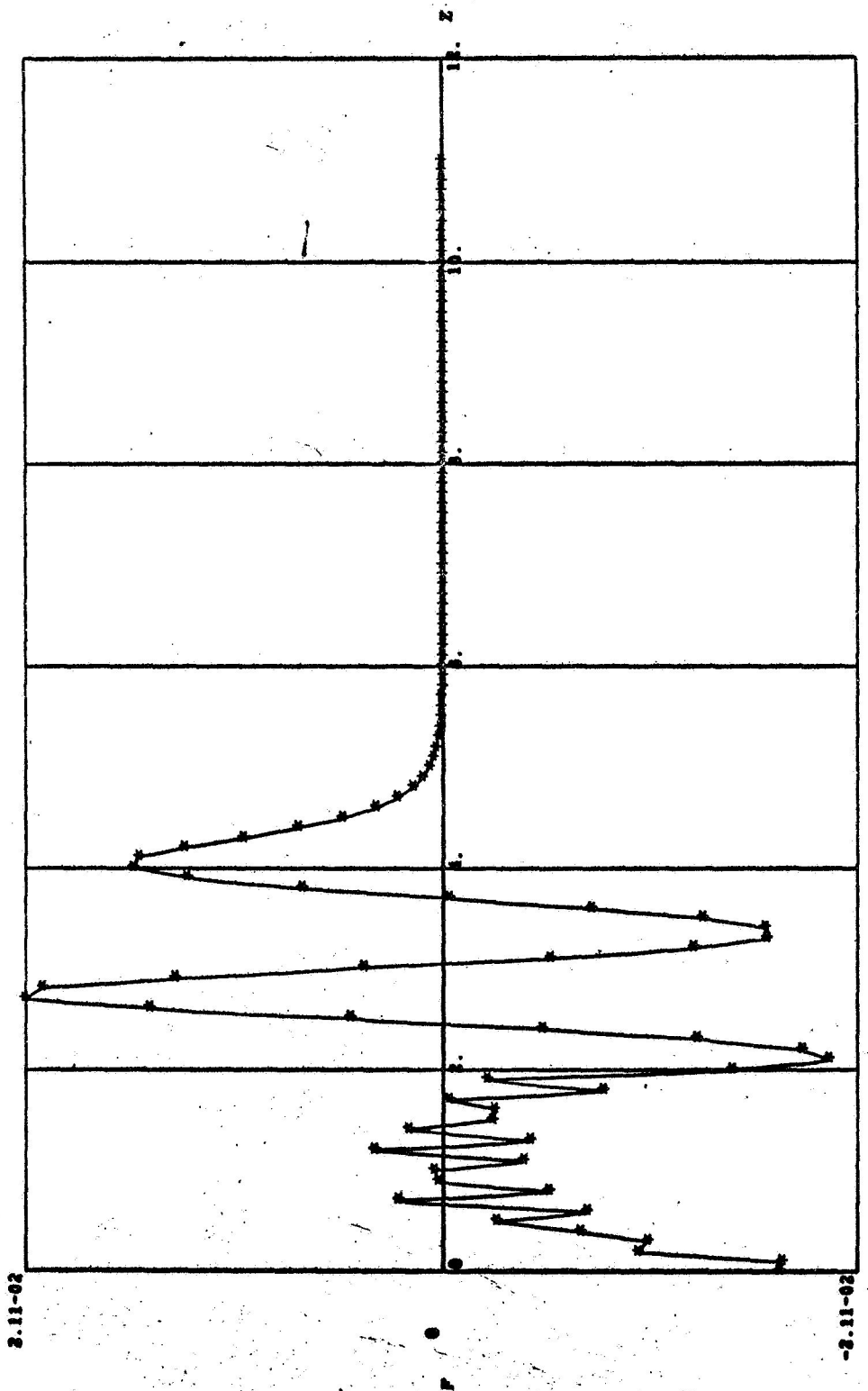

Figure 15d. Disturbance Stream Function

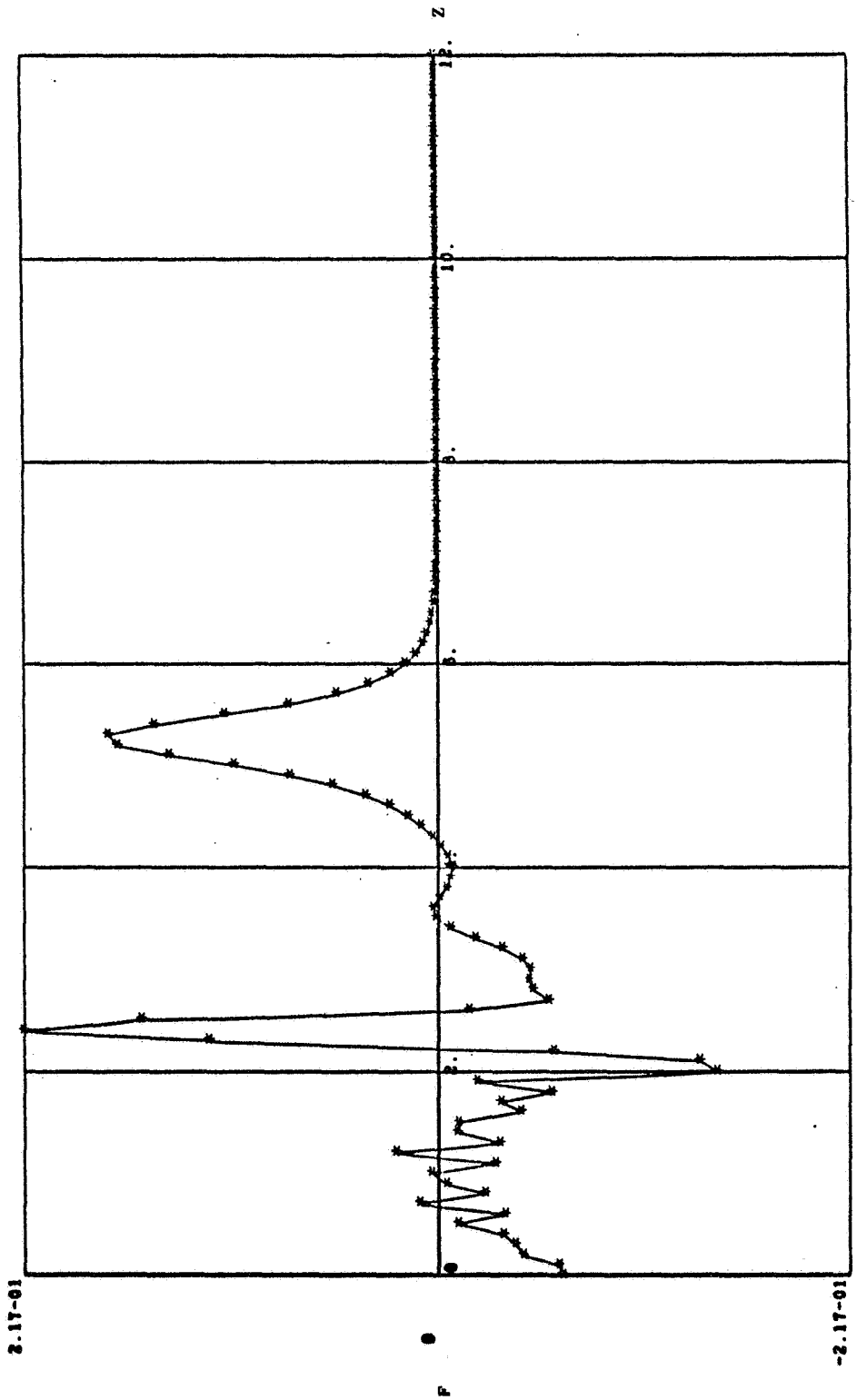

Figure 15e. Disturbance Stream Function

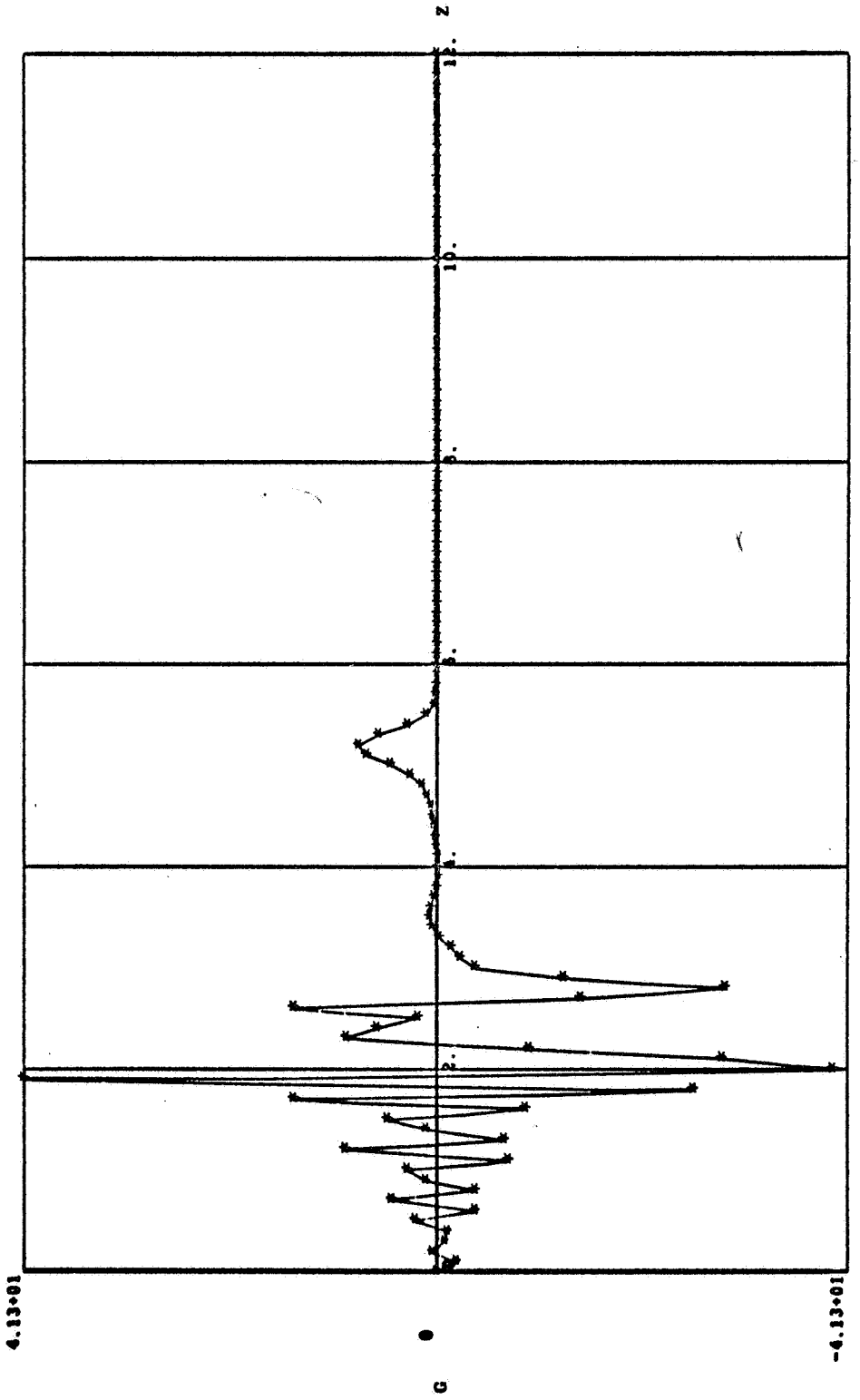

Figure 16a. Disturbance Vorticity

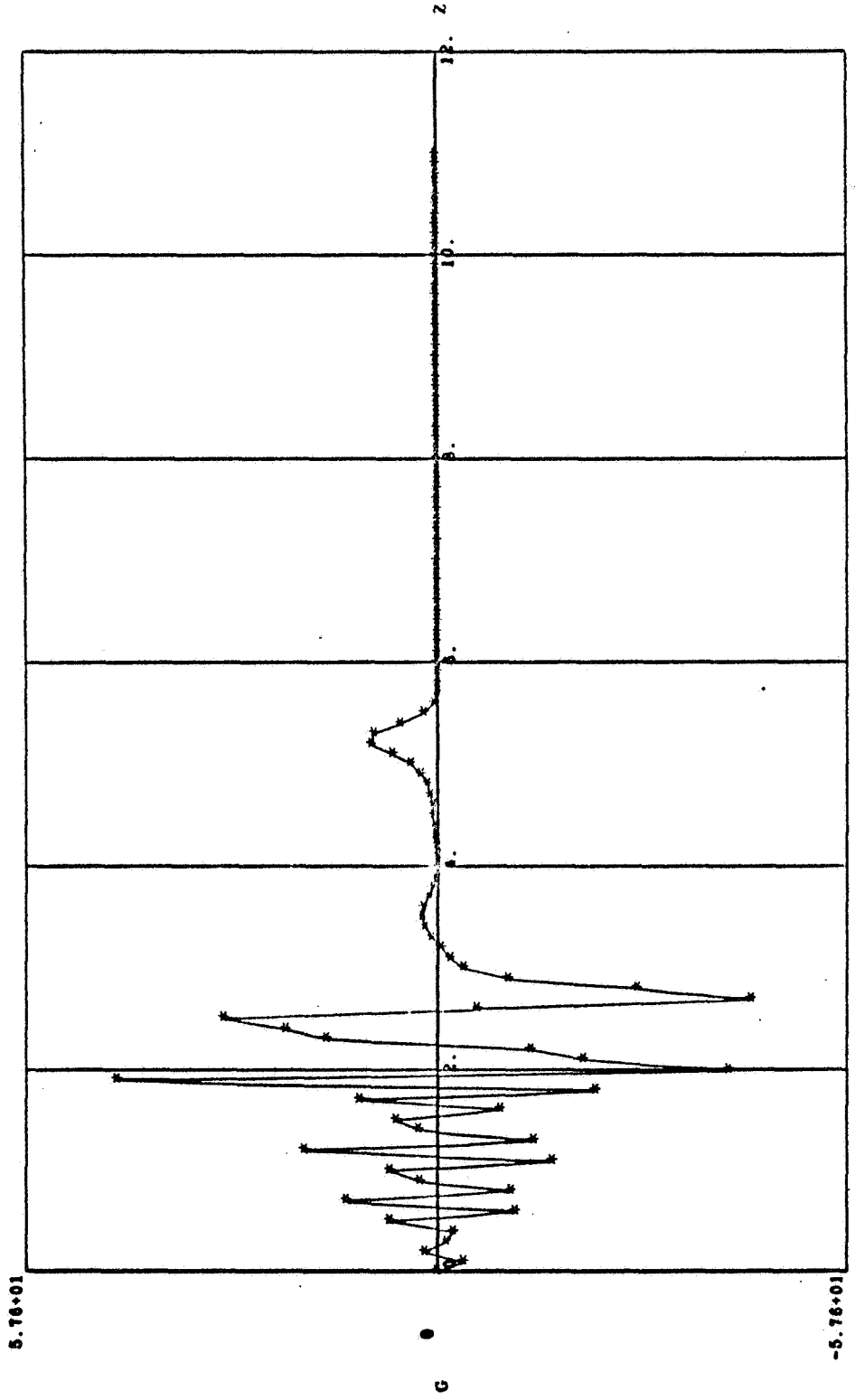

Figure 16b. Disturbance Vorticity

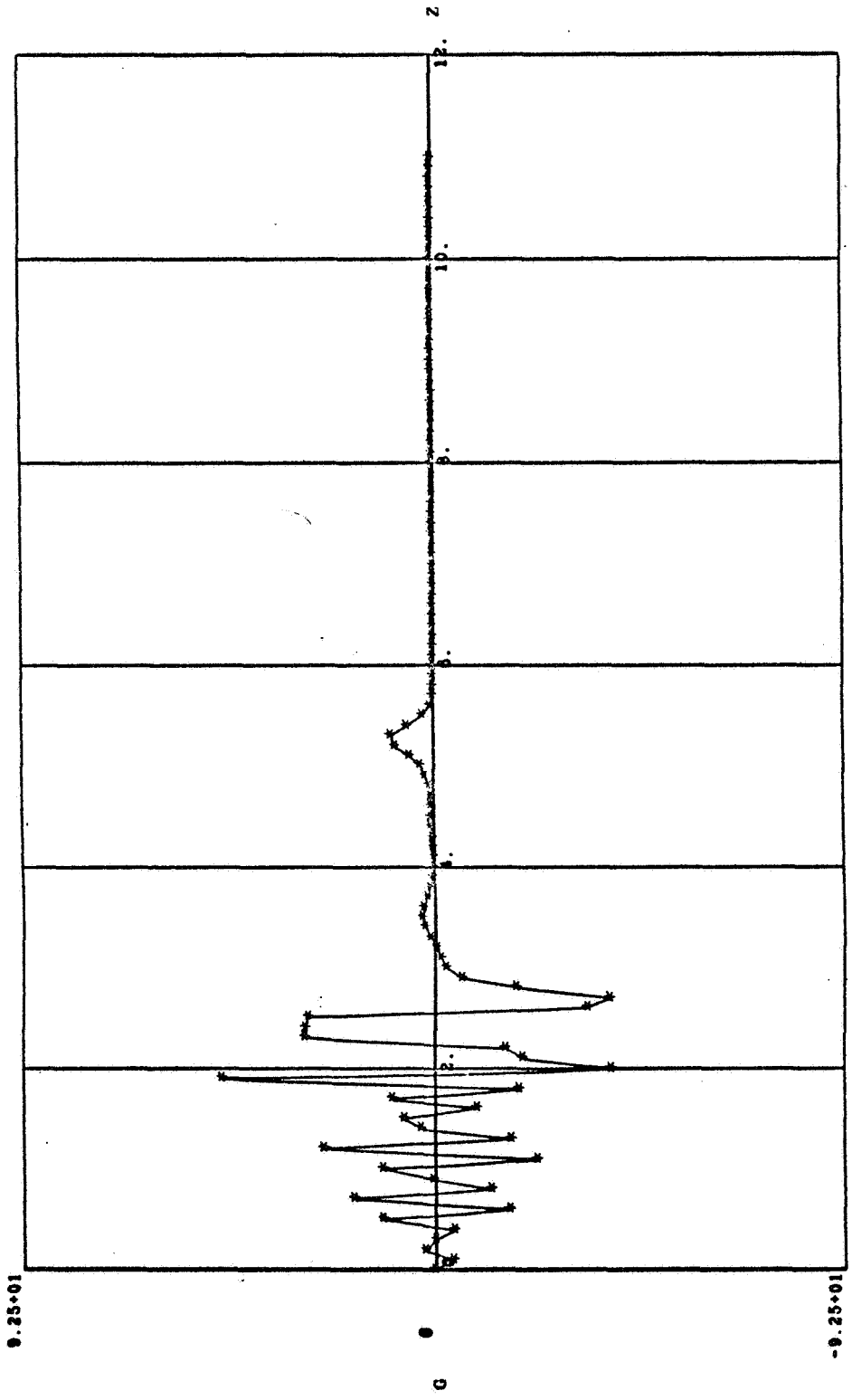

Figure 16c. Disturbance Vorticity

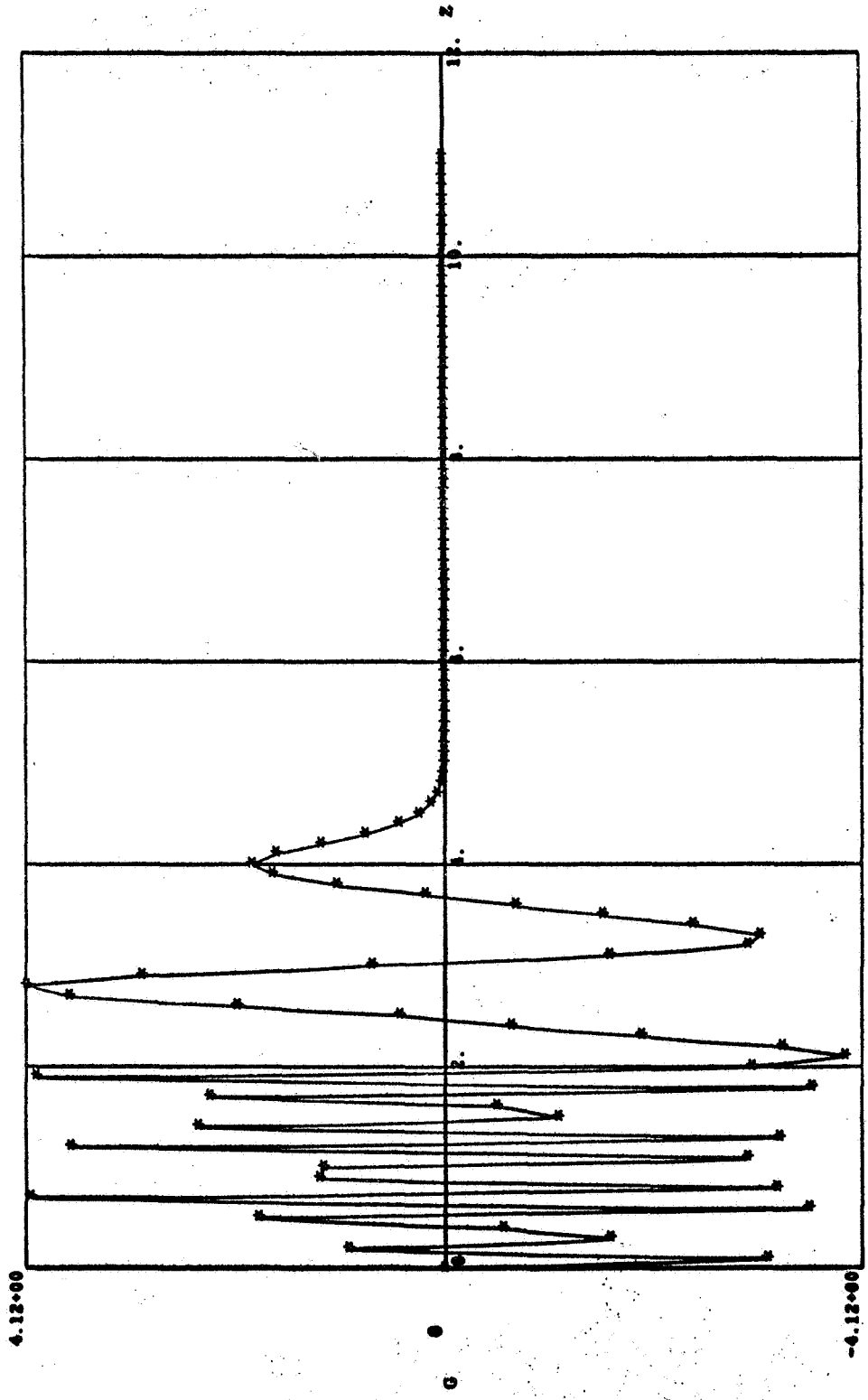

Figure 16d. Disturbance Vorticity

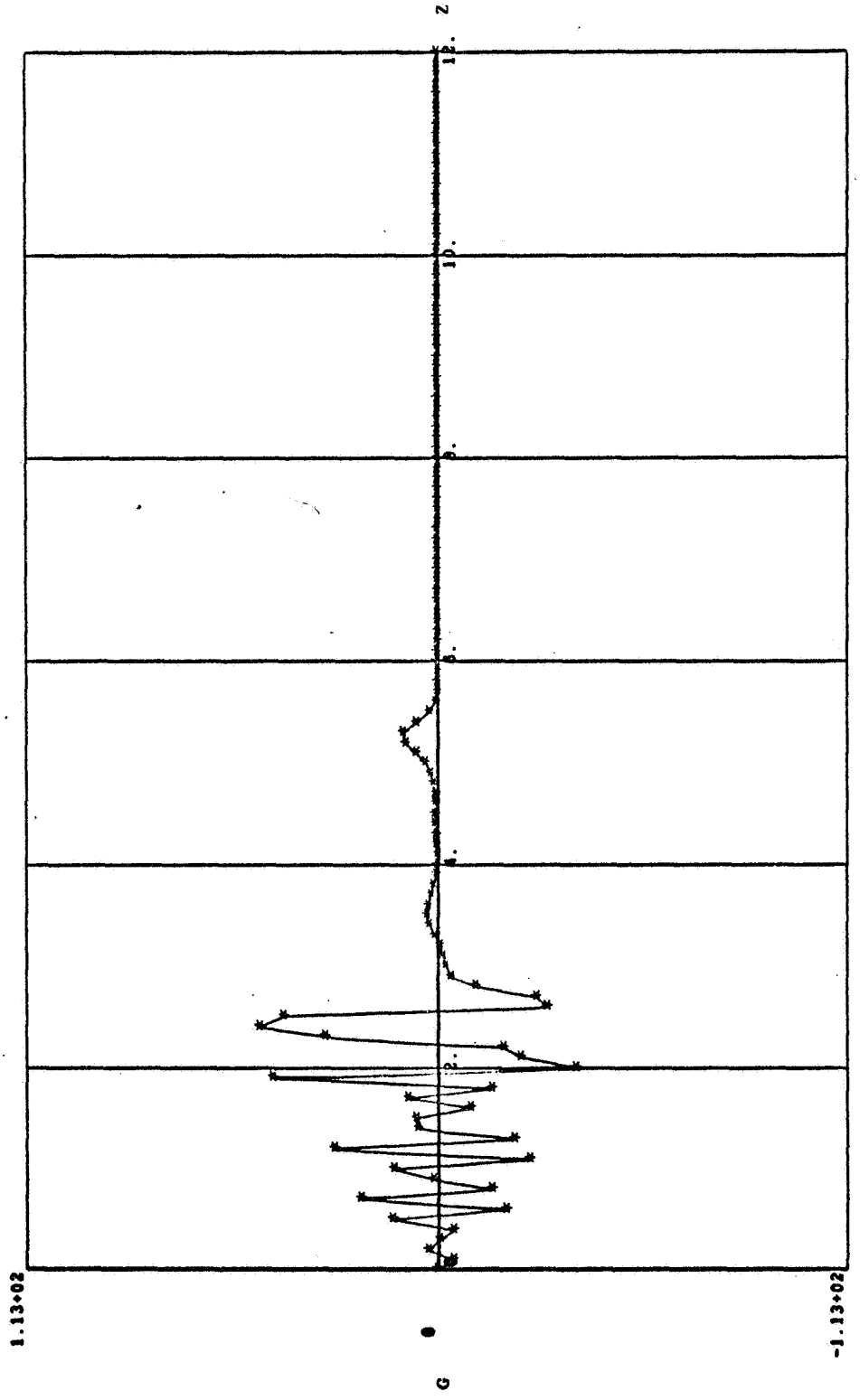

Figure 16e. Disturbance Vorticity

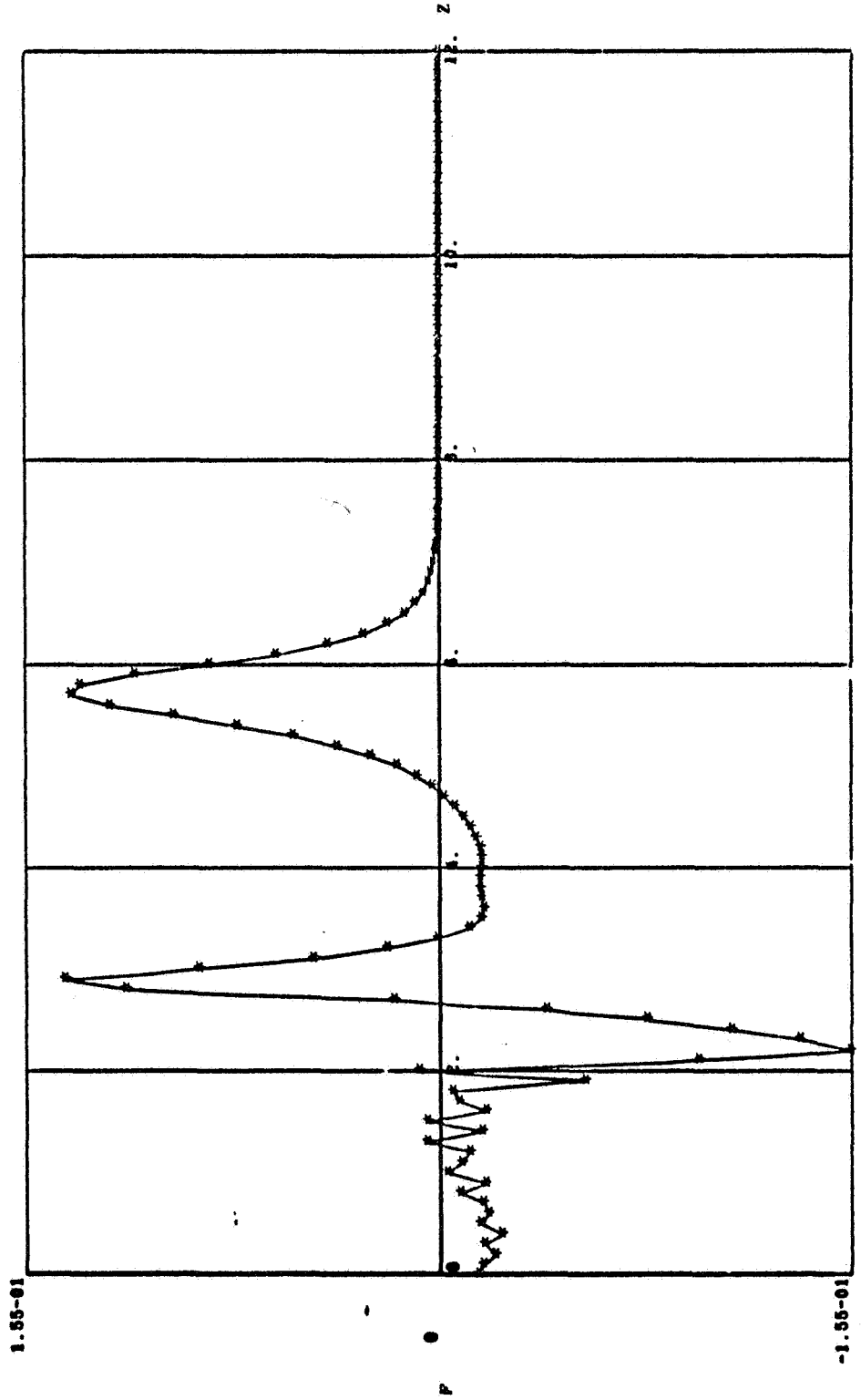

Figure 17a. Disturbance Stream Function

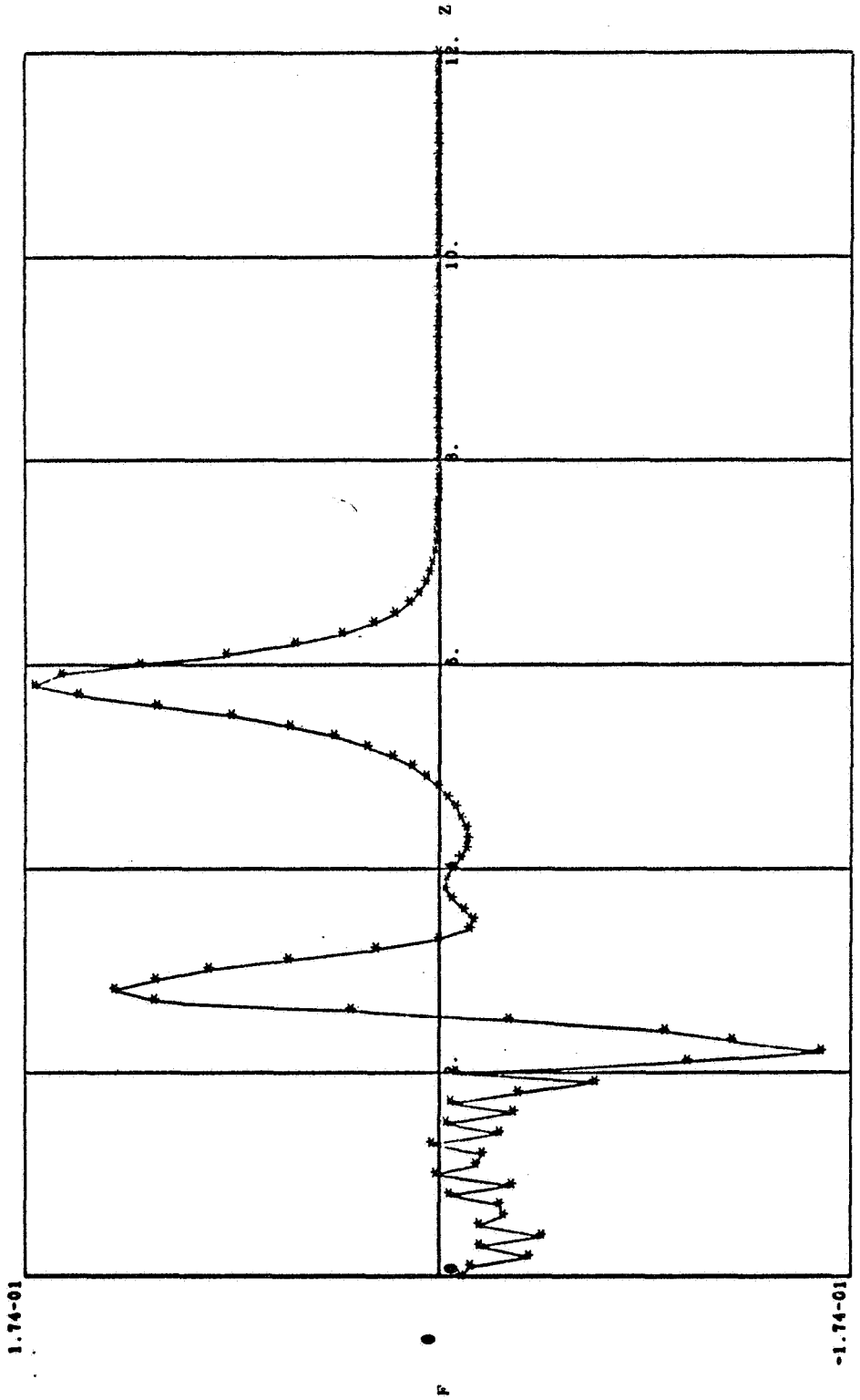

Figure 17b. Disturbance Stream Function

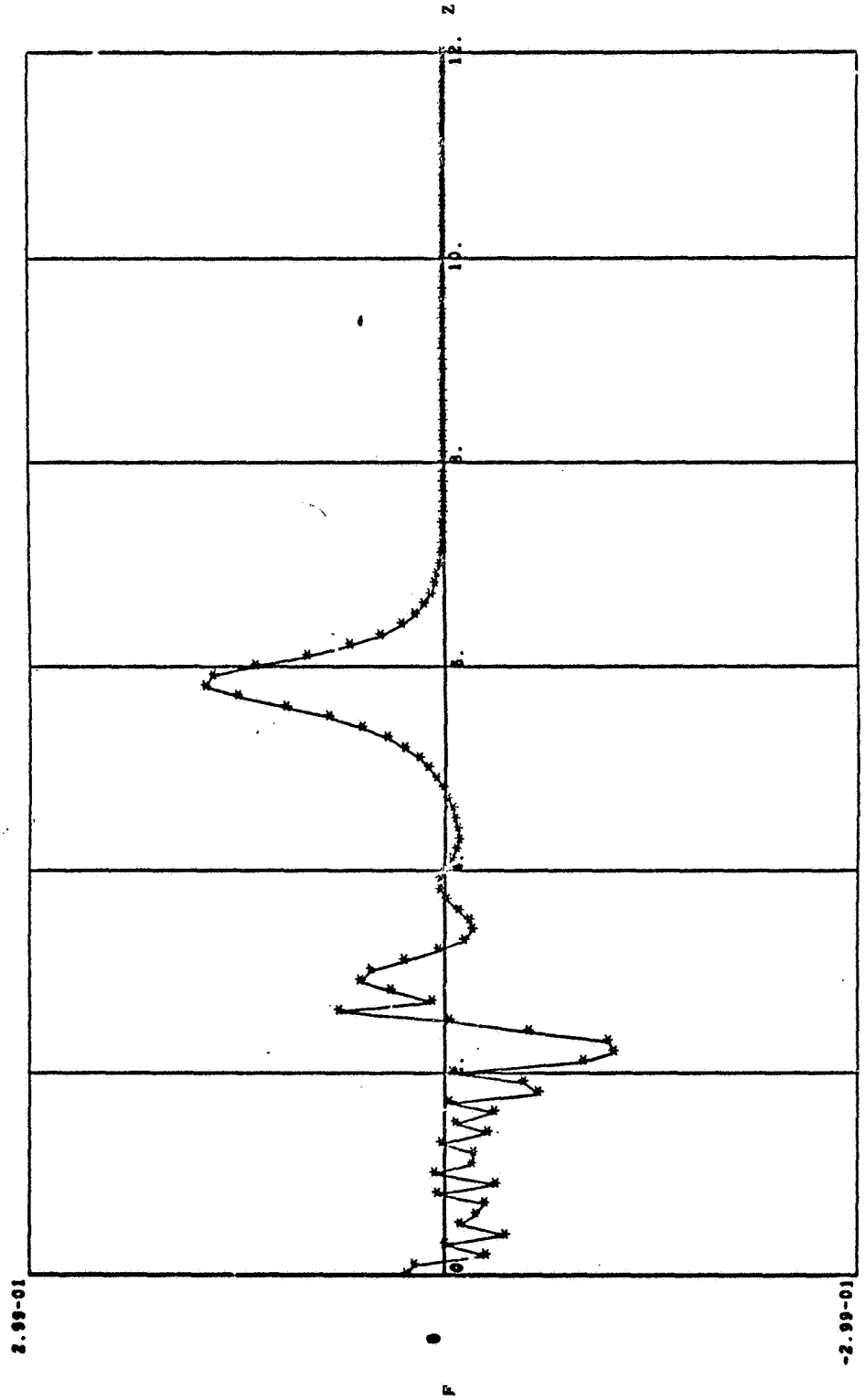

Figure 17c. Disturbance Stream Function

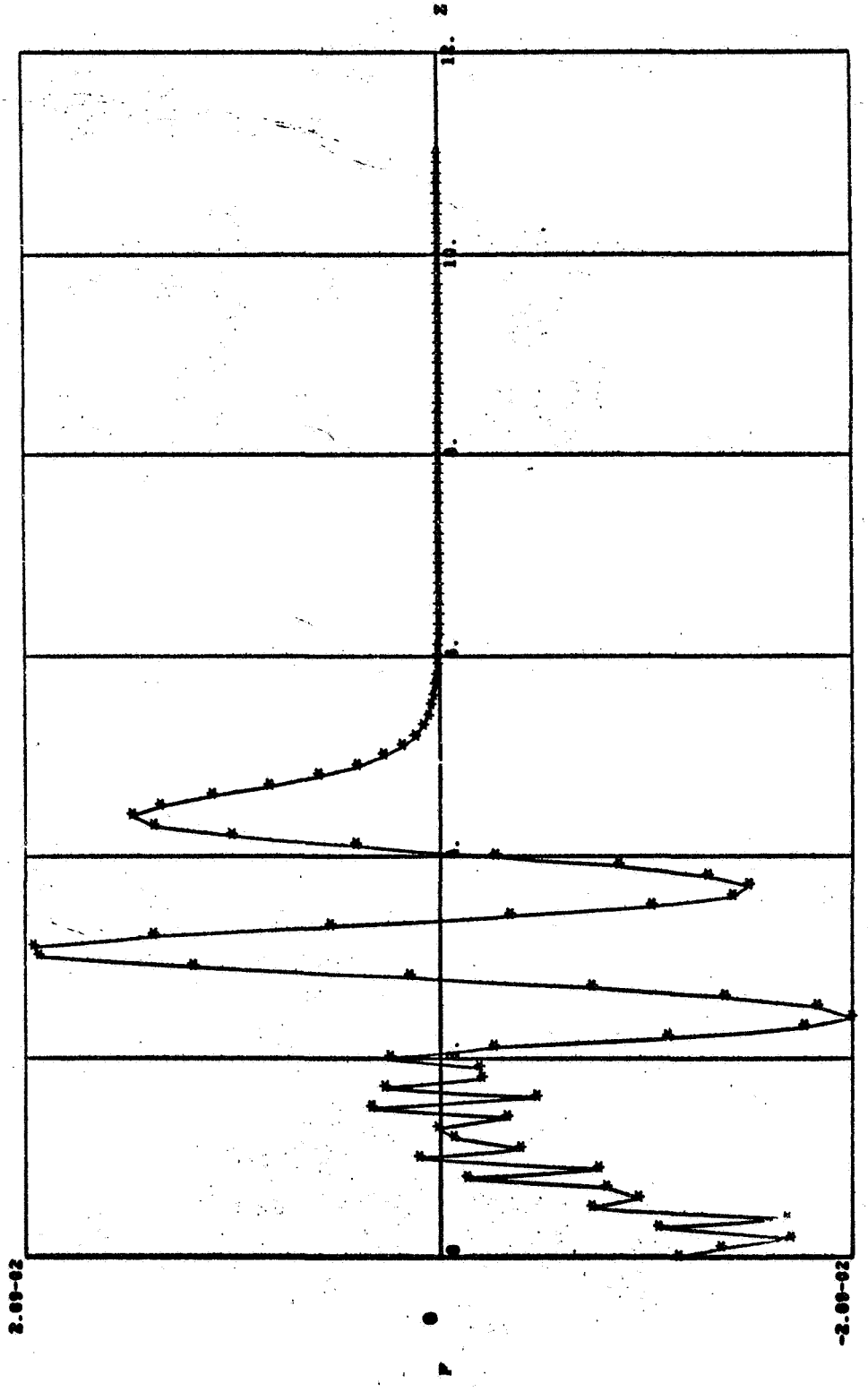

Figure 17d. Disturbance Stream Function

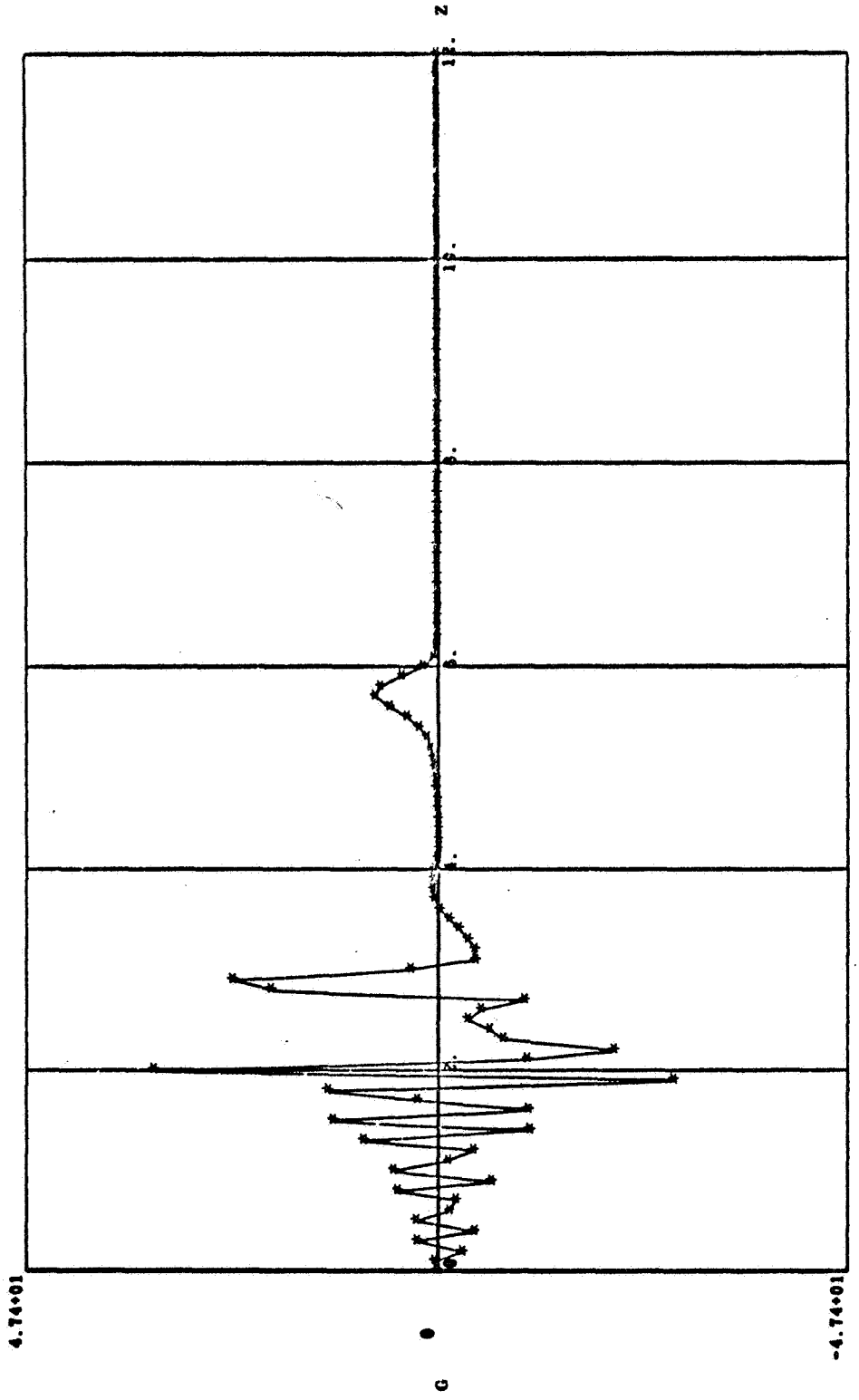

Figure 18a. Disturbance Vorticity

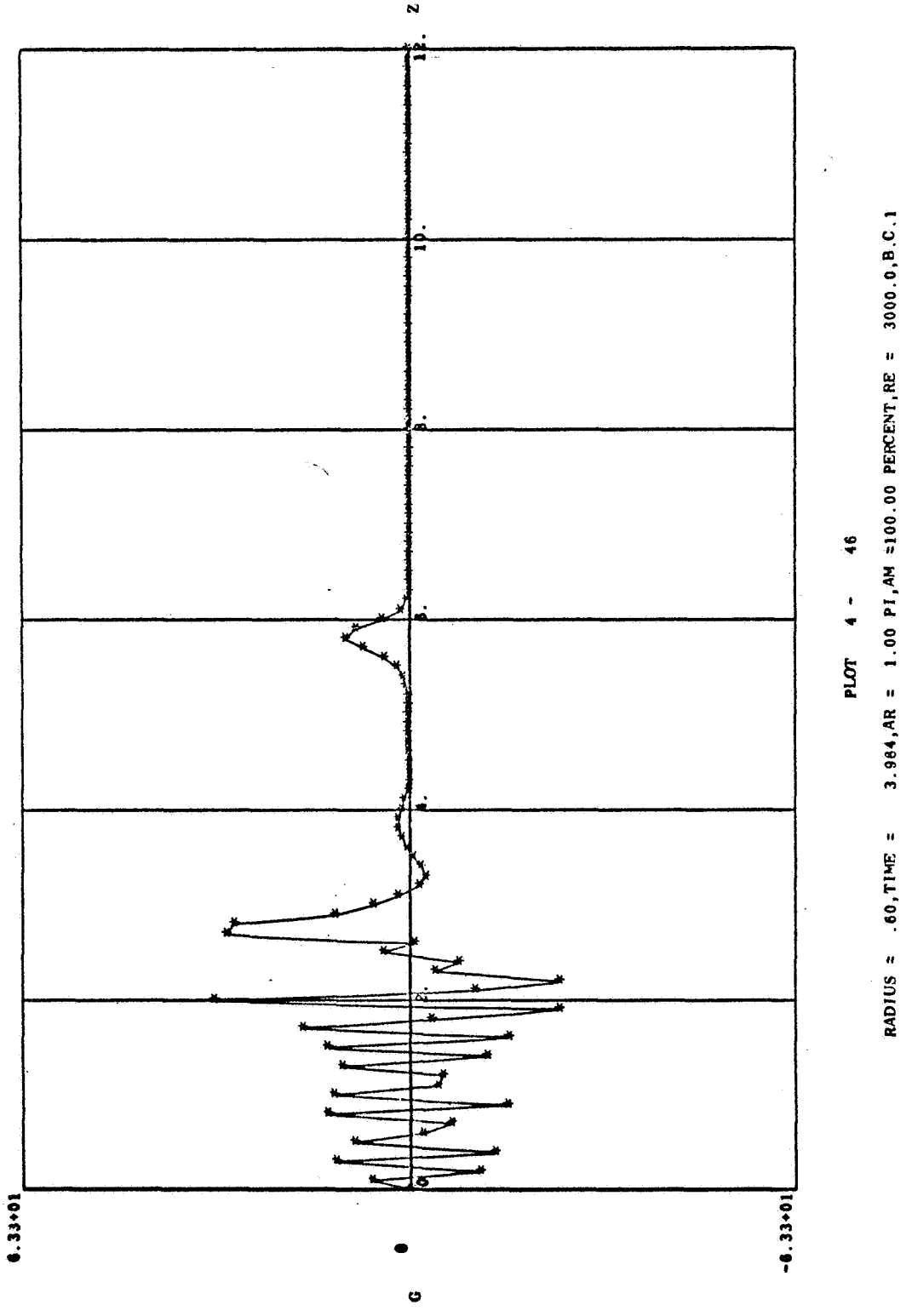

Figure 18b. Disturbance Vorticity

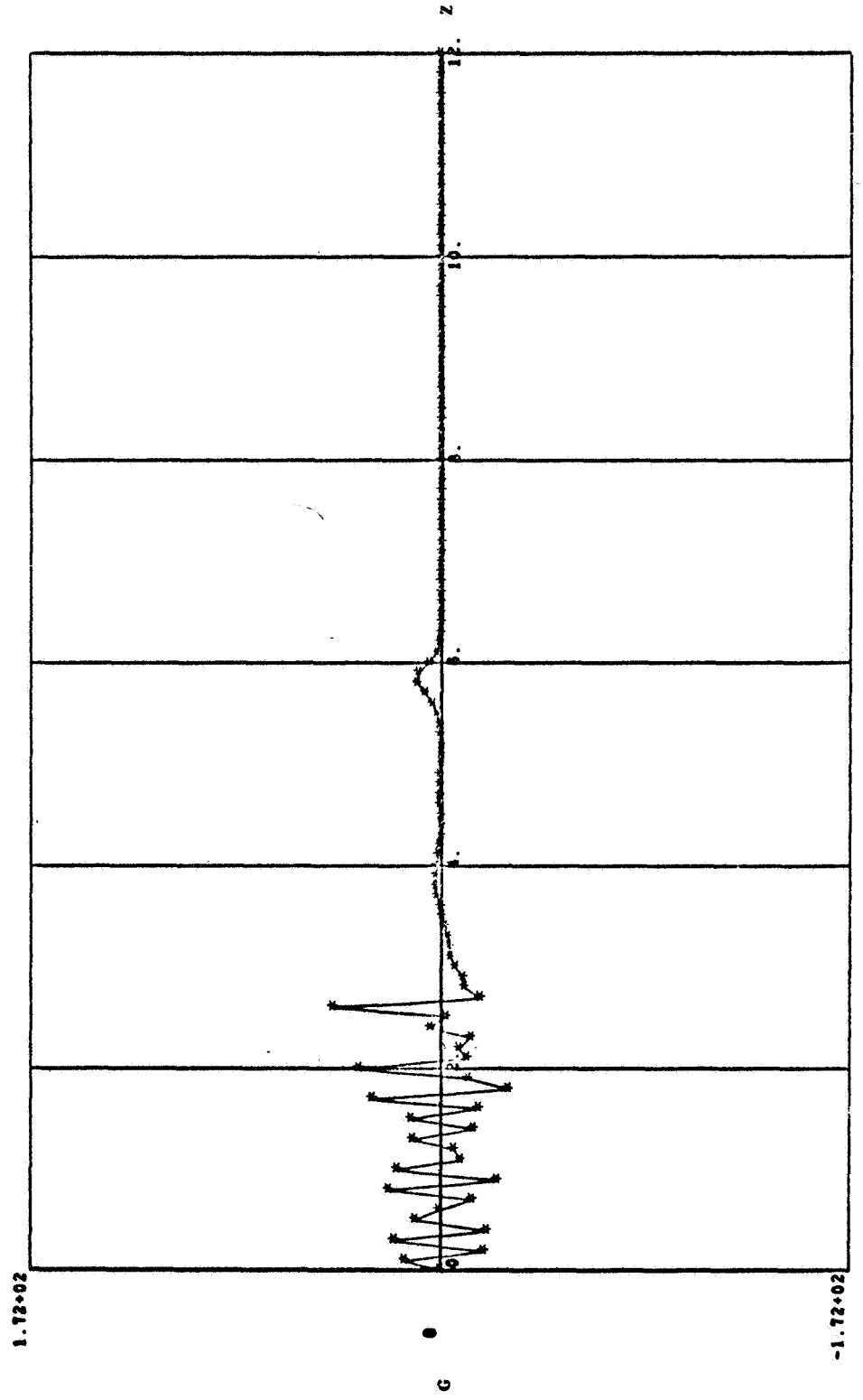

Figure 18c. Disturbance Vorticity

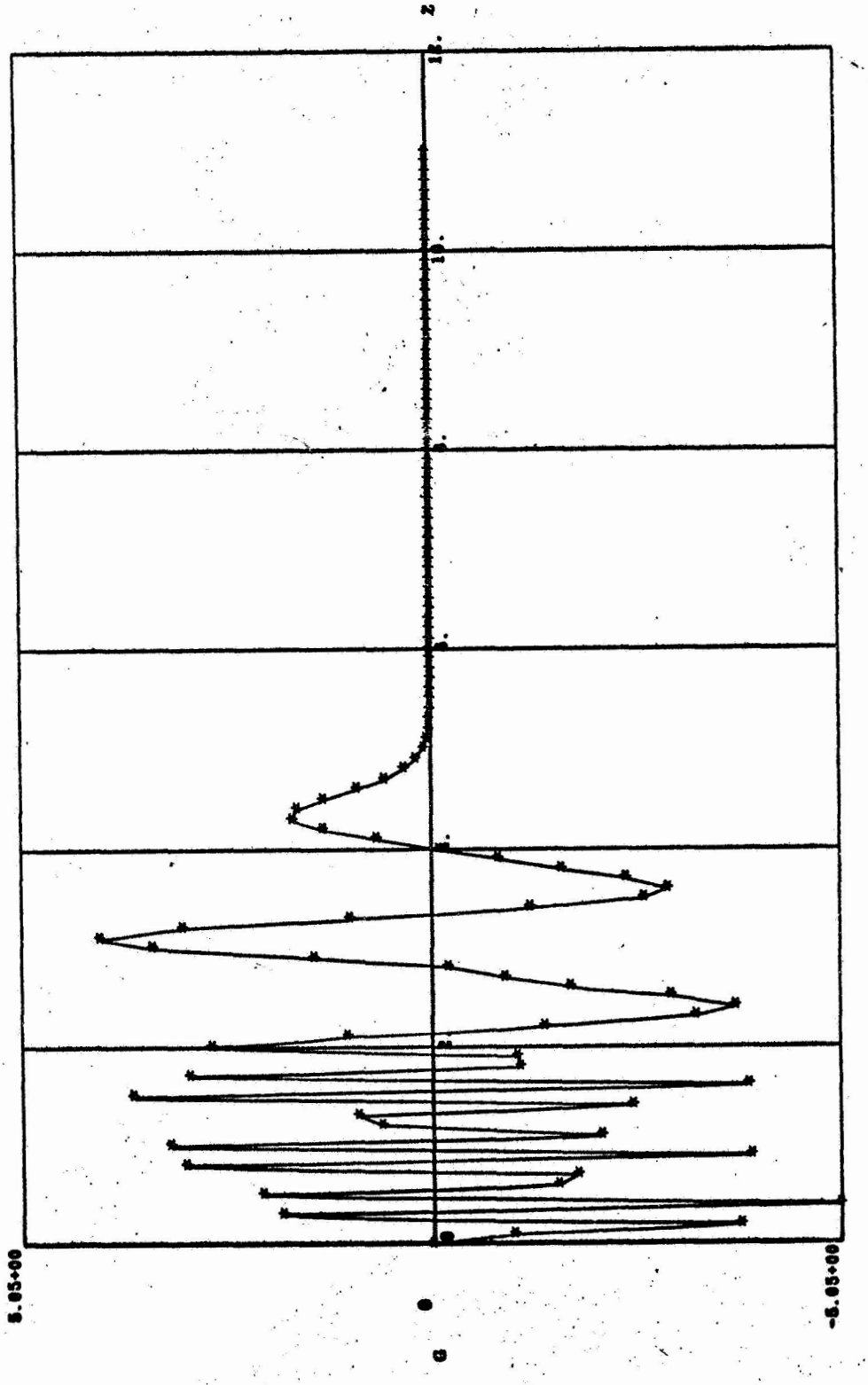

Figure 18d. Disturbance Vorticity

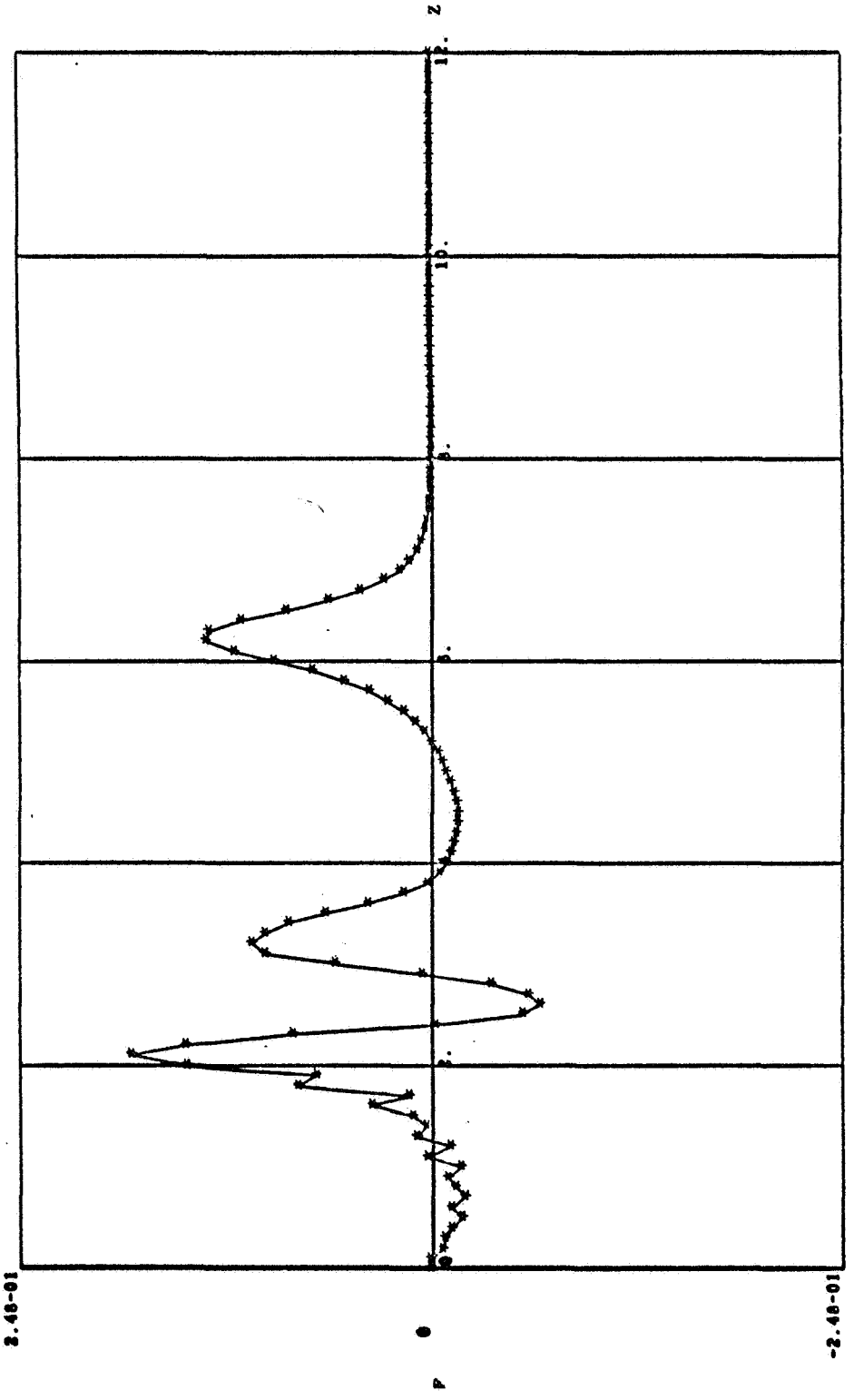

Figure 19a. Disturbance Stream Function

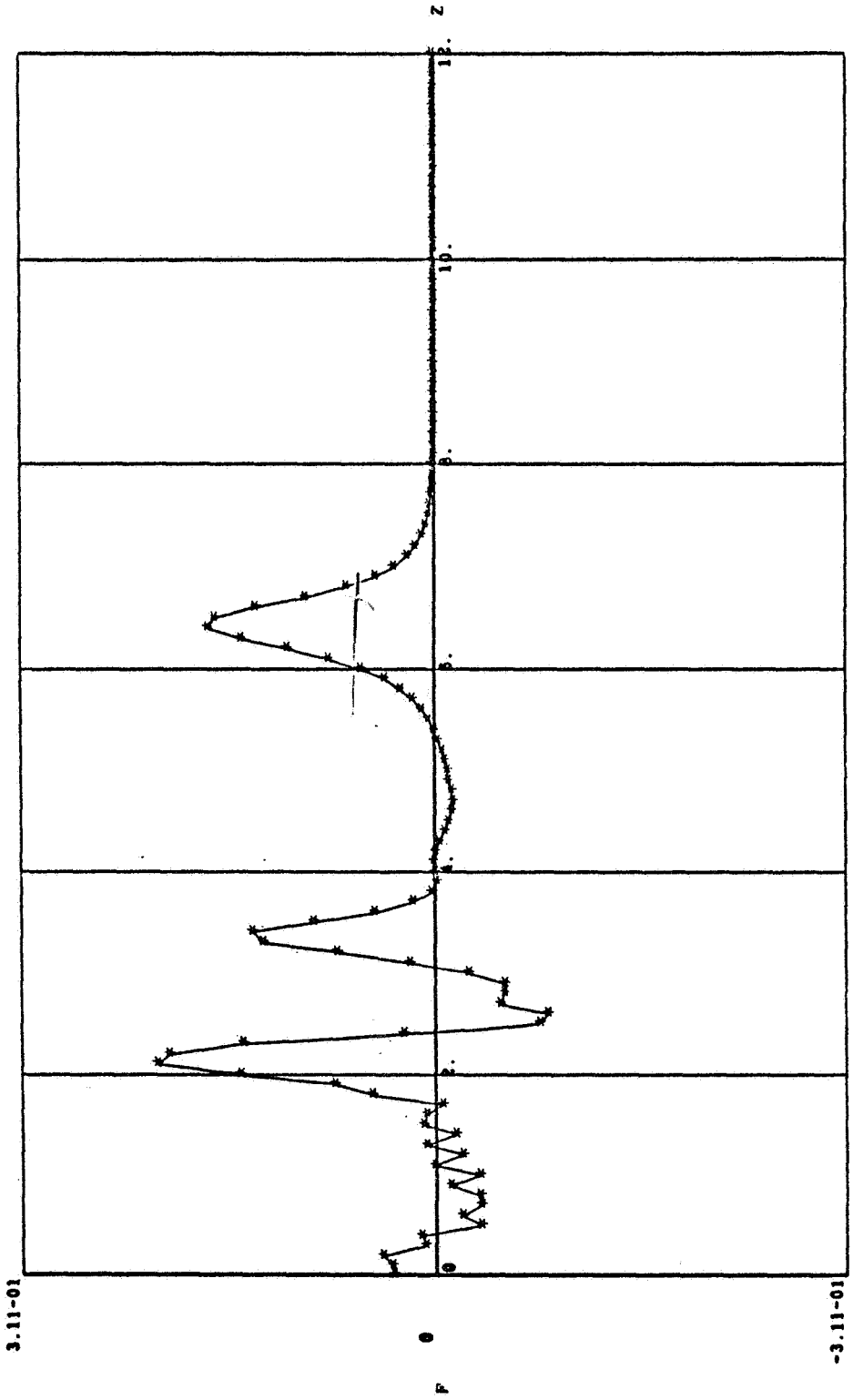

Figure 19b. Disturbance Stream Function

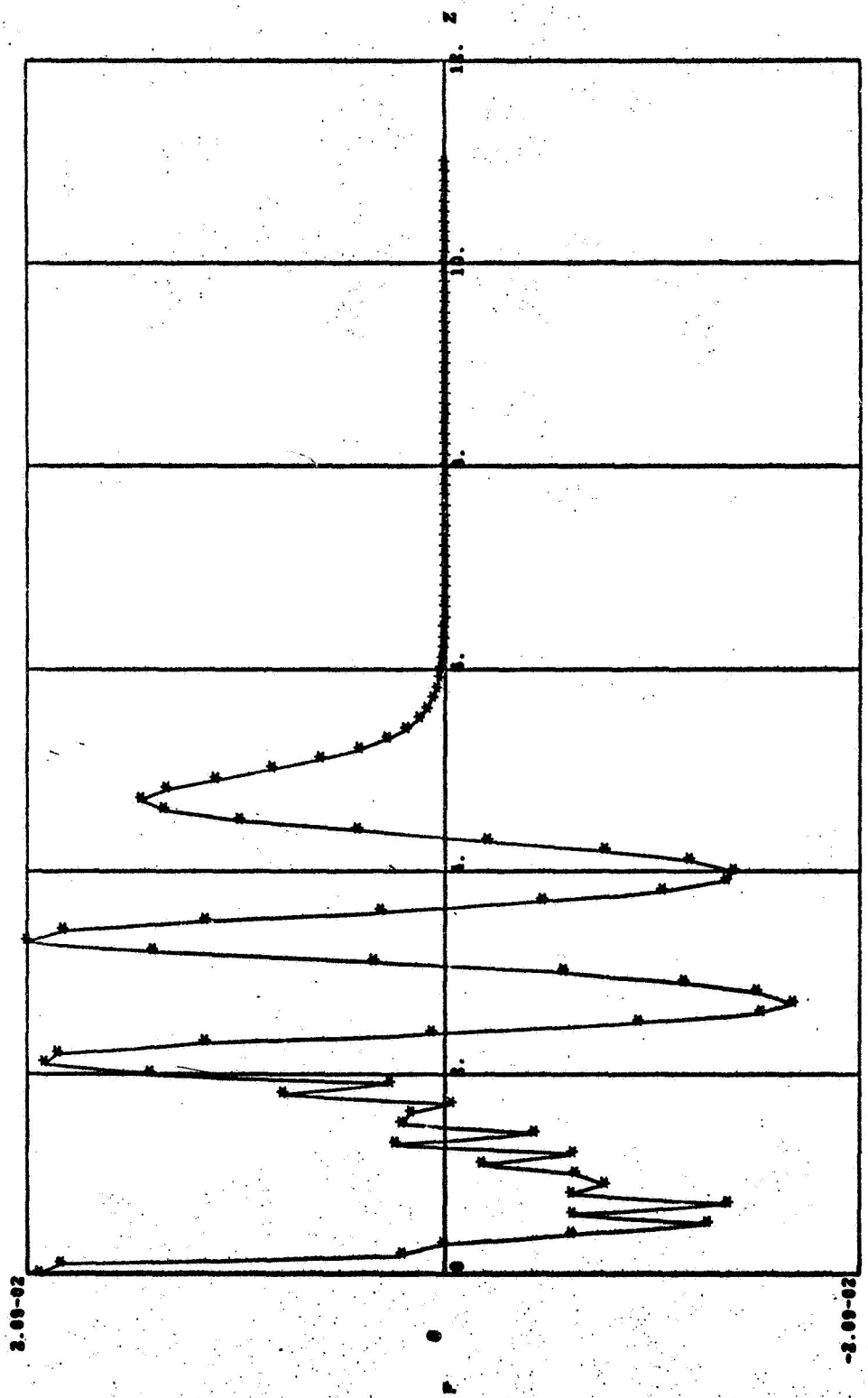

Figure 19c. Disturbance Stream Function

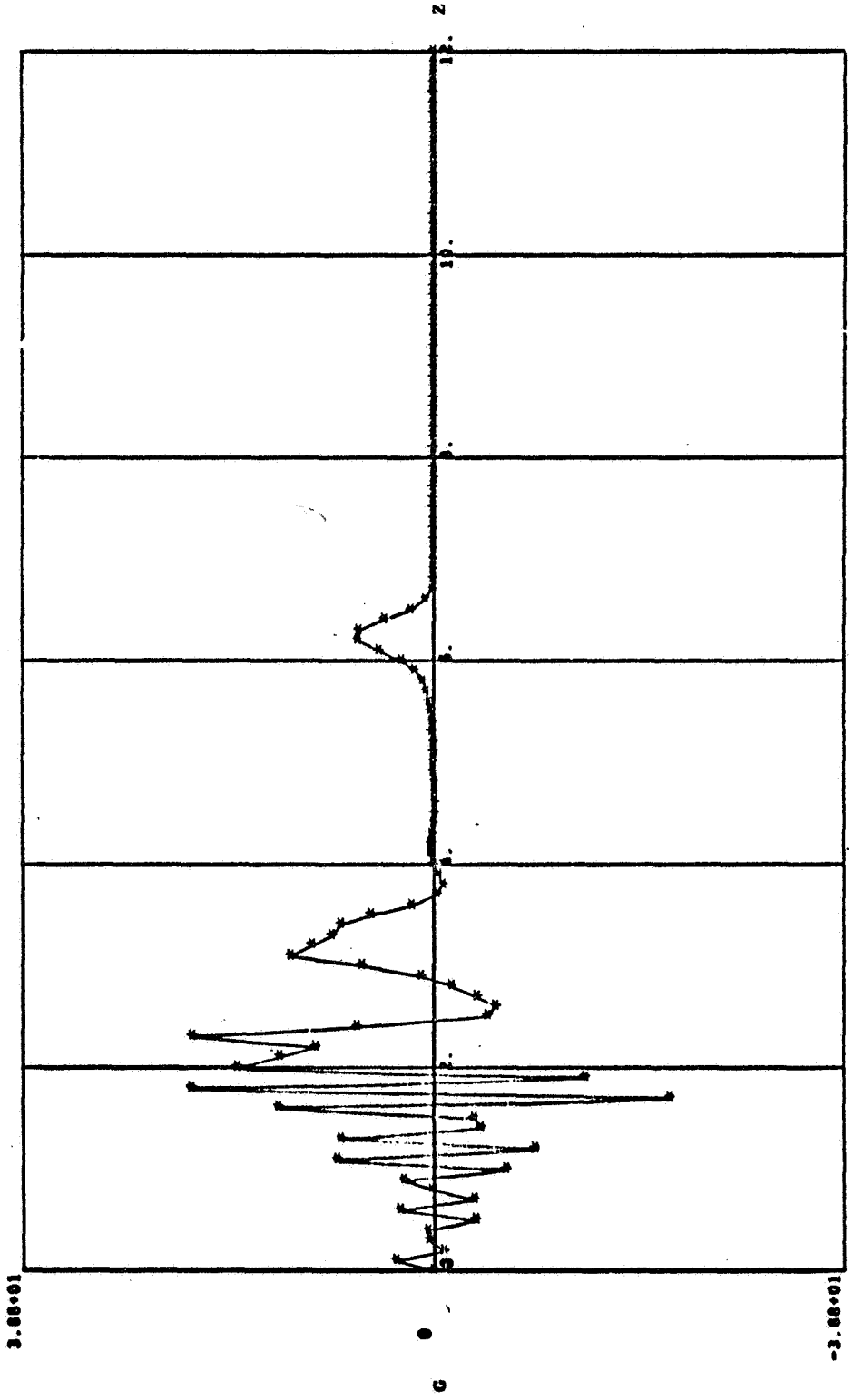

Figure 20a. Disturbance Vorticity

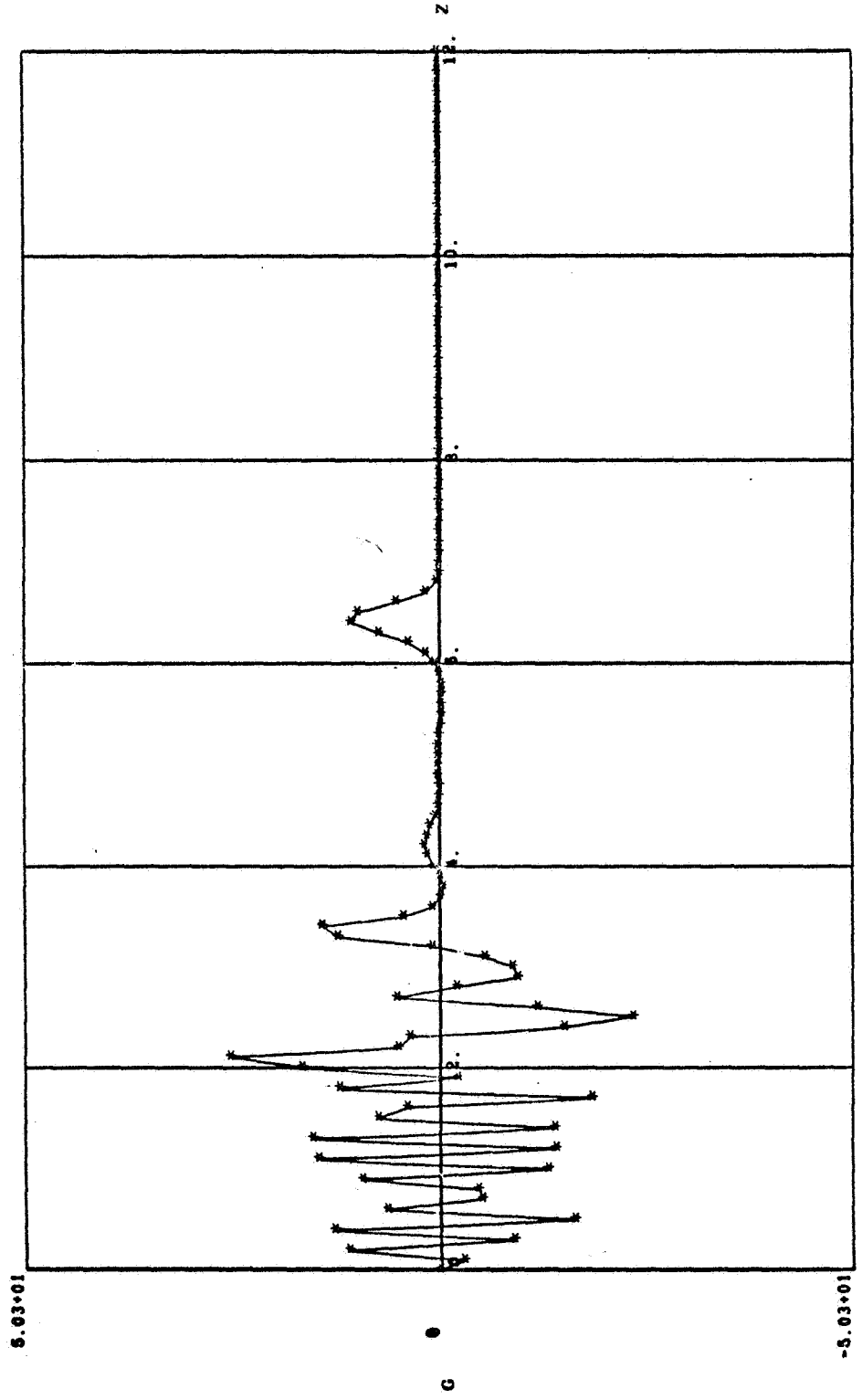

Figure 20b. Disturbance Vorticity

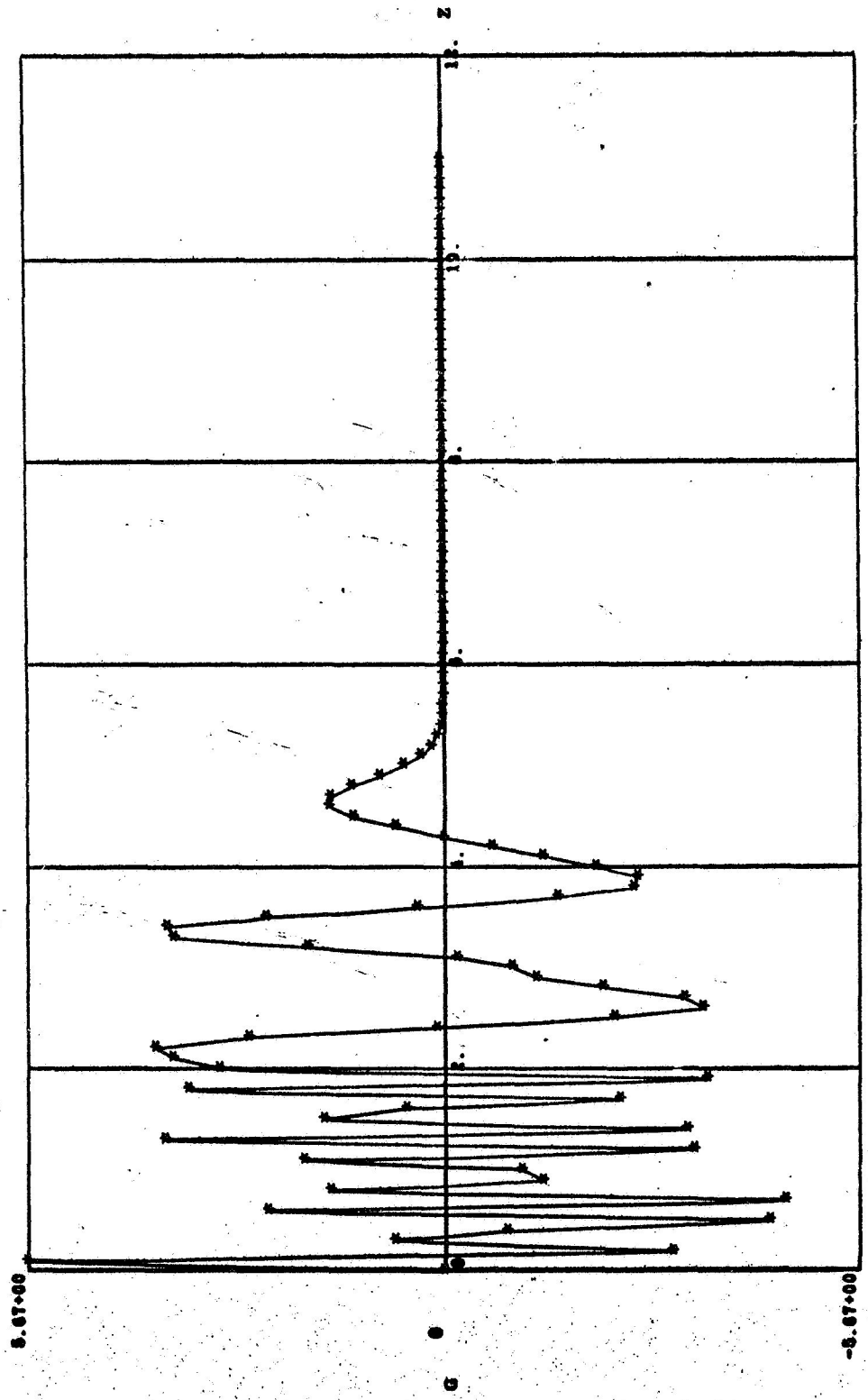

Figure 20c. Disturbance Vorticity

APPENDIX B

ERRORS IN THE USE OF NONUNIFORM MESH SYSTEMS

INTRODUCTION

Numerical studies of fluid-dynamics problems are quite often concerned with flow around solid bodies where fairly large velocity gradients are encountered. In the vicinity of the body, it is often convenient to use a mesh system which is smaller than the mesh system imposed over most of the flow field and which might even be a nonsquare mesh system. Examples of this approach are seen in the studies of Whitaker and Wendel [1] and Thoman and Szewcyzk [2]. This study is concerned with a comparison of the numerical error that arises in the solution of the Navier-Stokes equations when a nonsquare, nonuniform mesh system is used. This type of problem is of interest because the velocity (or vorticity or stream function) can change rather sharply and the effect of the change is more pronounced in certain regions than in other regions. Therefore, it is felt that by increasing the density of the mesh points in the regions of greatest change, a marked improvement in the overall accuracy of the solution could be effected without the expense of increasing the density of the grid system everywhere.

The problem chosen for study is that of Poiseuille flow in a pipe for which there is a well-known exact solution (see Schlichting [3]). This example arose during an investigation to determine numerically the onset of turbulence in Poiseuille pipe flow. The mathematical problem consisted of axisymmetrically perturbing the Poiseuille velocity distribution at some point in the pipe (see Crowder and Dalton [4]). Since the perturbation is expected to generate significant gradients of the vorticity and the stream function, it was felt desirable to use a denser mesh system in the vicinity of the perturbation as well as on the boundaries. The denser mesh system should allow for a more accurate representation of both the vorticity and the stream function. In checking the calculation procedure for the perturbed flow, it was noticed that varying numerical errors were obtained for the unperturbed solution when various nonuniform, nonsquare grid representations were used.

Investigation of the literature for nonuniform mesh systems showed the following: For a uniform mesh system, Young [5] gives the error term for a second partial derivative as behaving like $(h^2/4)\partial^4 U/\partial x^4$, where h is the uniform mesh spacing in the x direction. Young then gives a difference representation for the same second derivative over a nonuniform mesh system, i.e., when the mesh spacing goes like h on one side of the grid point in question and like sh $(0 < s \leq 1)$ on the other side. However, no error term

is given for the nonuniform mesh case. Analysis of the error involved yields that the error term goes like $(1 - s)(h/3)\partial^3 U/\partial x^3$. Hence, a lower order error in h is introduced for a nonuniform mesh system than for a uniform mesh system. It is also noted that for some physical problems $\frac{\partial^3 U}{\partial x^3}$ is significantly greater than $\frac{\partial^4 U}{\partial x^4}$. Hence, we choose to solve the problem of unperturbed Poiseuille pipe flow in order to obtain comparisons of the effect of the grid system on the accuracy of the finite-difference approximations to the Navier-Stokes equations.

GOVERNING DIFFERENTIAL EQUATIONS

A nondimensional axisymmetric form of the Navier-Stokes equations for viscous, incompressible flow in a circular pipe is

$$G_t - F_z\left(\frac{G}{r}\right)_r + \frac{F_r G_z}{r} = \frac{1}{R}\left[\left(\frac{1}{r}(rG)_r\right)_r + G_{zz}\right] \tag{1}$$

and

$$F_{zz} + r\left(\frac{F_r}{r}\right)_r = -rG, \tag{2}$$

where G is the vorticity, F is the stream function, and R is the Reynolds Number. The Reynolds Number is a parameter and is given by

$$R = \frac{\overline{W}D}{\nu},$$

where $\overline{W}$ is the average axial velocity component, D is the pipe diameter and ν is the kinematic viscosity of the fluid.

The boundary conditions for the above differential equations are:

$$G = 2r, \; F_z = 0 \text{ on } z = 0, \tag{3a}$$

$$G_z = F_{zz} = 0 \text{ on } z = L, \tag{3b}$$

$$G = F = 0 \text{ on } r = 0, \tag{3c}$$

$$F_r = 0, \; F = 0.25, \; G = -\frac{1}{r}\left(F_{rr} - \frac{F_r}{r}\right) \text{ on } r = 1, \tag{3d}$$

where $z = 0$ is the upstream boundary, $z = L$ is the downstream boundary, $r = 0$ is the centerline of the pipe, and $r = 1$ is the wall of the pipe. The initial conditions of the problem are given by

$$F = \frac{1}{2} r^2 - \frac{1}{4} r^4 \qquad \text{for} \begin{cases} 0 \le z \le L \\ 0 \le r \le 1, \end{cases} \tag{4a}$$

and

$$G = 2r. \tag{4b}$$

With the above boundary and initial conditions, equations (3) and (4), equations (1) and (2) admit to an analytic solution,

$$F = \frac{1}{2} r^2 - \frac{1}{4} r^4 \tag{5a}$$

and

$$G = 2r. \tag{5b}$$

This analytic solution is the steady flow solution to the above problem. Since we know this solution, we can use it as a comparison to determine the accuracy of the numerical procedures used to solve the mixed boundary-initial value problem.

For a derivation of the governing equations, see Schlichting [3]. For a discussion of the boundary conditions see Crowder and Dalton [4].

DIFFERENCE EQUATIONS

The solution of the differential equations is obtained by the use of the method of finite differences. For this technique, a net of grid points is introduced onto the region upon which the solution is to be found. We have chosen not to use equally spaced grid points, therefore any function Φ is given by

$$\Phi(r,z,t) = \Phi(r_i,z_j,t_n) = \Phi^n_{i,j},$$

where

$$r_i = \sum_{m=1}^{i} \Delta r_m,\ \Delta r_1 = 0,\ 1 \le i \le \text{Imax}\ (0 \le r_i \le 1), \tag{6a}$$

$$z_j = \sum_{m=1}^{j} \Delta z_m,\ \Delta z_1 = 0,\ 1 \le j \le \text{Jmax}\ (0 \le z_j \le L), \tag{6b}$$

and

$$t_n = \sum_{m=0}^{n} \Delta t_m,\ \Delta t_o = 0,\ \Delta t_{2m+1} = \Delta t_{2m},\ (0 \le t_n \le T). \tag{6c}$$

For the above grid, central differences in space are used while forward differences in time are used. The operators which we will use are defined as follows:

$$\Phi_z = (\Phi^n_{i,j})_z = \frac{1}{\Delta z_j + \Delta z_{j+1}}\left[-\frac{\Delta z_{j+1}}{\Delta z_j}\ \Phi^n_{i,j-1}\right.$$

$$\left. + \left(\frac{\Delta z_{j+1}}{\Delta z_j} - \frac{\Delta z_j}{\Delta z_{j+1}}\right)\Phi^n_{i,j} + \frac{\Delta z_j}{\Delta z_{j+1}}\ \Phi^n_{i,j+1}\right]$$

$$- \frac{\Delta z_j \, \Delta z_{j+1}}{3!} \Phi_{zzz}(r_i, \xi, t_n), \; z_{j-1} \le \xi \le z_{j+1} \tag{7a}$$

$$\Phi_{zz} = (\Phi^n_{i,j})_{zz} = \frac{2}{\Delta z_j + \Delta z_{j+1}} \left[\frac{1}{\Delta z_j} \Phi^n_{i,j-1} \right.$$

$$\left. - \left(\frac{1}{\Delta z_j} + \frac{1}{\Delta z_{j+1}} \right) \Phi^n_{i,j} + \frac{1}{\Delta z_{j+1}} \Phi^n_{i,j+1} \right]$$

$$+ \frac{(\Delta z_j - \Delta z_{j+1})}{3} \Phi_{zzz}(r_i, z_j, t_n)$$

$$- \frac{1}{12} (\Delta z_j^2 - \Delta z_j \Delta z_{j+1} + \Delta z_{j+1}^2) \Phi_{zzzz}(r_i, \xi, t_n),$$

$$(z_{j-1} \le \xi \le z_{j+1}), \tag{7b}$$

$$\Phi_r = (\Phi^n_{i,j})_r = \frac{1}{\Delta r_i + \Delta r_{i+1}} \left[\frac{\Delta r_{i+1}}{\Delta r_i} \Phi^n_{i-1,j} \right.$$

$$\left. + \left(\frac{\Delta r_{i+1}}{\Delta r_i} - \frac{\Delta r_i}{\Delta r_{i+1}} \right) \Phi^n_{i,j} + \frac{\Delta r_i}{\Delta r_{i+j}} \Phi^n_{i+1,j} \right]$$

$$\frac{\Delta r_i \, \Delta r_{i+1}}{3!} \Phi_{rrr}(\xi, z_j, t_n), \; (r_{i-1} \le \xi \le r_{i+1}), \tag{7c}$$

$$\Phi_{rr} = (\Phi^n_{i,j})_{rr} = \frac{2}{\Delta r_i + \Delta r_{i+1}} \left[\frac{1}{\Delta r_i} \Phi^n_{i-1,j} \right.$$

$$\left. - \left(\frac{1}{\Delta r_i} + \frac{1}{\Delta r_{i+1}} \right) \Phi_{i,j} + \frac{1}{\Delta r_{i+1}} \Phi^n_{i+1,j} \right]$$

$$+ \frac{(\Delta r_i - \Delta r_{i+1})}{3} \Phi_{rrr}(r_i, z_j, t_n) - \frac{1}{12} (\Delta r_i^2 - \Delta r_i \Delta r_{i+1}$$

$$+ \Delta r_{i+1}^2) \Phi_{rrrr}(\xi, z_j, t_n), \; (r_{i-1} \le \xi \le r_{i+1}) \tag{7d}$$

and

$$\Phi_t = (\Phi^n_{i,j})_t = \frac{1}{\Delta t_n} \left[\Phi^{n+1}_{i,j} - \Phi^n_{i,j} \right] - \frac{\Delta t_n}{2} \Phi_{tt}(r_i, z_j, \xi),$$

$$(t_n \le \xi \le t_{n+1}). \tag{7e}$$

Using equation (7) allows equation (2) to be approximated by

$$\rho_k F_{i,j}^{n+1,k+1} - \left(F_{i,j}^{n+1}\right)_{rr}^{k+1} + \frac{1}{r_i}\left(F_{i,j}^{n+1}\right)_{r}^{k+1}$$

$$= \rho_k F_{i,j}^{n+1,k} + \left(F_{i,j}^{n+1}\right)_{zz}^{k} \tag{8a}$$

and

$$\rho_k F_{i,j}^{n+1,k+2} - \left(F_{i,j}^{n+1}\right)_{zz}^{k+2}$$

$$= \rho_k F_{i,j}^{n+1,k+1} + \left(F_{i,j}^{n+1}\right)_{rr}^{k+1} - \frac{1}{r_i}\left(F_{i,j}^{n+1}\right)_{r}^{k+1} \tag{8b}$$

The multipliers, ρ_k, in equation (8) are analogous to the Wachpress-Goode parameters. The Wachpress-Goode parameters are derived for Laplace's equation on a square region and are given by

$$\rho_k = b\left(\frac{a}{b}\right)^{\frac{k+1}{m+1}} \qquad k = 1,2,\cdots,m \tag{9}$$

where a and b are respectively the maximum and minimum eigenvalues of the operator matrix associated with the difference equations which approximate the Laplacian differential equation on a square, equally spaced grid (see Varga [6]). Since our differential equation is not the Laplacian and we allow our grid to be unequally spaced but rectangular over the axisymmetric flow field, then no analytic derivation of the values which ρ_k should have are available. Nevertheless, if we use the above formulation for the ρ_k for our problem, we find that the maximum and minimum eigenvalues of the operator matrix for the radial derivatives are always larger and smaller, respectively, than those for the operator matrix for

the axial derivatives. Therefore a and b are taken as the maximum and minimum eigenvalues of the operator matrix for the radial derivatives. Numerical experimentation also showed that with this choice of a and b that use of five parameters for the iteration was optimal. The actual values of the ρ_k used in the calculations are given in Table 1. Again, using equation (7) allows equation (1) to be approximated by

$$\left[\frac{1}{\Delta t_{n+1}} + \frac{1}{r_i^2}\left(F_{i,j}^{n+1}\right)_z + \frac{1}{r_i^2 R}\right] G_{i,j}^{n+1}$$

$$- \left[\frac{1}{r_i}\left(F_{i,j}^{n+1}\right)_z + \frac{1}{r_i R}\right]\left(G_{i,j}^{n+1}\right)_r - \frac{1}{R}\left(G_{i,j}^{n+1}\right)_{rr}$$

$$= \frac{1}{\Delta t_{n+1}} G_{i,j}^{n} - \frac{1}{r_i}\left(F_{i,j}^{n}\right)_r \left(G_{i,j}^{n}\right)_z + \frac{1}{R}\left(G_{i,j}^{n}\right)_{zz} \qquad (10a)$$

and

$$\frac{1}{\Delta t_{n+2}} G_{i,j}^{n+2} + \frac{1}{r_i}\left(F_{i,j}^{n+2}\right)_r \left(G_{i,j}^{n+2}\right)_z - \frac{1}{R}\left(G_{i,j}^{n+2}\right)_{zz} =$$

$$\left[\frac{1}{\Delta t_{n+2}} - \frac{1}{r_i^2}\left(F_{i,j}^{n+1}\right)_z - \frac{1}{r_i^2 R}\right] G_{i,j}^{n+1}$$

$$+ \left[\frac{1}{r_i}\left(F_{i,j}^{n+1}\right)_z + \frac{1}{r_i R}\right]\left(G_{i,j}^{n+1}\right)_r + \frac{1}{R}\left(G_{i,j}^{n+1}\right)_{rr}, \qquad (10b)$$

where we allow the time step, Δt_m, to vary from step to step in the solution process subject to the restriction

$$\Delta t_{2m+1} = \Delta t_{2m+2} \qquad (11)$$

The time step is used as a parameter to speed the iteration process and to insure convergence. The time step is selected such that the average number of iterations for the solutions at the

TABLE 1

ρ_k for use in equation (8)

Grid	ρ_k
	14.4554279116205
	45.5195753385026
I	143.339356791502
	451.370010651717
	1421.34645414991
	14.4366669994227
II	46.5707761839117
and	150.231157542023
III	484.625822152668
	1563.33873305511
	14.6371115664442
IV	46.5190382231239
and	147.844805813021
VI	469.874000856377
	1493.33333333333
	14.5031251532618
	33.1157808959826
V	75.6150783201431
	172.656054444876
	394.235036169115

2m + 1 and 2m + 2 times to converge is kept near a minimum.

For the derivatives involved in the boundary conditions, we use the differentiated Lagrangian interpolation formulas to obtain their finite-difference representation

$$G^n_{i,1} = 2r_i, \tag{12a}$$

$$(F^n_{i,1})_z = 0, \tag{12b}$$

$$(G^n_{i,Jmax})_z = 0, \tag{12c}$$

$$(F^n_{i,Jmax})_{zz} = 0, \tag{12d}$$

$$G^n_{1,j} = 0, \tag{12e}$$

$$F^n_{1,j} = 0, \tag{12f}$$

$$G^n_{Imax,j} = -(F^n_{Imax,j})_{rr} + (F^n_{Imax,j})_r \quad , \tag{12g}$$

$$F^n_{Imax,j} = 0.25 \tag{12h}$$

and

$$(F^n_{Imax,j})_r = 0 . \tag{12i}$$

The initial conditions are given by

$$G^o_{i,j} = 2r_i \tag{13a}$$

and

$$F^o_{i,j} = \frac{1}{2} r_i^2 - \frac{1}{4} r_i^4. \tag{13b}$$

The difference equations, equations (8) and (10), are solved on various grids, specified later, subject to the boundary and initial condi-

tions, equations (12) and (13). The method of solution used is an adaptation of the Alternating Direction Implicit Method of Peaceman and Rachford given by Young [5].

Before explaining the calculation procedure, we set forward the convergence tests that are applied. For the stream function we used

$$|F_{i,j}^{n,\ell,k+2m} - F_{i,j}^{n,\ell,k}| \leq \epsilon_f \left[\max_{i,j} |F_{i,j}^{n,\ell,k+2m-1}|\right], \tag{14}$$

where m is the number of ρ values used in the iterative procedure and k is the stream-function iteration counter. We chose ϵ_f such that $\epsilon_f \geq 1.0 \times 10^{-5}$.

The tests used for convergence of the vorticity are

$$|G_{i,j}^{n,\ell+1} - G_{i,j}^{n,\ell}| \leq \epsilon_{g_i} \left[\max_{i,j} |G_{i,j}^{n,\ell}|\right] \quad i \neq \text{Imax}, \tag{15a}$$

and

$$|G_{\text{Imax},j}^{n,\ell+1} - G_{\text{Imax},j}^{n,\ell}| \leq \epsilon_{g_b} \left[\max_{j} |G_{\text{Imax},j}^{n,\ell}|\right]. \tag{15b}$$

In equations (14) and (15) ℓ is the vorticity iteration counter. Equation (15a) was used where i < Imax and equation (15b) was used when i = Imax. We demanded that $\epsilon_{g_b} = 2\epsilon_{g_i}$, and that $\epsilon_{g_i} \geq \epsilon_f$ at all iterations.

The solution to the difference equations is accomplished iteratively by first advancing the vorticity using equations (10a) and (10b) for alternate time steps. Then equation (8) is iterated to convergence and the vorticity is recalculated on the basis of

the updated stream function. This sequence is continued until the vorticity converges. Then the process is begun again with the alternate equation (10a) and/or (10b) for the next time step.

GRID SYSTEM

The notation used for specifying a grid, (a, b, c), means that, starting at position a, increment by c until b is reached. The grids which we will compare are the following:

Grid I r_i = (0.0, 0.5, 0.1), (0.5, 0.7, 0.05), (0.7, 0.9, 0.1), (0.9, 1.0, 0.05)
z_j = (0.0, 1.9, 0.1), (1.9, 2.1, 0.05), (2.1, 5.0, 0.1)

Grid II r_i = (0.0, 0.5, 0.1), (0.5, 1.0, 0.05)
z_j = (0.0, 1.9, 0.1), (1.9, 2.1, 0.05), (2.1, 5.0, 0.1)

Grid III r_i = (0.0, 0.5, 0.1), (0.5, 1.0, 0.05)
z_j = (0.0, 0.2, 0.05), (0.2, 1.9, 0.1), (1.9, 2.1, 0.05), (2.1, 4.8, 0.1), (4.8, 5.0, 0.05)

Grid IV r_i = (0.0, 1.0, 0.05)
z_j = (0.0, 5.0, 0.1)

Grid V r_i = (0.0, 1.0, 0.1)
z_j = (0.0, 5.0, 0.1)

Grid VI r_i = (0.0, 1.0, 0.05)
z_j = (0.0, 5.0, 0.05)

Grids I, II, and III were used because they give a dense grid system in the region of the disturbance function and/or the flowfield boundaries. Grid IV gives an additional density in the radial

direction, which is the direction of most uncertainty in the difference approximations.

Grids V and VI furnish comparisons of the results on square grids as well as an estimate of the grid-size convergence.

The problem which was of major interest to the authors was the stability of Poiseuille pipe flow. For this problem it seemed desirable to have a denser mesh system in the vicinity of the point at which the disturbance is applied (r = 0.6, z = 2.0). Therefore, this is the common property of the nonuniform grids. In order to cut computation time it is also desirable to keep the number of mesh points to a minimum so the grids are made as sparse as possible.

The experimental error analysis of the solution of the difference equations on the above grids which we present is shown for both single- and double-precision calculations of the solution for each grid. We define the errors e(F) and e(G) at any grid point by

$$e(F_{i,j}) = (F_{i,j} - \tilde{F}_i)/\tilde{F}_i \tag{16a}$$

$$e(G_{i,j}) = (G_{i,j} - \tilde{G}_i)/\tilde{G}_i \tag{16b}$$

where $\tilde{F}$ and $\tilde{G}$ are true solutions given by equation (5) and F and G are calculated from equations (8) and (10) with boundary and initial conditions, equations (12) and (13).

The relevant quantities for comparison are

$$\overline{e(F)} = \frac{1}{N} \sum_i \sum_j e(F_{i,j}), \tag{17a}$$

$$\overline{e(G)} = \frac{1}{N} \sum_{i} \sum_{j} e(G_{i,j}), \tag{17b}$$

$$\overline{e_I(G)} = \frac{1}{N_1} \sum_{i=1}^{Imax-1} \sum_{j} e(G_{i,j}) \tag{17c}$$

and

$$\overline{e_B(G)} = \frac{1}{Jmax} \sum_{j} e(G_{Imax,j}) \tag{17d}$$

where N = (Imax)(Jmax) and N_1 = N - Jmax. The absence of limits on the summation implies summing over the range of the index.

RESULTS

The solution to equations (8) and (10) was obtained at four consecutive time steps for each grid system. The errors, as specified by equation (17), at each of these time steps are presented in Tables 2-5, (the second number in each column is the power of 10 which should multiply the first number in order to obtain the true value) which show that Grid II is the best of the nonuniform Grids I, II and III and that Grid I is the worst mesh system tested based on a comparison of the errors. The mesh systems with uniform grid spacing, Grids IV, V and VI, are all significantly better than Grids I, II and III. The grid system with 0.05 square spacing, Grid VI, gives a better representation of the stream function and boundary vorticity than was obtained from Grid IV, the uniformly spaced, nonsquare mesh system. However, Grid IV gives a better representation of the interior vorticity than does Grid VI. The

grid system with 0.1 square spacing, Grid V, has less error for all times shown as seen in Tables 2-5; this is true for both single and double precision. The overall vorticity values are seen to have the least error for both single- and double-precision computation on Grid V for the three greatest time values as seen in Tables 3-5. Grid VI has the least error for both single- and double-precision calculation of the interior vorticity for all time levels shown. However, the error in boundary vorticity for Grid VI is greater than that for Grid V. Therefore, we rank the grid systems in order of increasing preference from the standpoint of errors produced in the solutions as follows: I, III, II, IV, VI, and V. Also due to the magnitude of the change in the errors, it is evident that use of double-precision calculations for the nonuniform grids, Grids I, II and III, effects no appreciable improvement in the accuracy of the solution. For the uniform grids, Grids IV, V and VI, double-precision calculations show an improvement consistent with the increased number of available digits for the computation.

The increase in the error of the boundary vorticity over the interior vorticity obtained in all of the solutions is expected. Since the value of the boundary vorticity is calculated by differencing the stream function, any errors in the stream function are magnified in the value obtained for the boundary vorticity. This magnification is an inverse function of step size in the radial direction. Therefore, the errors in the values of the boundary

TABLE 2

Mean Relative Error

Time Step 1

Time 0.01

Grid System	$\overline{e(F)}$	$\overline{e(G)}$	$\overline{e_I(G)}$	$\overline{e_B(G)}$
I S*	1.815 -3	-1.041 -2	-4.859 -5	- .1451
I D**	1.819 -3	-1.045 -2	-4.815 -5	- .1457
II S	3.240 -3	-4.216 -3	-1.996 -5	-6.716 -2
II D	3.245 -3	-4.272 -3	-1.953 -5	-6.807 -2
III S	3.240 -3	-4.227 -3	-2.002 -5	-6.734 -2
III D	3.245 -3	-4.278 -3	-1.955 -5	-6.816 -2
IV S	-1.232 -5	4.385 -5	-4.288 -7	9.293 -4
IV D	-5.564 -15	1.601 -14	-6.432 -17	3.376 -13
V S	-3.211 -6	1.930 -6	-6.908 -7	-1.432 -5
V D	-1.739 -15	-2.086 -14	-1.010 -16	-2.193 -14
VI S	-1.492 -5	4.991 -5	-4.278 -7	1.057 -3
VI D	-4.248 -15	1.562 -14	-7.876 -17	3.297 -13

---

* S indicates single-precision calculation

** D indicates double-precision calculation

TABLE 3

Mean Relative Error

Time Step 2

Time 0.02

Grid System	$\overline{e(F)}$	$\overline{e(G)}$	$\overline{e_I(G)}$	$\overline{e_B(G)}$
I S*	1.808 -3	-1.015 -2	-9.736 -5	- .1408
I D**	1.813 -3	-1.020 -2	-9.651 -5	- .1415
II S	3.236 -3	-4.103 -3	-3.993 -5	-6.505 -2
II D	3.242 -3	-4.157 -3	-3.914 -5	-6.592 -2
III S	3.236 -3	-4.113 -3	-4.007 -5	-6.520 -2
III D	3.242 -3	-4.162 -3	-3.924 -5	-6.601 -2
IV S	-1.242 -5	4.308 -5	-9.236 -7	9.232 -4
IV D	-5.504 -15	1.595 -14	-1.083 -16	3.372 -13
V S	-3.584 -6	-5.065 -7	-1.244 -6	6.872 -6
V D	-1.744 -15	8.332 -16	-2.201 -16	1.137 -14
VI S	-1.484 -5	4.593 -5	8.741 -7	9.819 -4
VI D	-4.281 -15	1.510 -14	-1.498 -16	3.201 -13

* S indicates single-precision calculation

** D indicates double-precision calculation

TABLE 4

Mean Relative Error

Time Step 3

Time 0.031

Grid System	$\overline{e(F)}$	$\overline{e(G)}$	$\overline{e_I(G)}$	$\overline{e_B(G)}$
I S*	1.801 -3	-1.017 -2	-1.488 -4	- .1404
I D**	1.806 -3	-1.007 -2	-1.467 -4	- .1391
II S	3.233 -3	-4.057 -3	-6.076 -5	-6.400 -2
II D	3.238 -3	-4.099 -3	-5.948 -5	-6.470 -2
III S	3.233 -3	-4.065 -3	-6.100 -5	-6.412 -2
III D	3.238 -3	-4.105 -3	-5.966 -5	-6.478 -2
IV S	-1.308 -5	4.197 -5	-1.438 -6	9.102 -4
IV D	-5.545 -15	1.596 -14	-1.608 -16	3.384 -13
V S	-4.646 -6	-6.380 -7	-1.882 -6	1.180 -5
V D	-1.765 -15	5.457 -16	-3.315 -16	9.317 -15
VI S	-1.493 -5	4.540 -5	-1.310 -6	9.796 -4
VI D	-4.374 -15	1.395 -14	-2.305 -16	2.975 -13

* S indicates single-precision calculation

** D indicates double-precision calculation

TABLE 5

Mean Relative Error

Time Step 4

Time 0.042

Grid System	$\overline{e(F)}$	$\overline{e(G)}$	$\overline{e_I(G)}$	$\overline{e_B(G)}$
I S*	1.794 -3	-9.901 -3	-2.003 -4	- .1360
I D**	1.800 -3	-9.942 -3	-1.971 -4	- .1366
II S	3.230 -3	-3.993 -3	-8.159 -5	-6.266 -2
II D	3.235 -3	-4.042 -3	-7.989 -5	-6.347 -2
III S	3.229 -3	-4.067 -3	-8.187 -5	-6.385 -2
III D	3.235 -3	-4.047 -3	-8.012 -5	-6.355 -2
IV S	-1.359 -5	4.088 -5	-1.921 -6	8.968 -4
IV D	-5.559 -15	1.570 -14	-1.889 -16	3.335 -13
V S	-4.543 -6	-1.130 -6	-2.455 -6	3.698 -5
V D	-1.781 -15	-4.780 -16	-4.236 -16	9.493 -15
VI S	-1.534 -5	4.914 -5	-1.723 -6	1.066 -3
VI D	-4.359 -15	1.467 -14	-3.110 -16	3.142 -13

* S indicates single-precision calculation

** D indicates double-precision calculation

vorticity are seen to be consistent with the grid system used.

The results which are presented in Tables 2-5 could be expanded to show individual errors at grid points, or to show errors for each grid line but this is unnecessary since the values presented are indicative of the results everywhere.

The reason that the interior mean vorticity increases with time is that the errors in the boundary vorticity are spread inward slowly as the solution progresses. For time step 1 the points at which the vorticity is significantly in error are on the boundary only. At time step 4, the next two interior grid lines also show noticeable error in the vorticity. Table 6 shows the computing time expended to calculate the solutions for the four time steps presented in Tables 2-5.

The sequence of times obtained for either single- or double-precision calculations, using the same convergence criteria, is as expected since the time required to compute the solution increases with an increasing number of grid points. However, when we compare the times involved between single- and double-precision calculations, we note that double-precision calculation takes less time for Grid V than does single-precision. This is the reverse of what happens for all the other grids. Therefore, from the standpoint of computation time involved in the calculation, the grids are ranked in increasing order of preference as VI, III, IV, II, I and V for single-precision and as VI, IV, III, II, I and V

TABLE 6

Computation Time in Minutes

Grid	I	II	III	IV	V	VI
Single Precision	1.16	1.38	1.51	1.48	.95	2.79
Double Precision	1.22	1.54	1.60	1.72	.83	3.32

for double-precision calculation. Hence, the preferred grid system from this standpoint is Grid V with double-precision calculations.

SUMMARY

On the basis of the results obtained, we conclude that calculation of the stream function and vorticity for Poiseuille pipe flow is most accurately and efficiently accomplished using double-precision calculations on Grid V, a square, equally spaced mesh system of 0.1 grid size. This result is in direct contrast with the original hypothesis set out in the introduction, i.e., that non-uniform and nonsquare grids should allow an increased accuracy in the representation of the vorticity and stream function.

References

1. S. Whitaker and M. M. Wendel, Numerical solution of the equations of motion for flow around objects in channels at low Reynolds numbers. Appl. Sci. Res. 12-A, 91 (1962).

2. D. C. Thoman and A. A. Szewczyk, Numerical Solutions of Time-Dependent Two-Dimensional Flow of a Viscous Incompressible Fluid over Stationary and Rotating Cylinders. Heat Transfer and Fluid Mechanics Laboratory, Department of Mechanical Engineering, University of Notre Dame, Technical Report 66-14 (1966).

3. H. Schlichting, Boundary Layer Theory, McGraw-Hill, 6th ed. 1968.

4. H. J. Crowder and C. Dalton, "On the stability of Poiseuille pipe flow." submitted to J. Fluid Mech. (1969).

5. D. M. Young, Jr., "The numerical solution of elliptic and parabolic partial differential equations." in Survey of Numerical Analysis, Edited by John Todd. McGraw-Hill, 380 (1962).

6. R. S. Varga, Matrix Iterative Analysis. Prentice-Hall (1963).